1-1-2007

Optimization of the effect of corrosion on bond behaviour between steel and concrete

Zahir Aldulaymi
Ryerson University

OPTIMIZATION OF THE EFFECT OF CORROSION ON BOND BEHAVIOUR BETWEEN STEEL AND CONCRETE

By

Zahir Aldulaymi

BASc. of Civil Engineering

Mosul University, Iraq, 1988

A Thesis

Presented to Ryerson University

in partial fulfillment of the

requirements for the degree of

Master of Applied Science

in

Civil Engineering

Toronto, Ontario, Canada, 2007

OPTIMIZATION OF THE EFFECT OF CORROSION ON BOND BEHAVIOUR BETWEEN STEEL AND CONCRETE

By
© Zahir Aldulaymi 2007
Master of Applied Science
in
Civil Engineering
Ryerson University
Toronto, Ontario, Canada

ABSTRACT

This research program consists of laboratory study of corrosion phenomenon in reinforced concrete and further analytical study of the experimental results obtained by Amleh (2000). The laboratory study examined the influence of increasing levels of corrosion on the progressive deterioration of bond between the steel and concrete and determined the extent to which the various water to cement (w/c) ratio in concrete mixtures influence the corrosion of the steel reinforcement as well as the chloride ion penetration.

The influence of corrosion on the bond characteristics of the reinforcing bars in pullout test specimens made with two different w/c ratios and two different concrete cover thicknesses were investigated using control specimens to study the effect of the concrete cover ratio and the concrete compressive strength. The two w/c ratios were 0.47 and 0.37, with two concrete cover thicknesses of 40 mm and 65mm. Hence, the effect of w/c ratio on different parameters like rate of corrosion, compressive strength and the effect of concrete cover thickness on the corrosion rate were studied.

An accelerated electrochemical corrosion procedure was used to develop four levels of corrosion including no corrosion to complete corrosion, with over 25 percent steel bar weight loss due to corrosion, with wide longitudinal cracks.

This research study clearly indicated that the bond stress-slip response of the embedded bar in the pullout specimen, was adversely affected by the width of the crack, and the level of corrosion. The crack width was found to develop faster and longer in specimens with lower compressive strength and as a result the maximum bond strength in the pullout test is affected significantly by the number and size of cracks and thus, the level of corrosion. For a given crack width due to corrosion, it is observed that the available bond strength is higher for larger concrete cover thicknesses than for smaller cover thicknesses. Certainly, the quality of concrete in terms of its permeability is equally important for the corrosion protection

A relationship between the effect of w/c ratio on chloride ingress was developed to count for the deterioration in bond stress, and the induced current used in corroding the specimens of Amleh (2000) and of this investigation program were incorporated to consider for the lack of chloride ion content measured due to the shorter immersing time in this investigation and the high current used to force the specimens to corrode in the accelerated corrosion process.

ACKNOWLEDGMENT

First ALLAH is praised for the aid and guidance.

I would like to express my deepest gratitude and appreciation to Dr. Lamya Amleh for her continuous advice and support since the beginning and through the whole research, her support and valuable remarks were greatly useful and helpful to achieve effective and beneficial results.

The experimental work was carried out at the Ryerson University Civil Engineering Department concrete laboratory. The great help of the department to use all the facilities is highly appreciated. I would like to thank the laboratory technical staff, Mr. Nidal Jaalouk and Mr. Dan Peneff for their help.

Warm love to my mother, praying for her and all the family members the patience and easiness for what we are going through.

Sincere thanks to my brother Samir for his valuable support, assistance, and endless help. Special thanks also for my other brothers and my sister for their support and constant encouragement.

A special gratitude is owed to my wife Zeena for her infinite love and tender, without her support, patience, and encouragement, the completion of this research would not have been possible to me. Therefore, I embrace the opportunity to dedicate this thesis to her.

To:

THE SYMBOL .....

THE ICON.....

MY LATE FATHER .....

TABLE OF CONTENTS

LIST OF FIGURES

LIST OF TABLES

LIST OF SYMBOLS

NaCl : Sodium chloride.

w/c : Water-to-cement ratio.

f_c : Concrete compressive strength.

f_t : Splitting tensile strength.

K : Material intrinsic permeability.

Δh : Drop in hydraulic head (m).

η : Fluid dynamic viscosity (N.sec/m^2).

ρ : Fluid density (Kg/m^3).

g : Gravity acceleration (m/sec^2).

J : Flux rate ($kg/m^2.sec$).

D_{eff} : Effective diffusion coefficient (m^2/sec).

dC_{cl}/d_x : Concentration gradient (Kg/m^4)

C_{cl} : Concentration of chloride ion.

erf : Error function.

C_s : Surface concentration.

i : Liquid absorbed per unit of surface (g/m^2 for mass or m^3/m^2 for volume).

t : Time (sec).

S : Concrete sorptivity ($g/(m^2 \cdot s^{1/2})$ for mass change or $m/s^{1/2}$ for absorbed volume).

Rr : Relative rib area.

c/d_b : Concrete cover thickness to the bar diameter.

Tc : Tensile strength of concrete.

A_{ct} : Area of the concrete subjected to tension.

ΔT : Change in the bar tensile force along a distance ΔL .

ΔL : Distance along the beam length between the two considered section.

u : Bond stress (MPa).

ML : Mass loss of steel bar subjected to corrosion.

Cl^- : Chloride ion concentration at the steel bar surface.

CHAPTER 1
INTRODUCTION

1.1 General

Chloride-induced corrosion of reinforcing steel in concrete bridge decks, parking garage slabs and marine structures has been identified as the primary cause of concrete deterioration. The distress in concrete is caused basically by several interactive factors and characterized mainly by severe environment, unsuitable materials, inadequate construction practices and specifications in conjunction with structural weakness.

In many parts in the world, the deterioration of concrete structures is mainly caused by the corrosion of the reinforcing steel and the associated volumetric expansion of the corrosion products. The steel bar shows a high resistance to corrosion, when it's embedded in concrete where the cement paste provides an alkaline environment that protects the steel bar from corrosion. This protection comes from the ferric oxide passive layer which forms around the steel in concrete. This layer is stable in high alkaline concrete (pH $\approx$ 11 to 13) Bavarian et al (2002). The factors influencing the passivity of the reinforcing bars are the water cement ratio, permeability and electrical resistance of concrete, Bavarian et al (2002). These factors determine whether corrosive agents like carbonation and chloride ion can penetrate the concrete pore to the passive layer.

The potential consequences of the corrosion problem can be summed up in the continuous reduction in strength, stiffness, durability, and designed life time of concrete structural elements reinforced with conventional steel. Corrosion of reinforcing steel in concrete has caused catastrophic failures in some specific cases, resulting in injury and death, such as the collapse of the Berlin Congress Hall, Isecke (1982) and of a parking garage in Minnesota, Borgard *et al.* (1990).

According to the Federal Highway Association, the infrastructure deficiencies due to corrosion in the United States present a $1.3 trillion Elsener (2001). In Canada, however,

there is no accurate number of the infrastructure deficiency, but some studies found that the cost of rehabilitation for corrosion of reinforcing steel is estimated to be about $3 billion per year in Canada, Davis (2000). The total cost of Canada's infrastructure is estimated between 3-5 trillion dollars, and because of lack of funding the related political decision leading to deferred maintenance, the current infrastructure deficit is well over $100 billion, Amleh (2000).

It should be emphasized that the reinforcing steel is provided in reinforced concrete to resist the tensile forces, and to produce controlled cracking within that zone. However, corrosion not only deteriorates the steel bar and its function of transferring the tensile stresses, but it deteriorates the concrete by spalling of the cover. Therefore, corrosion of the reinforcement has a strong influence on the bond behaviour at the interface between the steel reinforcement and concrete. As corrosion of the reinforcing steel progresses, the bond strength between the reinforcing steel and concrete diminishes progressively, and major repairs or replacement is needed. While much has been written about the problem, and numerous reports have appeared which discuss how this corrosion can be controlled, only limited data are available about its influence on the bond behaviour at the steel-concrete interface.

1.2 Methods of Corrosion Resistance

There are two major measures, active and passive, that have been developed and successfully implemented to control, minimize the corrosion risk. The passive measurements are designed to be used for protecting the healthy concrete elements that suffer no corrosion problems against potential corrosion attack. These passive measurements include using high performance concrete with added admixtures, such as superplasticizers, or mineral admixtures, as fly ash and silica fumes, or using corrosion inhibitors that can improve the stability of the passive layer of the steel, or through using epoxy coated or galvanized reinforcing bars or applying sealers to the finished concrete surface. An adequate thickness and impermeability of the concrete cover over the steel reinforcement provides both physical and chemical protection by providing an alkaline and electrically resistive medium in the immediate vicinity of the steel surface, besides providing a physical and chemical barrier to the ingress of moisture, oxygen, carbon

dioxide, chlorides and other aggressive agents. According to RILEM (1987), the efficiency of the concrete cover in preventing corrosion is dependent on many factors collectively referred as its "quality", Amleh (2000).

On the other hand, the use of active corrosion control systems is assigned to treat the salt contaminated concrete elements minimizing the rate of corrosion; this can only be done using cathodic and anodic protection, Elsener (2001).

1.3 Corrosion and Structural Safety

Bond between the reinforcing steel and the concrete is dependent on cohesion, adhesion at the steel interface and the mechanical interlocking between the lugs of the reinforcing steel bar and the surrounding concrete. Corrosion can result in the loss of the cross-sectional area and gradual deterioration of bond between the concrete and the reinforcing steel with increasing levels of corrosion. Besides being extremely costly, both phenomena can endanger structural safety and severely influence the serviceability of the structure. Over the past few decades, considerable research has been undertaken on bond, tension stiffening and crack width control to ensure system serviceability through control of crack width and deflections in structural concrete elements. However, little research work has been undertaken to evaluate the effect of corrosion on bond characteristics at the steel-concrete interface, tension stiffening and the width of spacing of cracks. The corrosion of reinforcing steel, which impairs the overall durability, can perhaps impair structural safety more due to the deterioration of bond at the steel-concrete interface, than due to a loss in the cross-sectional area unless the bar size is too small (Amleh and Mirza, 1999).

1.4 Scope and Objective of This Study

The investigations of the influence of corrosion on the bond behaviour between the reinforcing steel and the concrete reported here were carried out under pullout testing relative to four stages of corrosion: no corrosion, corrosion corresponding to hairline cracking, and two postcracking levels explained thereafter. The appearance of the first

visible hairline crack was defined as first level of corrosion. Corrosion is measured as the loss of metal of the reinforcing steel bar relative to the original reinforcing steel bar weight.

Reinforced concrete that is exposed to deicing salts and marine environments is particularly susceptible to chloride-induced corrosion. A well-designed, durable, low permeability concrete mixture will provide some protection against chloride-induced corrosion of reinforcement.

The objective of this study is focused on investigating the bond properties between the reinforcing steel and the surrounding concrete, using different w/c ratio concrete mixtures, and determining the effect of deleterious agents on these properties, especially the effect of chloride ion concentration on bond deterioration and modeling this effect to estimate the residual bond capacity. The main objective is to determine as to what extent the various water/cements ratio of concrete mixtures influence the corrosion of the reinforcement as a function of the chloride-ion penetration phenomenon.

Using the data obtained by Amleh (2000), a model represents the residual bond capacity has been derived, and then verified with data obtained in this investigation, from 32 pullout specimens with different diameters and w/c ratios.

1.5 Structure of Thesis

This thesis consists of six chapters; Chapter 1 consists of a brief introduction to the corrosion problem, scope and objective of the study and the thesis structure. Chapter 2 presents some of the latest literature review of the mechanisms of reinforcement corrosion and the main causes of the breakdown of the protective mechanisms, which have been the subject of intensive research over the past few decades. It discusses the characteristics of the concrete that are relevant to reinforcement corrosion, and how the concrete environment protects the embedded steel. Chapter 3 consists of a description of the experimental program of the accelerated corrosion testing to simulate the corrosion conditions in the pullout specimens that underwent the accelerated testing. In addition, it presents the concrete mix parameters, the physical, chemical, and mechanical properties

of the materials used, the properties of the concrete mixture including the test results of the fresh and hardened concrete, and description of specimens' preparation and the tests setup. Finally, the experimental program of the pullout testing of the specimens that was performed after achieving the required corrosion conditions is presented.

Chapter 4 presents the discussion of the results that were obtained from the pullout-tests. Chapter 5 presents an overall discussion of the analytical investigation of the experimental results obtained by Amleh 2000, and by this investigation. Chapter 6 consists of a brief summary of the experimental and analytical work as well as the conclusions and recommendations for further research and development of the influence of corrosion on bond behaviour at the steel-concrete interface are included.

CHAPTER 2

LITERATURE REVIEW

The corrosion of steel reinforcement is of the greatest concern in the deterioration of the infrastructure around the world, and therefore, this chapter will discuss the factors that cause and control corrosion of steel in concrete, as several metals will corrode under certain conditions when embedded in concrete. Factors influencing the electrochemical process are also discussed, and some protective measures that can be utilized are presented.

This chapter does not attempt a total review of all of the tests on corrosion of the embedded steel in the concrete, but rather the results of some tests that have an impact on corrosion of embedded steel in concrete are reviewed. Special attention is given to the research that has investigated the influence of corrosion on bond behaviour.

In addition, the behaviour of a reinforced concrete member is influenced to a considerable degree by the bond between the concrete and the reinforcing steel, and cracking. This chapter presents some basic information on bond between the concrete and the reinforcing steel, and the associated slip and cracking in reinforced concrete. The mechanics of slip of deformed bars versus plain bars in concrete is discussed. The stress redistribution and deformations in concrete associated with the bond are also presented.

2.1 MECHANISMS OF CORROSION OF EMBEDDED STEEL IN CONCRETE

Corrosion is the process of the transformation of a metal to its "native" form which is the natural ore state, often as oxides, chlorides or sulphates. This transformation occurs because the compounds such as the oxides "involve" less energy than pure metals, and hence they are more stable thermodynamically. The corrosion process does not take place directly but rather as a series of electrochemical reactions with the passage of an electric current. Corrosion also depends on the type and nature of the metal, the immediate environment, temperature and other related factors. The corrosion may be defined as the destructive attack of a metal by chemical or electrochemical reaction with its environment.

2.1.1 Corrosion in Reinforcing Steel

Corrosion of steel embedded in concrete affects the mechanical properties of the steel bar such as strength and ductility. Corrosion products occupy a larger volume from the uncorroded steel bar developing high pressure to the surrounding concrete leading to cracking and spalling or delamination of the concrete cover, Neville (1995). Also, corrosion of the reinforcing steel bars causes changes in the profile of the bar ribs and a loss in the adhesion of the steel-concrete interface, Cabrera & Ghodussi (1992). As the corrosion progresses, the growing pressure created by the corrosion products will eventually force the concrete off the steel bar, and causing the reinforcement to lose any protection against corrosion and also losing a significant part of its bond resistance to transfer forces from the reinforcing steel to the surrounding concrete, Amleh (2000).

2.1.2 Principles of Corrosion

The corrosion of iron may occur by several mechanisms. Corrosion may initiate by bacterial action, certain bacteria (desulphovibrio desulphuricans), Berkely and Pathmanaban (1990), by direct oxidation (burning), or by acid attack, and by chemical attacks. Such corrosion is of little concern in the concrete. Indirect oxidation (electrochemical corrosion) as a result of dissimilar or non-uniform metals or dissimilar environments is of paramount importance in the deterioration of most concrete structures. Also, corrosion of the reinforcing steel in concrete by electrolysis due to "stray electrical currents" and hydrogen embrittlement due to "stress corrosion" are also relevant. In summary, the corrosion of the reinforcing steel in concrete occurs generally by an electrochemical reaction in the presence of moisture and oxygen, which is believed to be the essential cause for all of the corrosion distress that occurs.

2.1.3 Electrochemical Reactions

Corrosion of steel by galvanic actions where the highly alkaline environment and the accompanying passivating effect may be destroyed occurs because of three principle causes: the carbonation of concrete, the ingress of chloride ions into concrete to destroy the passive layer of oxides on the steel bar surface, and the leaching of the alkalies by the streaming water. It must be emphasized that corrosion is possible only if sufficient moisture and

oxygen are available. This electrochemical process causing corrosion of the reinforcing steel in the concrete is similar to the action that takes place in a flashlight battery which involves an anodic reaction, consisting of oxidation of the iron, and a cathodic reaction where this reaction consumes any electrons produced during oxidation of the iron, an electrical conductor, and an electrolyte.

The chloride ion in the concrete plays a major role in the onset of corrosion; the chloride ion content of the concrete indicates the corrosion level and the severity of structure deterioration.

For the corrosion to initiate, the passive layer should be penetrated by the chloride as follow:

$$Fe^{++} + 2Cl^{-} \longrightarrow FeCl_2$$

$$FeCl_2 + 2H_2O \longrightarrow Fe(OH)_2 + 2HCl.$$

The consequences of this penetration are the formation of corrosion products as mentioned above and the reduction of the bar diameter, thus losing the composite action and reducing the load carrying capacity. Neville (1995).

2.1.4 Morphology of Corrosion Process

The morphology of the corrosion process depends on the distribution of anodes and cathodes on the steel bar surface and on their relative areas. If the anodes and the cathodes are irregularly distributed on the steel surface and change their position during the corrosion process, the attack will be more or less uniform. However, if the anodes are located at fixed point and the anodes/cathode area ratio is very small, localized attack will develop.

The corrosion rate is considered to be cathodically controlled when the cathodic process is slower. Figure 2.1 represents the log of the absolute current, *I*, versus the potential, *E*, by polarizing each half-cell and demonstrates the cathodic control as the cathode has larger polarization. The corrosion rate is considered to be anodically controlled when the anodic

process is slower and is shown in Fig. 2.2. There are two types of corrosion-rate controlling mechanisms ACI Committee 222 Report, (2002):

(1) The cathodic diffusion, where the rate of oxygen diffusion through the concrete determines the rate of corrosion.
(2) The development of a high resistance path, when there is a large distance between the anodic and cathodic areas such as several feet apart, and hence, the resistance of the concrete may be of great importance.

2.1.5 Concrete as an Electrolyte

An understanding of some of the elements of concrete structure is essential for discussing the factors influencing the corrosion. Concrete consists of a cement paste and coarse and fine aggregates, and the aggregates usually do not play a significant role in the electro-chemical corrosion process. Basically, the cement paste phase of the concrete acts as the electrolyte for the transportation of ions and the ionic current.

Mehta and Monteiro (1992) and others have described the composition of the hydrated cement paste, which consists of two phases - the hydrated minerals and the pore solution (liquid phase). The basic parameters which control steel corrosion are:

(1) The volume and composition of the pore solution.
(2) The size and distribution of pores.
(3) The presence of $Ca(OH)_2$ in the hardened paste.

Corrosion in reinforced concrete structures is associated with transport properties of concrete. These properties determine the amount of aggressive materials permitted into concrete. There are three main transport properties, permeability, diffusion and sorptivity.

2.1.5.1 Permeability

Permeability is defined as the rate of flow of a fluid under pressure in a porous material. This transport property is highly affected by the porosity and the pore structure. The pore

structure can be defined through pore size, distribution, shape, and connectivity. The porosity of a material is defined as the ratio of the volume of all the pores in a material to the whole volume. Hence the pore structure affects the permeability, and the pore size affects the permeability in a way that the larger the pores, the easier the water or fluid to flow through. The distribution of the pores plays a big role in the flow of fluids within the concrete. The connectivity can help the flow of liquid through the concrete. If the pores are connected, fluids are allowed to move in many paths of flow, but if they are disconnected the fluid is trapped and cannot move on.

The concrete coefficient of permeability can be defined by use of Darcy's law:

$$\frac{dq}{dt}\frac{1}{A} = \frac{K'\rho g}{\eta}\frac{\Delta h}{L} \qquad (2.1)$$

where: dq/dt : Flow rate of water (m^3/sec)

A : Cross-sectional area

K : Material intrinsic permeability

Δh : Drop in hydraulic head (m)

L : Depth of flow (m)

η : Fluid dynamic viscosity (N.sec/m^2)

ρ : Fluid density (Kg/m^3)

g : Gravity acceleration (m/sec^2)

The coefficient of permeability K, can be found through the following relationship:

$$K = \frac{K'\rho g}{\eta} \text{ (m/sec)} \qquad (2.2)$$

2.1.5.2 Diffusivity

Diffusivity is defined as the spread of fluids in concrete under a concentration gradient. For this to occur, the concrete must have a continuous liquid phase and there must be a chloride ion concentration gradient, Stanish *et al.* (1997). Chloride ion diffuses only when dissolved in water, and the diffusion is more effective when the pore system is fully saturated, Bertolini *et al.* (2004). There are two types of flow in which diffusion can be

analyzed; steady state flow and non-steady state flow, the steady state flow described by Fick's first law:

$$J = -D_{eff}\frac{dC_{cl}}{dx} \tag{2.3}$$

where: J = flux rate ($kg/m^2.sec$)

D_{eff} = effective diffusion coefficient (m^2/sec)

$\frac{dC_{cl}}{dx}$ = concentration gradient (kg/m^4)

C_{cl} = concentration of chloride ion

x = position variable

The non – steady state flow, where diffusion in concrete falls under this type of flow, and is described by Fick's second law

$$\frac{\partial C_{cl}}{\partial t} = D_{eff}\frac{\partial^2 C_{cl}}{\partial x^2} \tag{2.4}$$

This function is integrated under the assumptions:

$C_{cl\,(x=0,t>0)} = C_s$ (surface concentration is constant at any time)

$C_{cl\,(x>0,t=0)} = 0$ (initial C at any point other than the surface = 0)

The solution is:

$$\frac{C_{cl}(x,t)}{C_s} = 1 - erf\left(\frac{x}{2\sqrt{D_{eff}t}}\right) \tag{2.5}$$

where, $C_{cl}(x,t)$ = concentration at distance x from the concrete surface at time t

C_s = surface concentration

erf = error function

It's worth mentioning that in concrete, Fick's second law does not apply correctly unless a diffusion coefficient (determined experimentally) is applied. This is due to the binding of some diffusing agents by components of the cement matrix.

2.1.5.3 Sorptivity

Sorptivity is defined as the ingress of water into non-saturated structure driven by capillary forces, Bentz *et al.* (2001). Porous concrete absorbs more water and faster than a dense concrete. The following relationship has been empirically derived by Bertolini (2004) from the observation of experimental data and is only correct for very porous materials or in the early stages of capillary action.

$$i = S\,(t)^{1/2} \qquad (2.6)$$

where:
i : liquid absorbed per unit of surface (g/m^2 for mass or m^3/m^2 for volume)
t : time (sec)
S : concrete sorptivity ($g/m2\,.\,s^{1/2}$) for mass change or $m/s^{1/2}$ for absorbed volume)

The values of concrete sorptivity depend on a variety of factors, but the main factor is the degree of drying to which the samples have been subjected.

2.1.6 Concrete Cover Thickness

The thickness of concrete cover is an important factor in delaying the corrosion initiation. The larger the concrete cover the longer the time required for the chloride to reach the reinforcing steel surface. The low permeability and the concrete cover thickness can compensate each other (Neville 1995). For this reason standards often specify a combination of cover thickness and concrete strength, such that a higher concrete strength and a lower concrete cover and vise versa.

However, this is not always right; for example, a thick concrete cover does not compensate a highly permeable concrete. Besides, thick concrete cover may have an

adverse effect if not associated with steel due to shrinkage cracks and thermal stresses. Typically, the concrete cover should not exceed (80 – 100) mm, unless otherwise decided by the structural designer. Small thickness of concrete cover should also be avoided, because despite the low penetrability of concrete, cracks for whatever reason, local damage, and misplacing of steel could result in rapid transportation of chloride ions to the surface of the reinforcing steel.

2.2 BOND BETWEEN REINFORCING STEEL AND CONCRETE

Bond is defined as the transfer of shear forces across the interface between concrete and reinforcing steel. It is the interaction between the reinforcing steel and the surrounding concrete where forces are transferred from concrete to steel and vise versa. (Amleh, and Gosh, 2006).

The relative movement of the bar takes place with respect to the surrounding concrete is called slip. In deformed steel bars, when slip starts, the chemical adhesion forces are lost. As further slip takes place, the friction forces are reduced, leaving most of bond transfer to the mechanical interlocking Figure 2.3.

Therefore, bond strength in deformed steel bars is comprised of three components (Figure 2.3),

a- Adhesion: is the chemical bond created on the interface between the steel bar and the surrounding concrete. This bond is relatively weak; it is lost due to the service load or shrinkage of the concrete.

b- Friction: unlike the adhesion bond, the friction bond is a very dependant on the surface characteristics of the steel bar. After the adhesion bond is destroyed, some frictional slip happens before the full bearing capacity at the ribs is mobilized. The ACI Committee 408 (1994) suggested based on the work of Treece and Jirsa (1989) that the friction contributes up to 35% of the ultimate strength governed by the splitting of the concrete cover.

c- Mechanical interlock: The profile of the steel bar and the geometry of the ribs dictate the amount of the mechanical bond generated between the steel bar and the concrete. At higher loading levels, the bearing against the ribs is considered the most significant stress transfer mechanism. This transfer is due to the mechanical interlocking between the steel ribs and the concrete keys. The slip of a deformed bar may occur in two ways, either through pushing the concrete away from the bar by the ribs, i.e. wedging action, or through crushing of the concrete by the ribs.

Bond in plain steel bars has two mechanisms only; chemical adhesion and the friction between the reinforcing steel bar and the surrounding concrete.

2.2.1 Effect of Bar Profile on Bond Strength

Since the theory of reinforced concrete is based on the bond transferred between the steel bar and the surrounding concrete, this transfer is made possible by the resistance to relative motion or slippage between the concrete and the surface of the embedded steel bar.

Previous bond researches, Rehm (1961); Lutz, Gergely, and Winter (1966); Soretz, and Holzenbein (1979); Kimura, Hideka and Jirsa (1992); Darwin and Ebeneze,(1993) involved pullout and beam-end tests of regular and specially machined bars, and showed that the geometry and shape of bar deformations play a big role in the bond strength of anchored bars. They concluded that the increase in the height of the rib and decrease in the spacing between ribs; would increase rib bearing area-to rib shearing area ratio and would improve the bond performance. The ratio of rib bearing area-to rib shearing area is called the relative rib area (Rr) which is defined as the ratio of the projected rib area (normal to bar axis) to the product of the nominal bar perimeter by the center-to-center rib spacing. It was also concluded that an increase in the rib face angle above 45 deg would result in a higher bond performance Figure 2.3.

Choi and Lee (2002) studied the effect of rib geometry of deformed bars on bond behavior and found that the effective rib face angle is between 25 and 35 degrees which is less than the 45 degrees, and the relative rib area has a low effect on the bond strength of the deformed bars when they are not confined by transverse reinforcement.

Lutz, *et al.* (1966) studied the action of bonding forces, and the associated slip and cracking for bars with various surface properties and found that a higher rib face angle would be less affected by grease and any other friction-reducing agents than a flatter rib face angle bars. If the rib face angle was 90 degrees, than the entire bond between the steel bar and concrete would be produced by the bearing of the concrete key, and the friction between the concrete and the steel would be unnecessary. However, a 90 degree rib face angle of steel bar could have insufficient compaction of the concrete in front of the rib which would adversely affect the bond strength. While, in plain bars, the bond strength is produced from the friction and adhesion between the steel bar and the surrounding concrete, and the loss of them would destroy the bond.

2.2.2 Effect of Geometry and Shape

David, (1941), investigated the effect of different bar geometry on bond stress. He found that the stress transmission from the loaded end to the free end was higher in case of plain bars than that of ribbed bars. Also, he observed that the stress in the ribbed steel bar was higher near the loaded end than that of plain bars, and this may be attributed to the increase of bond resistance due to the ribs action, which is not available in plain bars.

Maslehuddin *et al.* (1990) conducted a study to evaluate the surface conditions of steel bar on the bond between the reinforcing bar and the concrete. The objective of the study was to investigate the effect of different rust degrees on the surface of the steel bar and their corresponding effect on bond with concrete. Several bar diameters were subjected to atmospheric exposure. The results indicate that the 16 mm diameter bar showed no change in bond with concrete, whereas the 32 mm diameter bar showed a slight increasing in bond with concrete. They attributed this to the smaller bar diameters which showed some filling of rust between the lugs, and thus producing a plane surface effect

compared to the ribbed bars, while in bigger diameters the increase of the roughness due atmospheric exposure and rust formation, slightly increased the bond.

2.2.3 Effect of Rib Angle, Rib Spacing, and Rib Height

Cairns and Abdullah (1994) studied the effect of the reduction of bond stress in fusion-bonded epoxy-coating reinforcement and evaluated the variation in bond stress with rib face angle for machined bars. . Figure 2.4 shows the variation in rib face angle from 30 to 75, with the bond stress and the corresponding slips. At slips 0.01 and 0.1 mm, the bond stress slightly increases with the increase in the rib face angle. At the failure load (slip 1 mm), the bond stress increases with the increase of rib angle from 30 to about 55 or 60. This may be attributed to the increase of bearing force due to the increase of bearing area. It should be mentioned that the large increase in the rib face angle can result in an insufficient concrete compaction below the rib and this factor should be taken in to consideration to design the rib face angle. Researchers observed that the ribs act as wedges and the concrete in front of the ribs crushes gradually, resulting in a pullout-type failure and found that the concrete in front of the ribs undergoes gradual crushing (Figure2.5).

2.2.4 Effect of Casting Position and Concrete Confinement on The Bond Strength

According to Park and Paulay (1975), the load-bond slip relationship for deformed bars is mainly affected by the quality of concrete in front of the steel bar rib. The quality of concrete depends on the position of casting. Figure 2.6 shows different positions of casting and their effect on the bond-slip relationship. Soft and porous layer is formed under the bar when the concrete is poured perpendicular to the length of the reinforcement bar (number 3 in Figure 2.6). This results in a weaker bond compared to the other positions due to the weak nature of the concrete under the bar.

In plain steel bars; the effect of casting position is even more severe. Figure 2.7 shows the effect of casting position of a 16 mm bar. Curves number (1) and (3) reflect heavy corroded and pitted bars, while curves number (2) and (4) reflect the plain steel. It is noticed that the bond strength is adversely reduced in horizontal bars compared to

vertical bars. Furthermore, it is expected that the bond in the top bars will have weaker bond with concrete than the bottom bars, since air and water will be greater under the top bars. In addition, the relative movement of concrete due to settlement; further weakens the bond under the top bars. The extent of bleeding of concrete and water permitted to escape from the form are dictating the amount of settlement Park and Paulay (1975).

Welch and Patten (1967) studied the effect of bleeding and settlement and compared the bond performance of bars surrounded by concrete in leaky timber molds and in well-sealed steel moulds. In the latter they also delayed the placing of the concrete by 40 minutes. Figure 2.8 demonstrates their results, curves number (1) and (2) refer to the delayed placing for top and bottom bars and curves (3) and (4) refer to the leaky timber mold placing for the same bars. This shows the effect of concrete settlement on bond, particularly for top bars. The ACI code recognizes this phenomenon by requiring 40% excess development length for top-cast deformed bars.

It has been found that the increased concrete cover would increase the resistance against splitting, since bond tends to fail abruptly in the case of deformed bars surrounded by light confinement; the longitudinal cracks accompanied by slip on the rib face break out through the entire cover thickness. Yet it would not increase the bond proportionally to the increased cover. In large size bars, the beneficial effect is not significant; in fact the effect on the formation and widths of cracks under service load condition is the governing criterion in selecting an appropriate value for allowable average bond stress. Medium sized top bars appear to benefit more from added cover. If the concrete cover thickness to the bar diameter (c/d_b) value is high, failure occurs by shearing of the concrete between the ribs. The critical value of c/d_b at which the failure mechanism changes from cover splitting to concrete shearing at the steel – concrete interface has been evaluated as 2.5 by Orangun *et al.* (1977), Jirsa *et al.* (1979), and by Reynolds (1982)

Stirrups prevent cracks along the embedded bars from opening specially if they are spaced closely, and enable greater bond forces to be transmitted. The aim of confinement by means of stirrups or transverse reinforcement is to prevent a failure along a potential

splitting crack and to enforce, if necessary, a shear failure, which is associated with the maximum attainable bond strength.

2.2.5 Modes of Bond Failure

Principally, two types of failure can occur under monotonically increasing loads Rehm (1961) and Lutz and Gregely (1967): Slip of the deformed bars can occur because of the crushing of concrete in front of the ribs, and splitting of the concrete by wedging action. Coronelli and Gambarova (2000) have developed a model to predict both the pressure around a corroded bar (which plays a fundamental role, but cannot be measured) and the bond strength at the onset of pull-out in a short anchorage. Bond degradation is shown to be caused by the loss of confinement in specimens with light stirrups and small covers, and by the simultaneous degradation of the steel concrete interface due to the loss of cohesion and friction caused by the corrosion products; these critical situations may affect markedly the structural behaviour. For medium and large covers, with heavy stirrups or a combination of stirrups and skin reinforcement, the confinement around the bar is not impaired by cover splitting, but still the interface deteriorates owing to the pressure exerted by the corrosion products, and its deterioration must be considered.

2.2.5.1 Splitting Bond Failure

Splitting bond failure happens in concrete at the smallest distance outward from the steel bar (Figure 2.9), or the relatively small concrete cover around the steel bar. It also happens when there is largely spaced confinement to the concrete. This phenomenon, of cover splitting, happens when the tangential tensile stresses in the concrete cover, caused by the radial outward pressure, exceed the tensile strength of the concrete.

2.2.5.2 Pullout Failure.

Pullout failure results from shearing off the concrete keys in a cylindrical plane tangential to the steel bar ribs leaving the concrete keys on the bar ribs (Figure 2.10). This type of failure happens when there is a large concrete cover and/or a good confinement to the concrete around the bar.

2.2.6 Cracking Behavior

Cracking of concrete occurs when the tensile stresses at a certain location exceed the tensile stress of concrete. With plain steel, when a crack occurs and the steel is separated from the concrete, the bond is lost completely in the vicinity of the crack. In case of deformed steel bars, the bond is not lost completely, and the forces are transmitted by means of interlocking between the ribs and the concrete keys as depicted in Figure 2.11 which is based on the study of the nature of cracking around a deformed bar by Goto (1971). In Beeby's study (1979) in reference to Goto's study (1971) on crack development; suggested that with slight loading, the crack width at the surface of the bar develops with a minimal width. With further loading the adhesion adjacent to the crack is lost causing a transfer of the load to the ribs of the bar and internal cracks are developed adjacent to the main crack. More loading will result in developing successive cracks in greater distances from the main crack. Stresses in the steel will reach a local peak at the crack, while between the cracks; the steel stress is lower due to stress transfer to the concrete around it. This stress transfer produces bond stresses.

2.2.7 Measurement of Bond

Many different types of bond measurement technique have been developed to investigate the bond characteristics of steel reinforcement in concrete. These are the pullout specimens both the (concentric and eccentric), tension specimen, different beam tests and semi-beam tests.

2.2.7.1 Pullout Test

Pullout specimen is a simple way of testing relative bond behaviour of embedded steel in concrete. However, the results of this test are not intended to establish bond strength values for design purposes, because it does not directly represent the stress state in concrete beams. Nevertheless, this test method is largely used, when relative but not absolute bond resistance is pursued, for example testing different lugs geometry and size for slip resistance, or different concrete mixtures.

Pullout specimen consists of steel bar embedded in a concrete cylinder or prism. When tested, the cylinder is secured and a force is applied to pull out the steel bar. The force and the slip of the bar then measured, Figure 2.12.

2.2.7.2 Tension Test

Tension specimen consists of a steel bar symmetrically embedded in cylindrical concrete specimen, Figure 2.13. The load is applied on the two ends of the steel and stresses are transmitted to the concrete throughout the bond till at some cross-sections of the concrete the stresses transmitted are larger than the tensile strength of concrete ($Tc = f_t A_{ct}$), where f_t is the tensile strength of the concrete and A_{ct} is the area of the concrete subjected to tension, cracks are developed. Formation of a crack in the concrete section is attributed to the loss of adhesion between the steel bar and surrounding concrete, and the bond is maintained by the bearing of the concrete on the lugs. In the process of transferring forces from steel bar to the concrete and vice versa, a relative slip takes place between the steel bar and concrete which leads to the opening of cracks in concrete. In the pullout test the concrete is under compression which causes an increase in the bond strength. That is why the pullout specimens are not recommended by the ACI Committee 408 to be used to determine the development length as they represent the least realistic type.

2.2.7.3 Beam Test

Beam test method is the most representative test to the behaviuor of reinforced concrete in terms of the state of stresses, crack development and bond loss through out the loading process. Figure 2.14a, depicts a four-point loading of a beam.

In this test both the concrete and the steel are under tension. When crack initiates at the bottom of the loaded beam, the neutral axis relocates upward causing a reduction in the stresses capacity at the cracked section Figure 2.14b.

2.2.7.4 End Beam Test

It is more realistic test than the pullout test. The ASTM standard A944-99, adopts this type of bond specimens, it was established to compare the bond strength of steel bars to

concrete. It was experimentally found that the bond results obtained using the beam end specimens closely match those obtained using full-scale reinforced concrete members, Figure 2.15. In the beam end specimens, both the reinforcing and the surrounding concrete are subjected to tensile stresses. To achieve such state of stresses, the compressive forces must be located away from the reinforcing bar by a distance not less than the bonded length of the tested bar. Also a short length of the tested bar near the concrete free surface has to be unbonded from surrounding concrete to avoid conical failure.

2.2.8 Bond Characteristics of Reinforced Concrete

As it is well known that the concrete is good in compression and weak in tension, therefore the ductility of the concrete is negligible. To enhance the tensile properties of concrete, steel reinforcement is used to restore ductility and utilize the concrete section. The idea behind using the reinforcement in flexural members is to transfer tensile stresses from the concrete across the tension cracks to the reinforcement. To insure this state of stresses transfer, an adequate bond must be developed between the two materials.

The role of reinforcement steel in concrete element varies depending on static status of the element and the distribution of internal stresses. For cracked flexural members in the constant moment region, the reinforcement bar gradually carries the developed tensile forces from the concrete along the development length. The bar carries the tensile forces form one side of the cracked concrete section to the other side and the forces flow back to the surrounding concrete. In case of successive cracks in a constant moment region, the forces do not transfer from the steel to the surrounding concrete. In fact they continue to flow through the bar till they reach the next crack. The presence of bond between the concrete and the bar will cause the flow of tensile forces in and out the steel as in Figure 2.16 creating a phenomenon called tension stiffening Amleh (2000). This phenomenon could also be observed between any two successive cracks, where all tensile stresses are resisted by the steel. However, between two adjacent cracks, the tensile stresses are transferred to the surrounding concrete by bond stresses. In their study of crack opening near reinforcement bars in concrete structures, Watstein and Matthey (1959) have already

noticed that the concrete between cracks contributes to the carrying tensile loads. The contribution of concrete may be considered to increase the stiffness of tensile reinforcement.

Figure 2.17 shows the transfer of part of tensile forces between reinforcing bar and the surrounding concrete between two cracks through the bond along a shear span of a tension member.

Since the bond forces are transferred axially along the interface of the reinforcing bar, an average bond stress can be calculated depicting the distribution of tensile forces along the bar length.

$$u_{av} = \frac{\Delta T}{\Delta L \, \pi \, d_b} \qquad (2.7)$$

Where, u_{av} : Average bond stresses along a definite length ΔL .

ΔT : $(T2 - T1)$: Change in the bar tensile force along a distance ΔL .

ΔL : Distance along the beam length between the two considered section.

d_b : Nominal bar diameter.

Since the variation of tensile forces is due to the variation in the induced bending moment, equation 2.6 can be written in terms of the bending moments, Figure 2.18.

$$u_{av} = \frac{(M_2/jd_2 - M_1/jd_1)}{\Delta L \, \pi \, d_b} \qquad (2.7)$$

2.2.9 Previous Research

Almusallam, et al (1995) assessed the effect of different degrees of reinforcement corrosion on bond degradation, they studied the free-end slip and the modes of failure in

four degrees of corrosion (as a percentage of bar weight loss), as well as the effect of different crack widths and degradation of rib profile for the various degrees of corrosion. The results indicated that, as the degree of corrosion increases from 0 to 4% (as a percentage of bar weight loss), the ultimate load increases from 61 to 71 kN, whereas the corresponding slip at the ultimate load decreases from 0.68 to 0.238 mm (Figure 2.19 to 3.21). The results also indicated a decrease in the ultimate bond strength with rib profile degradation (Fig. 2.22).

Auyeung *et al.* (2000), evaluated the bond strength and bond-slip behavior of reinforcement bars corroded to various levels of corrosion. They found that when the corrosion mass loss approached approximately 2%, cracks started forming along the corroded bar and once the crack was formed, corrosion was accelerated due to the decrease in resistance for the liquid permeation. Also they found that when the mass loss exceeds 1%, there was a rapid decrease in bond strength (Figure 2.23). In addition to that, the corroded bars undergo less slip until the mass loss reaches approximately 2.0%, after this mass loss, the stiffness reduces consistently (Fig. 2.24).

An experimental work carried out by Rodriguez *et al.* (1997) under the Brite/Euram Project on corroded reinforced beams by means of adding calcium chloride to the mixing water and applying constant current density of about 100 $\mu A/cm^2$, concluded the following:

- Corrosion of reinforcement affects the performance of concrete beams, increasing the deflection and the crack width at the service load, and reducing the strength at the ultimate load.
- Corrosion of reinforcement modifies the type of failure in the concrete beams, whereas sound beams of the same ratio of reinforcement failed by bending, the corroded beams failed by shear bond failure in most of the cases (Figure 2.25)
- Pitting at the reinforcing steel has shown the most relevant damage in the beams with significant reduction in their load carrying capacity.

Hassan (2003) studied the effect bond of reinforcement in concrete with different types of mixtures and corroded bars, and he found the regular carbon steel bars showed higher

bond strength than the stainless steel bars for all concrete types. He also found that the effect of accelerated corrosion on the regular carbon steel bars was less than that on the stainless steel bars at the same corrosion stage. In terms of supplementary cementing materials he found that the use of theses materials in concrete decreases the cracks number due to corrosion.

Clark (1949) tested deformed bars in both beams and pull-out specimens, considering the bar size, bar's rib deformation pattern, concrete strength and development length as test variables. The objective was to determine the correlation between bond strength values obtained from beam and pull-out specimens for each of the above mentioned parameters. The author pointed out that the correlation between the results of the beam and pullout specimens is strong enough to give reliable estimates of the bonding efficiency of deformed reinforcing bars, and added that both the load-bond slip relations and the general behavior of the bars were similar in the two types of tests.

Mathey *et al.* (1961) investigated the bond strength of high yield strength deformed bars in beam and pull-out specimens by varying the bar diameter, and anchorage length. The authors adopted a new bond failure criterion in which he defined bond failure as a failure accompanied by excessive slip at the free end of the bar with only a slight increase in the bar force. The critical bond stress was defined to be the lesser of the bond stresses corresponding to either a free-end slip of 0.002 in. or loaded-end slip of 0.01 in.

Ferguson and Thompson (1965) focused on the development length of large sized, #11, high strength bars, $f_y > 75$ ksi. The concrete cover, beam width, stirrup ratio, and depth of concrete cast below the bar were the main variables. It was found that increasing concrete clear cover surrounding the bar generally increases ultimate bond strength with a rate of 60 psi/in of cover, but it did not improve the observed crack width on the surface under service loads. Also the beam width and shear were reported as factors affecting bond strength and that any further increase in development lengths more than 50 in will no longer cause decrease in bond strength.

Ingraffea *et al.* (1984) reported that, in general, there are four different sources that contribute to bond slip namely elastic deformation, crushing of concrete at points where concrete bears on steel ribs, secondary radial cracking, and longitudinal splitting cracking.

2.2.10 Descriptive Expressions for Bond

A number of expressions that predicts the bond strength based on the regression analysis of experimental result are presented. All the equations are based on bottom-cast bars results.

Orangun, Jirsa, and Breen (OJB) (1975, 1977) used the statistical analysis technique, to develop their equations. They developed two expressions; one to describe the bond strength of bars with confining transverse reinforcement and the other expression to describe the bond strength for those beams without transverse reinforcement. The database used included 62 beams, 57 of them were bottom cast bars, and five were either side or top cast bars. According to OJB (1977), for bars not confined with transverse reinforcement, the total bond force is given by:

$$\frac{L_d}{d_b} = \frac{(f_y/(f'_c)^{1/2}) - 200}{12\,[(C'_{min} + 0.4\,d_b)]} \qquad (2.8)$$

However, for bars confined with transverse reinforcement the total bond force is given by:

$$\frac{L_d}{d_b} = \frac{(f_y/(f'_c)^{1/2}) - 200}{12\,[(C'_{min} + 0.4\,d_b) + (A_{tr}\,f_{yt}/1500\,sn)]} \qquad (2.9)$$

Where, see Figure (2.17);

T_b: the total bond force (lb.)

f_c': concrete compressive strength measured using 6 x 12 in cylinders. (psi)

L_d: development/splice length. (in.)

C'_{min}: minimum of concrete covers surrounding the bar or half the clear spacing between bars, minimum of C_{si} and (C_b or C_{so}) (in.)

d_b: bar diameter. (in.)

A_{tr}: area of each stirrup or tie crossing the potential plane of splitting. (in.2)

s: spacing of transverse reinforcement. (in.)

n: number of bars being developed or spliced.

f_y: specified yield strength of the tested bar. (psi)

f_{yt}: yield strength of the transverse reinforcement. (psi)

Equations (2.8) and (2.9) are limited to cases in which splitting failure, rather than pullout failure governs. So the application, of the above two equations, is restrained by the following condition:

$$1/d_b \ [(C'_{min} + 0.4\, d_b) + (A_{tr}\, f_{yt} / 1500\, sn)] \leq 2.5 \qquad (2.10)$$

Darwin *et al.* (1992) reanalyzed the data used by Orangun *et al.* (1975, 1977) and including the effect of the relative value of C'_{max} and C'_{min}, Darwin *et al.* (1992) establish their expression for bars not confined with transverse reinforcement as given below.

$$\frac{L_d}{d_b} = \frac{(f_y/(f'_c)^{1/2}) - 300}{\dfrac{0.1177\,(C'_{min} + 0.5\, d_b)\,[0.08\,(C'_{max}/C'_{min}) + 0.92]}{d_b}} \qquad (2.11)$$

Where, see Figure (2.17a);

C'_{min}: minimum of concrete covers (bottom and side) surrounding the bar and half the clear spacing between bars, minimum of (C_b or C_{so}) and C_{si}, (in).

C'_{max}: maximum of concrete covers (bottom and side) surrounding the bar and half the clear spacing between bars, minimum of (C_b or C_{so}) and C_{si}, (in).

Darwin *et al.* (1996) used a large database including 133 splice and development length specimens with bars not confined by transverse reinforcement and 166 specimens with bars confined by transverse reinforcement. All the specimens were bottom cast bars. They concluded that $fc'^{1/4}$ provides a more accurate representation of the concrete strength on development and splice strength than the currently used $fc'^{1/2}$. They also integrated the effect of the relative rib area R_r in their expression because they observed that this factor has a significant effect on the bond strength of bars confined by transverse reinforcement. Based on their analytical study the best fit equation that can predict the development length for bars without transverse reinforcement confinement is:

$$\frac{L_d}{d_b} = \frac{(f_y/(f'_c)^{1/4}) - 2130\,[\,0.1\,(C'_{max}/C'_{min}) + 0.9]}{\dfrac{80.21\,(C'_{min} + 0.5\,d_b)\,[0.1\,(C'_{max}/C'_{min}) + 0.92\,]}{d_b}} \qquad (2.12)$$

And, for bars confined by transverse reinforcement, the following equation was obtained:

$$\frac{L_d}{d_b} = \frac{(f_y/(f'_c)^{1/4}) - 2130\,[\,0.1\,(C'_{max}/C'_{min}) + 0.9] - (66/A_b)}{\dfrac{80.21\,(C'_{min} + 0.5\,d_b)\,[0.1\,(C'_{max}/C'_{min}) + 0.92\,] + (35.33\,t_y\,t_d\,A_{tr})/sn}{d_b}} \qquad (2.13)$$

Where; C_{max}: maximum of (C_b, C_s)

C_b: clear bottom cover.

C_s: minimum of (C_{so}, C_{si} +0.25 in)

C_{so}: clear side cover.

C_{si}: half the clear spacing between bars.

C_{min}: the minimum of (Cb, Cs)

$t_r = 9.6\,R_r + 0.28 < 1.72$ and $t_d = 0.72\,d_b + 0.28$

N: total number of stirrups within the development length.

R_r: Relative rib area, is the ratio of the bearing area (projected rib area on a plane normal to the bar axis) to the shearing area (the surface area of the bar between 2 adjacent ribs), the shaded area in Figure (2.24b).

To ensure that the splitting mode of failure will govern, the above equation is applicable only if the following condition is met:

$$l/d_b \left[(C'_{min} + 0.5\,d_b)\,[\,0.1\,(C'_{max}/C'_{min}) + 0.9] + (35.3\,t_y\,t_d\,A_{tr})/sn\,\right] \leq 4.0 \qquad (2.14)$$

Zuo and Darwin (1998, 2000), expanded the work of Darwin et al. (1996b) by increasing the data base specially specimens made with high strength concrete (f_c' > 8000 psi). The data base they used reached 171 specimens containing bars confined by transverse reinforcement and 196 specimens containing bars confined by transverse reinforcement. All bars were bottom cast. Their results supported the early observation made by Darwin et al. that $f_c'^{1/4}$ accurately represent the contribution of concrete compressive strength to bond strength for bars not confined by transverse reinforcement. They also observed that $f_c'^{p}$ with p between ¾ and 1.0 best represent the effect of concrete strength on the contribution of confining of transverse reinforcement to bond strength. They selected p = 3/4 for their equation. For bars not confined by transverse reinforcement, the descriptive equation is:

$$\frac{L_d}{d_b} = \frac{(f_y/(f'_c)^{1/4}) - 2350\,[\,0.1\,(C'_{max}/C'_{min}) + 0.9]}{\dfrac{76.3\,(C'_{min} + 0.5\,d_b)\,[0.1\,(C'_{max}/C'_{min}) + 0.92\,]}{d_b}} \qquad (2.15)$$

However, for bars confined by transverse reinforcement, the descriptive equation is

$$\frac{L_d}{d_b} = \frac{(f_y/(f'_c)^{1/4}) - 2350\,[\,0.1\,(C'_{max}/C'_{min}) + 0.9]}{\dfrac{76.3\,(C'_{min} + 0.5\,d_b)\,[0.1\,(C'_{max}/C'_{min}) + 0.92\,] + (0.52\,t_y\,t_d\,A_{tr}/sn)\,(f'_c)^{1/2}}{d_b}} \qquad (2.16)$$

Where;

$t_r = 9.6\,R_r + 0.28 < 1.72$ and $t_d = 0.78\,d_b + 0.22$

To limit the applicability of the above two equations to cases in which a splitting failure governs:

$$1/d_b \left[(C'_{min} + 0.5\,d_b)\,[\,0.1\,(C'_{max}/C'_{min}) + 0.9] + (0.52\,t_y\,t_d\,A_{tr}/sn)\,(f'_c)^{1/2}\right] \leq 4.0 \qquad (2.17)$$

The ACI committee 408 database 10-2000 adopted and updated the expressions developed by Zuo and Darwin (1998, 2000), Equation (2.16) and (2.17), with minor numerical changes and rounding figures, to become the following two equations:

$$\frac{L_d}{d_b} = \frac{(f_y/(f'_c)^{1/4}) - 2400\,[\,0.1\,(C'_{max}/C'_{min}) + 0.9]}{\dfrac{76.3\,(C'_{min} + 0.5\,d_b)\,[0.1\,(C'_{max}/C'_{min}) + 0.92\,]}{d_b}} \qquad (2.18)$$

$$\frac{L_d}{d_b} = \frac{(f_y/(f'_c)^{1/4}) - 2400\,[\,0.1\,(C'_{max}/C'_{min}) + 0.9]}{\dfrac{76.3\,(C'_{min} + 0.5\,d_b)\,[0.1\,(C'_{max}/C'_{min}) + 0.92\,] + (0.52\,t_y\,t_d\,A_{tr}/sn)\,(f'_c)^{1/2}}{d_b}} \qquad (2.19)$$

Where: $t_r = 9.6\,R_r + 0.28 < 1.72$ and $t_d = 0.78\,d_b + 0.22$

The same restriction that applies to Zuo and Darwin (2000) expression applies to the ACI 408 committee equation:

$$1/d_b \left[(C'_{min} + 0.5\,d_b)\,[\,0.1\,(C'_{max}/C'_{min}) + 0.9] + (0.52\,t_y\,t_d\,A_{tr}/sn)\,(f'_c)^{1/2}\right] \leq 4.0 \qquad (2.20)$$

2.2.11 Design Expressions for Bond

The ACI 318 – 02, chapter 12, adopted the OJB equations for both cases of with and without transverse reinforcement confinement. The code used the same expressions for L_d/d_b but substituted f_y for f_s and incorporated four parameters namely; α, β, λ, and γ to account for the effect of bar location, epoxy coating, lightweight aggregate concrete, and reinforcement size factor respectively,. They also neglected the 200 number in the numerator of the OJB equation and multiplied the 1/12 constant by 0.9 to obtain 3/40 constant, and introduced the following expression:

$$\frac{L_d}{d_b} = \frac{3\,f_y\,\alpha\,\beta\,\lambda\,\gamma}{40(f'_c)^{1/2})(c+K_{tr})/\,d_b} \qquad (2.21)$$

Where: L_d: Development Length, (in).

d_b: Bar Diameter, (in).

f_y: Bar yield Strength, (psi).

α: reinforcement location factor; (top cast or bottom cast)

β: Coating factor (coated or uncoated bars)

λ: Light weight aggregate factor

γ: Reinforcement size factor (=0.8 for # 6 bars and smaller, and = 1 for otherwise)

f_c': Concrete compressive strength measured using 6 x 12 in cylinders, (psi).

$$K_{tr} = \frac{A_{tr}\,f_{yt}}{1500\,sn}$$

C'_{min}: minimum of concrete covers (bottom and side) surrounding the bar and half the clear spacing between bars, minimum of (C_b or C_{so}) and C_{si}. (in.).

A_{tr}: area of each stirrup or tie crossing the potential plane of splitting, (in^2).

f_{yt}: yield strength of the transverse reinforcement, (psi).

s: spacing of transverse reinforcement, (in).

n: number of bars being developed or spliced.

$$c = C'_{min} + 0.5\, d_b$$

To reduce the probability of pullout failure, the following requirement was imposed by the ACI-318-02

$$1/d_b \left[(C'_{min} + 0.5\, d_b) + \frac{A_{tr}\, f_{yt}}{1500\, sn} \right] \leq 2.5 \qquad (2.22)$$

The ACI committee 408 designed an expression from empirical equations involving the incorporation of a strength reduction factor, Φ, to ensure a realistic low probability of failure. The Φ factor for bond depends on the Φ factor for tensions and the load factors for dead and live loads. Based on a Monte Carlo analysis, Φ for bond is 0.82, in case the tension Φ factor is 0.90, the dead load factor is 1.2, and the live load factor is 1.6. For a tension Φ factor of 0.90, a dead load factor is 1.4, and a live load factor is 1.7 the Φ factor for bond will be 0.92. Based on that, the ACI committee 408 developed two expressions; one with the bond Φ factor of 0.82 and the other with Φ factor equals 0.92.

The 0.92 Φ factor was multiplied by the f_c' term in Equation (2.19), and the effect of the bar location during casting, presence of epoxy coating, and lightweight aggregate are considered in the design expression through multiplying the equation by α, β, and λ. After rounding the numbers the following formula was obtained:

$$\frac{L_d}{d_b} = \frac{(f_y/(f'_c)^{1/4}) - 2200\,[\,0.1\,(C'_{max}/C'_{min}) + 0.9]}{\dfrac{70\left[(C'_{min} + 0.5\,d_b)\,[0.1\,(C'_{max}/C'_{min}) + 0.92\,] + (0.52\,t_y\,t_d\,A_{tr}/sn)\right]}{d_b}} \qquad (2.23)$$

When the 0.82 Φ factor was multiplied by the f_c' term in equation (2.19), the following formula was obtained:

$$\frac{L_d}{d_b} = \frac{(f_y/(f'_c)^{1/4}) - 1970\,[\,0.1\,(C'_{max}/C'_{min}) + 0.9]}{\dfrac{62\left[(C'_{min} + 0.5\,d_b)\,[0.1\,(C'_{max}/C'_{min}) + 0.92\,] + (0.52\,t_y\,t_d\,A_{tr}/sn)\right]}{d_b}} \qquad (2.24)$$

A comparison was conducted by the ACI committee 408, and reported in the ACI committee 408 report in October 2001, between the predicted values for bond capacity (T_b) from the five descriptive equations for bars not confined by transverse reinforcement, [Equations (2.8), (2.11), (2.12), (2.15), and (2.18)] and the test results from ACI 408 database 10-2001. This database included 635 development and splice tests of uncoated reinforcing bars, and was limited to normal weight concrete specimens. The concrete compressive strengths for the test results included in the data base were obtained by testing concrete cylinders rather than cubes. The tests included in the data base could be classified according to the bar placement, 478 tests for bottom-cast, 111 tests for top-cast, and 46 tests for side-cast. The results of this comparison are shown in Table (2.1). Table (2.1) shows that for bars not confined by transverse reinforcement the average test/predicted ratio are within 3 percent. OJB equation shows the highest extremes between maximum and minimum test/predicted values, while the ACI 408 equation shows the smallest difference between them. The minimum scatter is exhibited by the expression obtained by Zuo and Darwin (2000) and ACI committee 408, as they give a coefficient of variation of 0.111. On the other hand, the highest value for the coefficient of variation, 0.202, was obtained from the test/predicted ratio comparisons made with the OJB equations. Figure (2.27) shows the relationship between the

test/predict ratio and the concrete compressive strength for the five different descriptive equations. It is clear that OJB (1977) and Darwin *et al.* (1992) equations, which consider the effect of concrete strength as $(f_c')^{1/2}$, exhibit a remarkable decrease in test/predict ratio as the compressive strength increases. The reason for this trend is that these two equations were formulated based on test results that included a narrow range of compressive strengths. On the other hand, the other three expressions, which considered the impact of concrete strength as $fc'^{1/4}$, demonstrate significantly less variation in the test/predict ratio, with a very slight increase in the ratio as the concrete strength increases from 3000 to 16000 psi. Another comparison was made, but this time for bars confined by transverse reinforcement using the four equations, [(2.9), (2.13), (2.16), and (2.19)], and the results are provided in Table (2.2). The average test/predicted ratios ranged from 1.074 for OJB (1977) to a low of 0.989 for Zuo and Darwin (2000). The best overall match was obtained by ACI 408 expression with an average test/predict ratio of 1.00 and a coefficient of variation of 0.12. In Figure (2.28), it is obvious that the test/predict ratio for the equations developed by Zuo and Darwin (2000) and ACI 408 committee are remarkably insensitive to the variation compressive strength. Because these two expressions consider the contribution of the concrete as a function of $fc'^{1/4}$ and the contribution of the transverse reinforcement as function of $fc^{3/4}$. However for the other two expressions, the contribution of the concrete and the contribution of the transverse reinforcement are treated differently. In OJB (1977) equation, the contribution for both concrete and transverse reinforcement is considered to be influenced by the concrete compressive strength as function of $(fc')^{1/2}$, while in Darwin *et al.* (1996) this contribution, for both concrete and transverse reinforcement, is considered to be function in $fc'^{1/4}$. That is why the OJB equation shows a high test/predict ratios for low strength concrete, and low test/predicted ratios for higher strength concrete as shown in Figure (2.28). In the contrast Darwin *et al.* (1996) expression, provides low ratios for lower strength concrete and high test/predict ratios as the strength increases.

Tables (2.3) and (2.4) provides another comparison done by the ACI committee 408 between the test/predict ratios for the different design expressions shown in equations, [(2.21), (2.23), and (2.24)]. The comparison reflects that the test/predict ratios for the

ACI 318-02 equation shows higher scatter than those for ACI 408. The test/predict ratio ranged from 0.704 to 2.192 for the bars confined with transverse reinforcement. Overall, the ACI 318-02 provides a higher average test/predict ratios and higher coefficients of variation than do the equations of the ACI committee 408. That implies that the ACI 318-02 requires longer development length than ACI 408. The ACI 408 equation, equation (2.24), that was based on load factors and strength reduction factors presented in chapter 9 of ACI 318-02 provides average test/predict ratios that are slightly higher than those given by the ACI 318-02.

2.2.12 Pullout – Slip Response

In design practice, the average bond resistance u is usually calculated assuming that it is uniformly distributed along the embedded bar length using the maximum bond stress. However, the bond stresses vary along the embedded length of the bar and knowledge of this distribution is essential. The distribution of the bond stress is dependent on the assumed relationship between the bond stress and slip.

The Comite Euro-International du Beton (CEB) (1991) Model Code equations were developed for the bond stress-slip relationship to describe both the ascending and descending branches as in Figure 2.29. The formulation consists of four parts:

1. $s \leq s_1$	$u = u_m (s/s_1)^a$	$0 \leq a \leq 1$	(2.25)
2. $s_1 < s \leq s_2$	$u = u_m$		(2.26)
3. $s_2 < s \leq s_3$	$u = u_m - (u_m - u_f)[(s - s_2)/(s_3 - s_2)]$		(2.27)
4. $s_3 < s$	$u = u_f = \eta u_f$	$0 \leq \eta \leq 1$	(2.28)

The CEB Model Code states that the ascending branch refers to the stage where the ribs on the reinforcement bear against the mortar matrix characterized by the local crushing and micro-cracking of the concrete. Hence, in the ascending branch; the bond stress increases according to a non linear function up to the point where s is equal to s_1 (Equation 2.25). The horizontal line between s_1 and s_2 refers to the advanced concrete crushing and shearing off between the ribs and is believed to occur only for the confined

concrete. During this stage, the bond stress is a constant maximum (Equation 2.26). The descending branch refers to the reduction of bond resistance due to the occurrence of splitting cracks along the steel bar (Equation 2.27). In the final stage; the horizontal part represents a residual bond capacity, which is maintained by the presence of transverse reinforcement (Equation 2.28).

Table (2.1) Test /predicted ratios for bars not confined by transverse reinforcement usingdescriptive equations.

	OJB (1975, 1977)*	Darwin *et al* (1992)	Darwin *et al* (1996)	Zuo and Darwin (2000)	ACI 408
Maximum	1.555	1.383	1.342	1.304	1.288
Minimum	0.505	0.528	0.719	0.729	0.724
Average	1.030	1.014	1.020	1.010	1.000
Standard Deviation	0.208	0.189	0.118	0.113	0.111
COV**	0.202	0.187	0.116	0.111	0.111

* Orangun, Jersa and Breen (1975, 1977)

** Coefficient of Variation

Table (2.2) Test /predicted ratios for bars confined by transverse reinforcement usingdescriptive equations.

	OJB (1975, 1977)*	Darwin *et al* (1996)	Zuo and Darwin (2000)	ACI 408
Maximum	1.902	1.479	1.309	1.333
Minimum	0.595	0.776	0.739	0.755
Average	1.074	1.052	0.989	1.002
Standard Deviation	0.255	0.132	0.119	0.121
COV**	0.238	0.125	0.121	0.120

* Orangun, Jersa and Breen [1975, 1977]

** Coefficient of Variation

Table (2.3) Test/predict ratio for bars not confined by transverse reinforcement using design expressions.

For f'c < 1000psi	ACI 318-02	ACI 408 (eq 2.23)	ACI 408 (eq 2.24)
Maximum	1.908	1.401	1.574
Minimum	0.756	0.749	0.843
Average	1.229	1.089	1.224
Standard Deviation	0.229	0.108	0.121
COV**	0.186	0.099	0.099

Table (2.4) Test/predict ratio for bars confined by transverse reinforcement using design expressions.

For f'c < 1000psi	ACI 318-02	ACI 408 (eq 2.23)	ACI 408 (eq 2.24)
Maximum	2.192	1.525	1.715
Minimum	0.704	0.845	0.951
Average	1.237	1.15	1.294
Standard Deviation	0.311	0.155	0.175
COV**	0.251	0.135	0.135

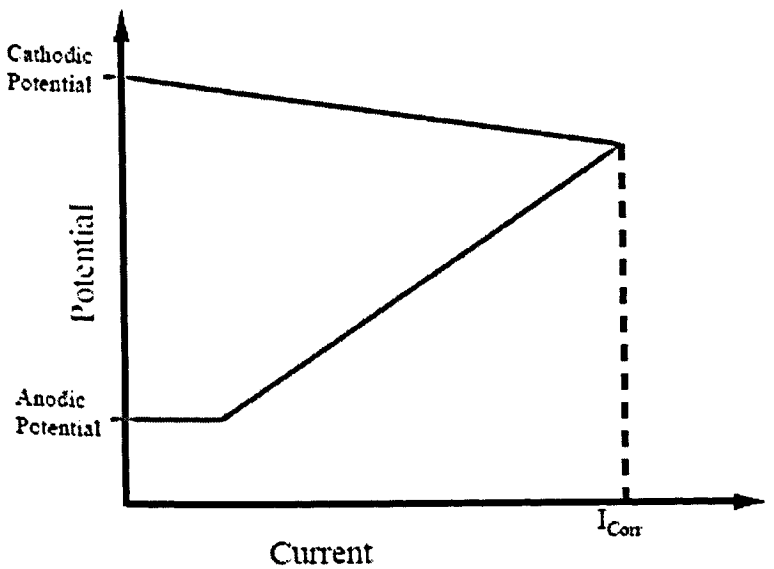

Figure 2.1 Potential vs Current plots for systems under cathodic control, Amleh (2000)

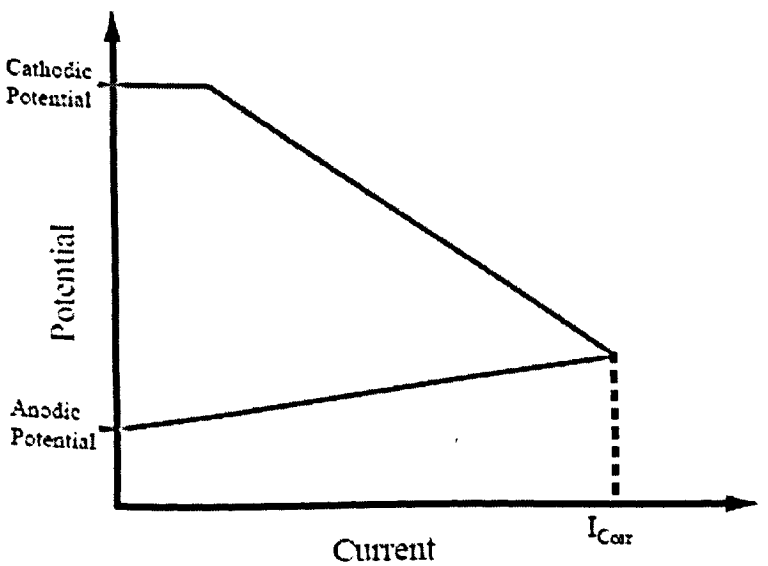

Figure 2.2 Potential vs Current plots for systems under anodic control, Amleh (2000)

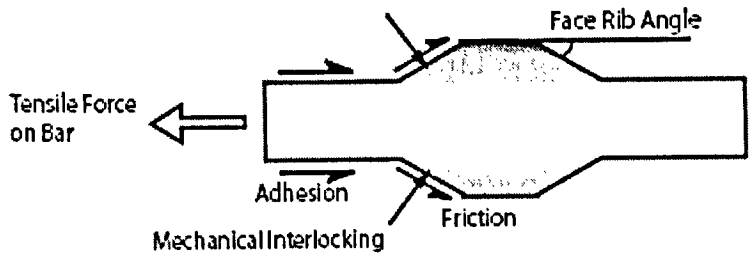

Figure 2.3 – Components of bond strength, Rehm (1961)

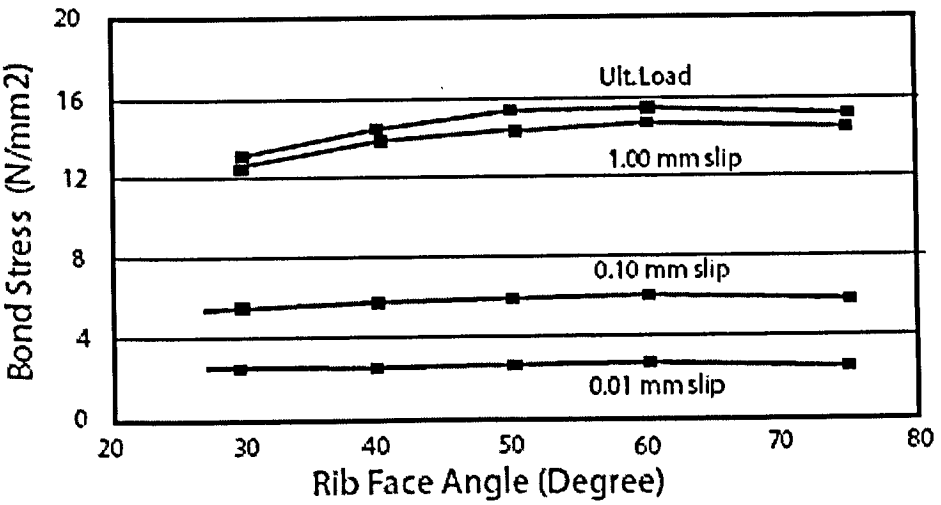

Figure 2.4 Variation in bond stress with rib face angle (Cairns an Abdullah 1994)

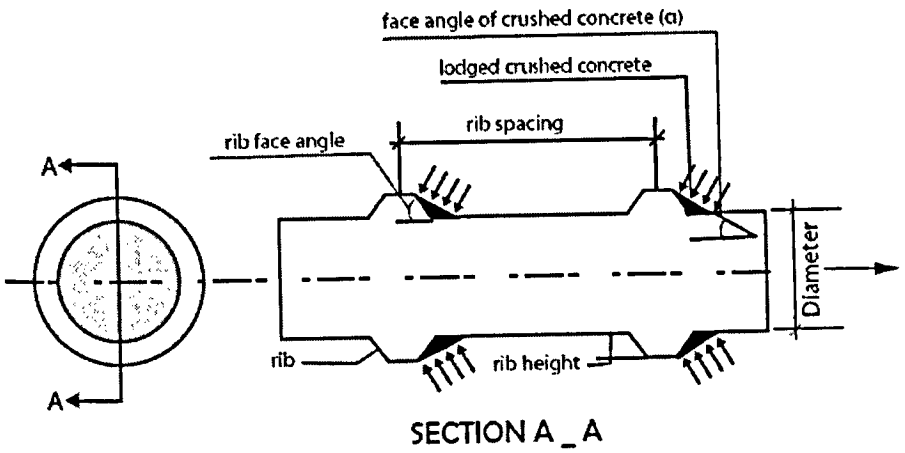

Figure 2.5 Flattened rib face angle by concrete crushing (Tepfers 1979)

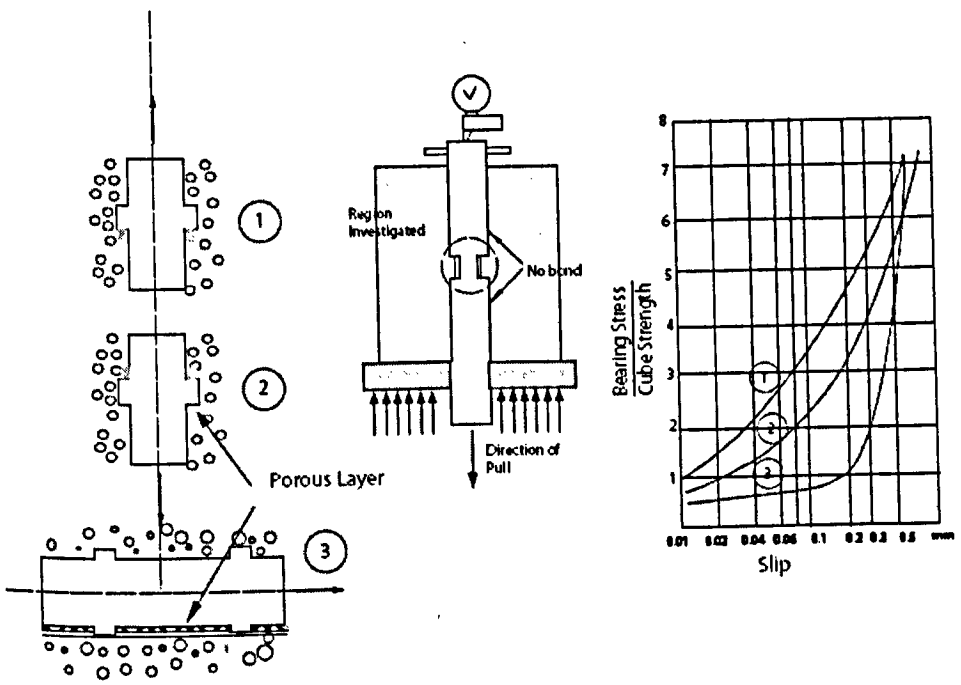

Figure 2.6: The influence of casting position on bond performance (Park and Paulay 1975)

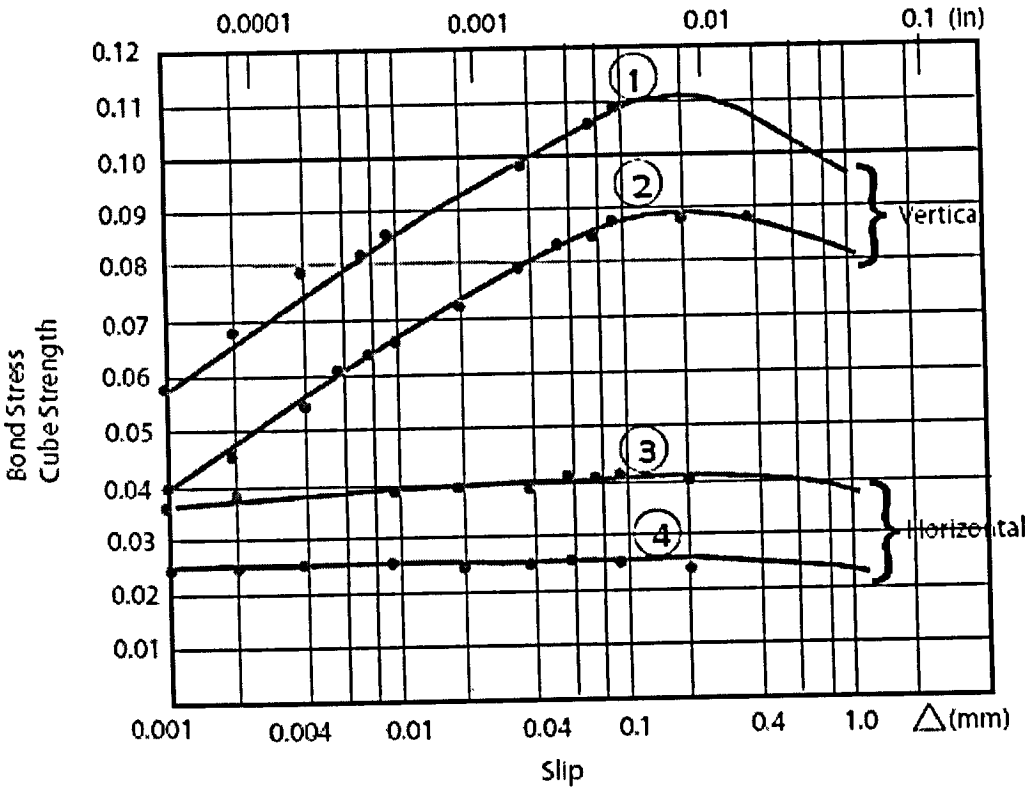

Figure 2.7: The load-slip relationship for No. 5 (16 mm) plain rounded bar in different casting positions (Park and Paulay 1975)

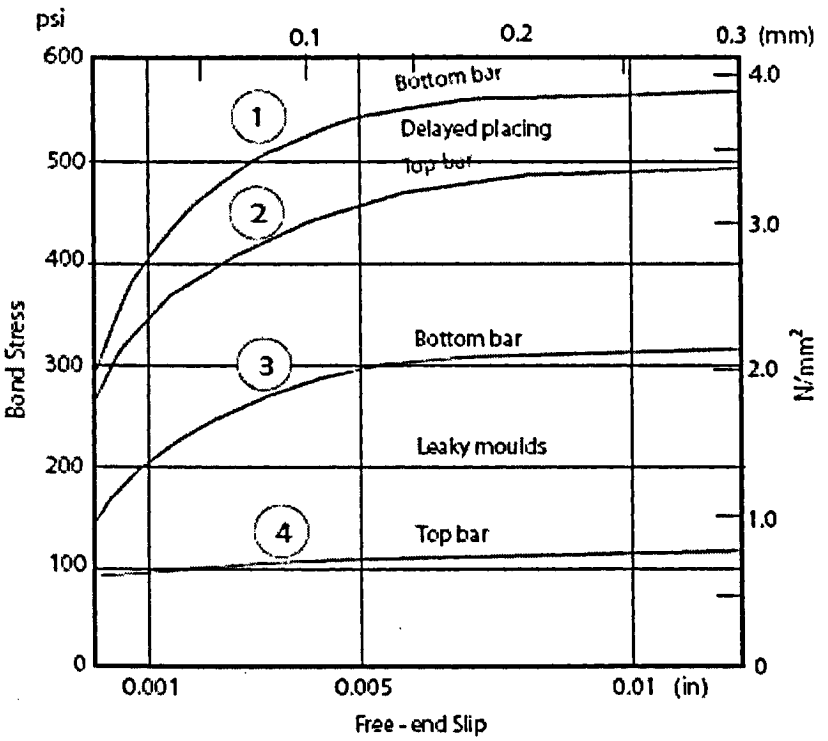

Figure 2.8: Bond stress-slip relationship for plain round bars as affected by settlement of fresh concrete. (Welch and Patten 1967)

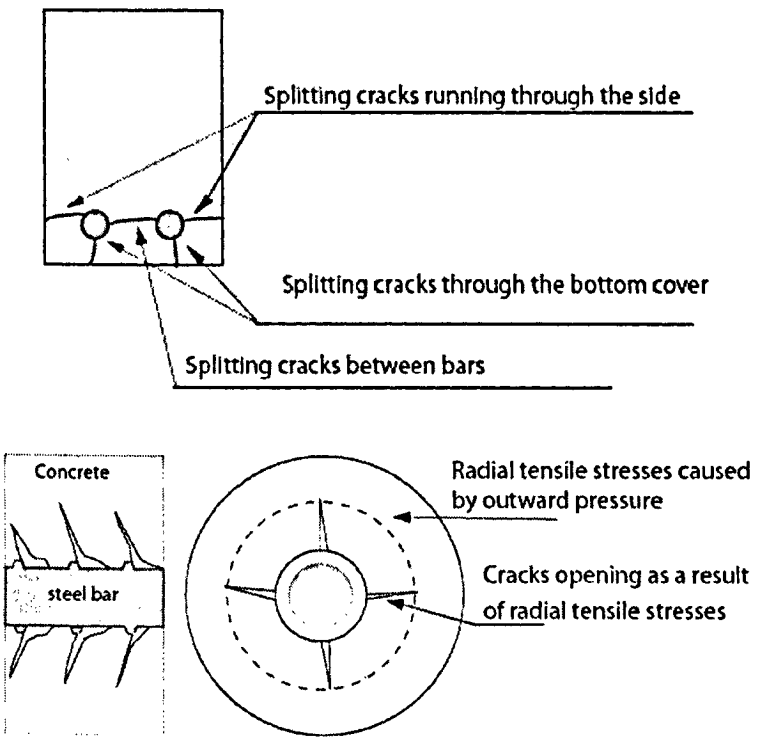

Figure 2.9 Splitting cracks running through concrete covers and between bars.

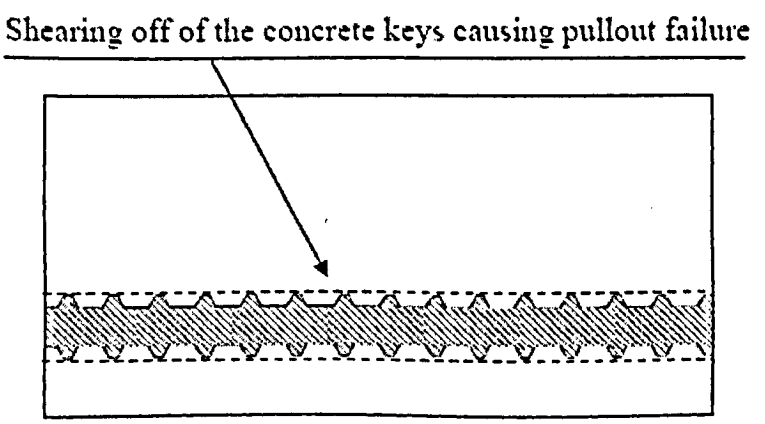

Figure 2.10 Pullout failure associated with shear cracks.

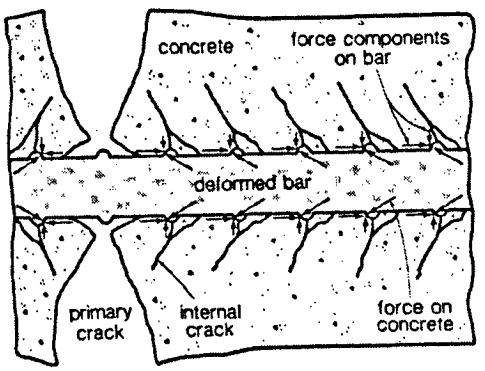

Figure 2.11 Formation of internal cracks (Goto, 1971)

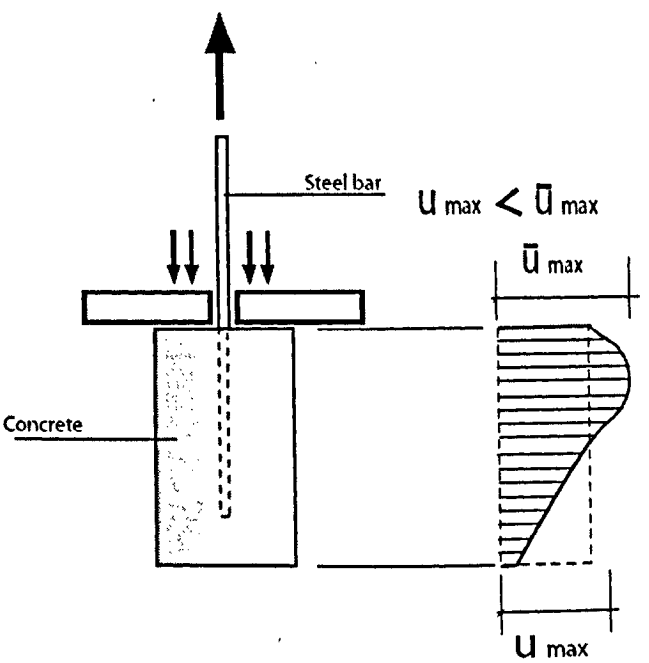

Figure 2.12 Pullout specimen

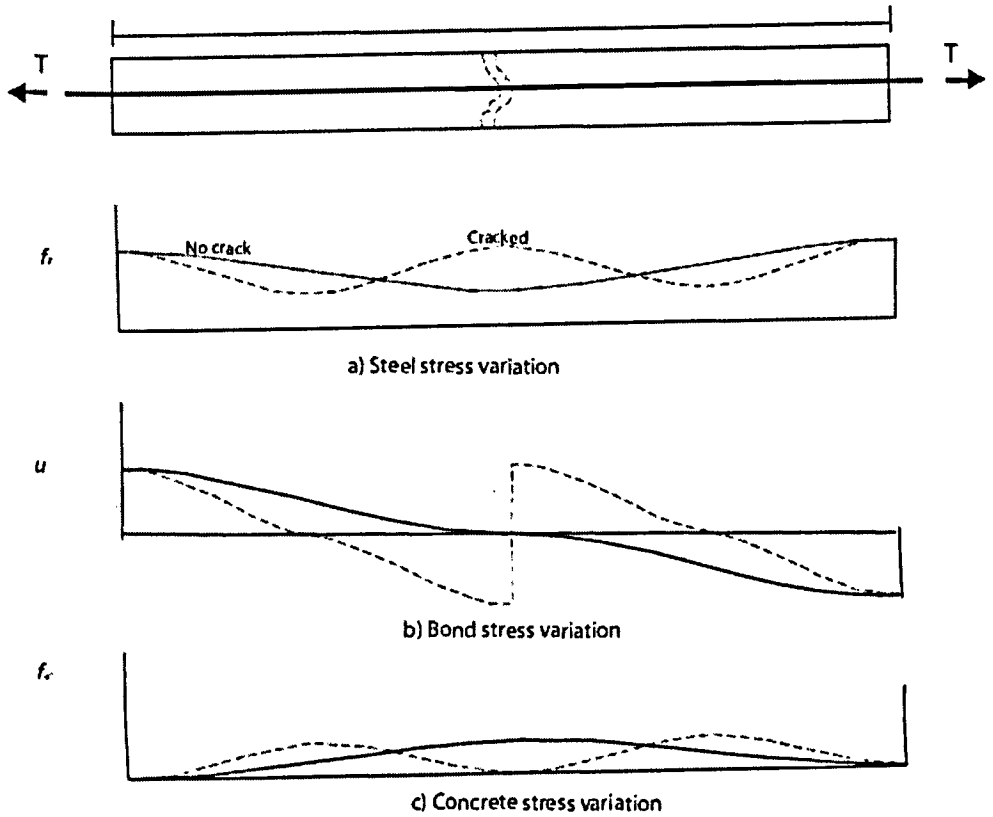

Figure 2.13 Tension specimen, Amleh (2000)

a)

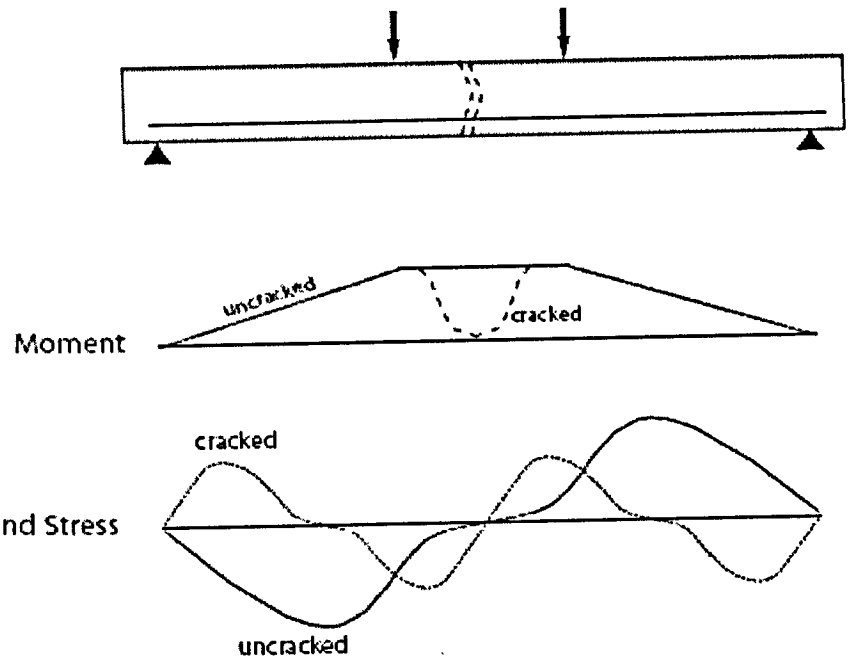

b)

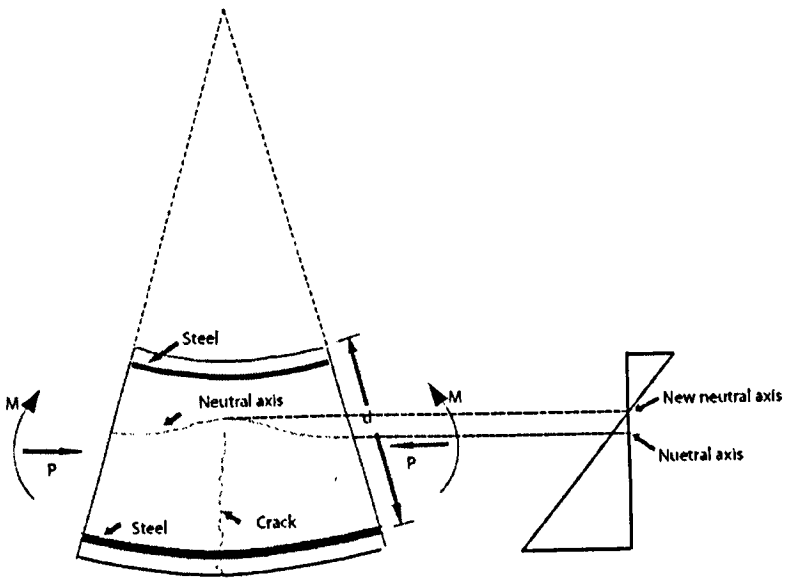

Figure 2.14 Beam loading

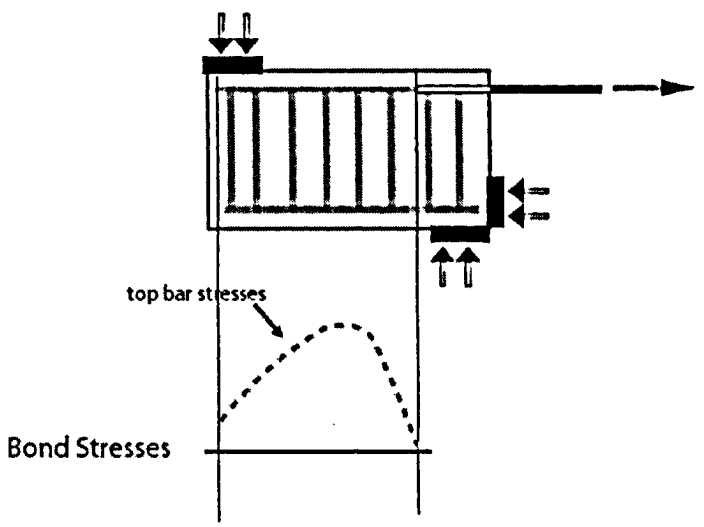

Figure 2.15 End beam specimen

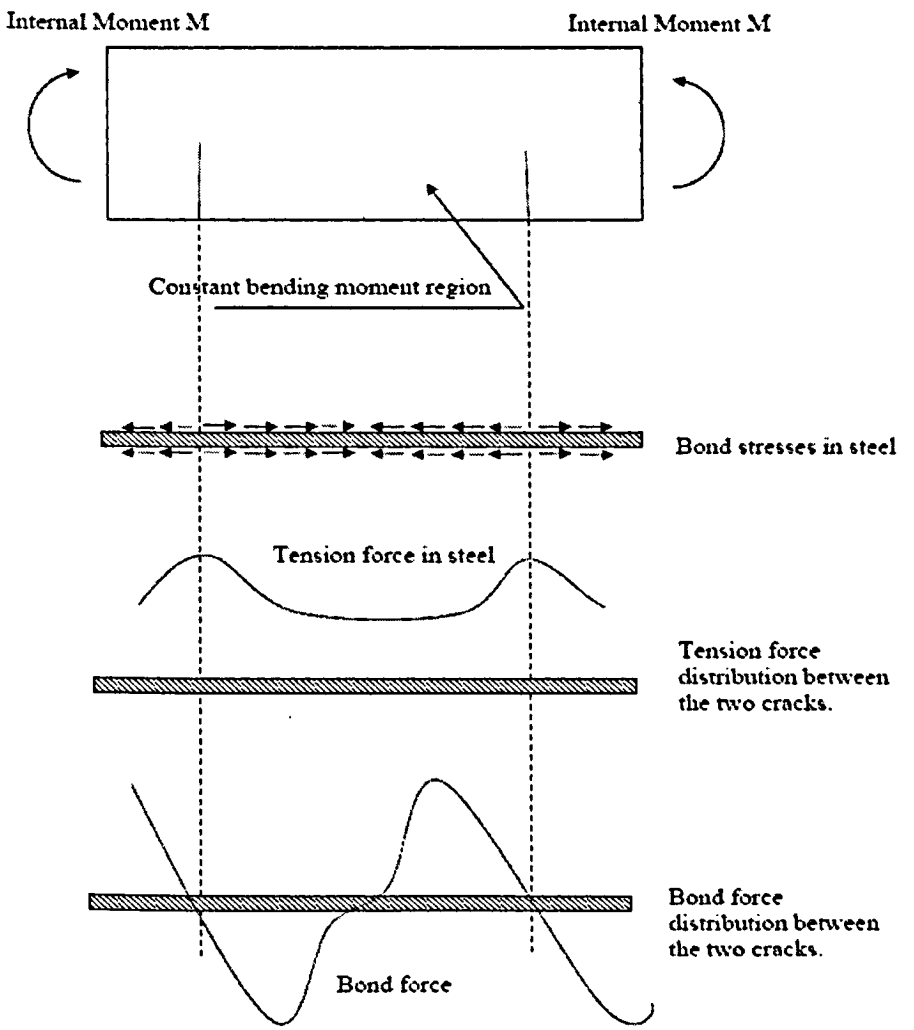

Figure 2.16 Tension and bond force distribution along the bonded length between two cracks; Alagroudi (2003)

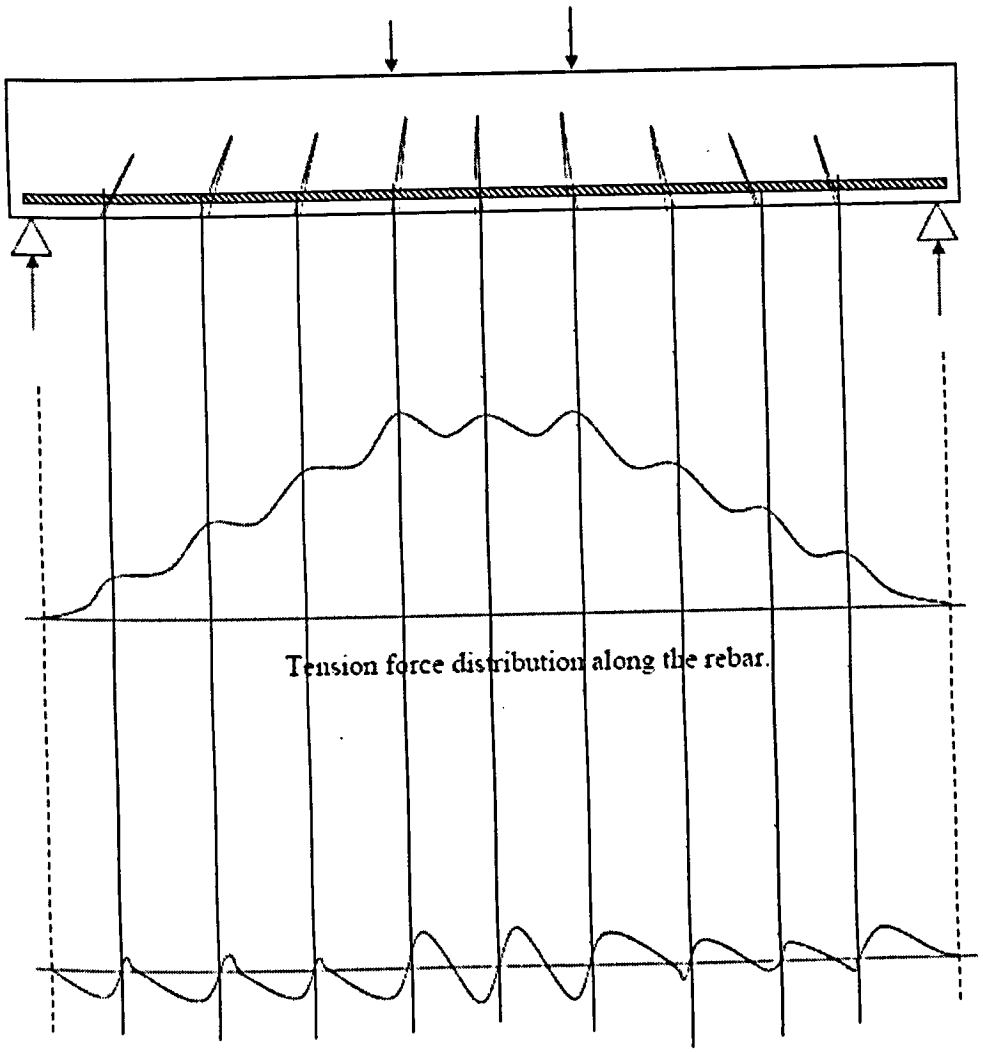

Figure 2.17 Tension and bond force distribution along the bar in the shear span; Alagroudi (2003)

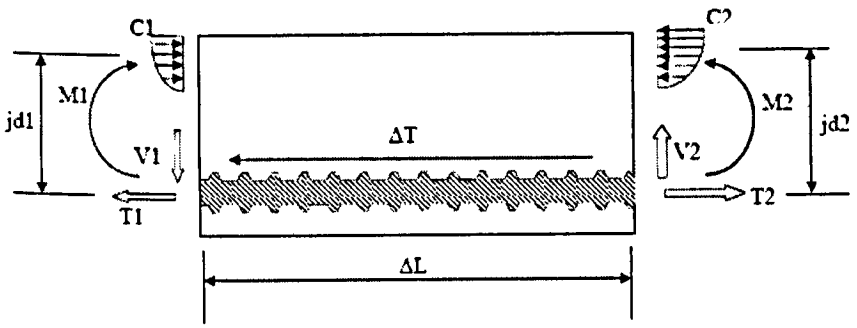

Figure 2.18 Bond Force develops in Flexural Members due to Moment; (Alagroudi 2003)

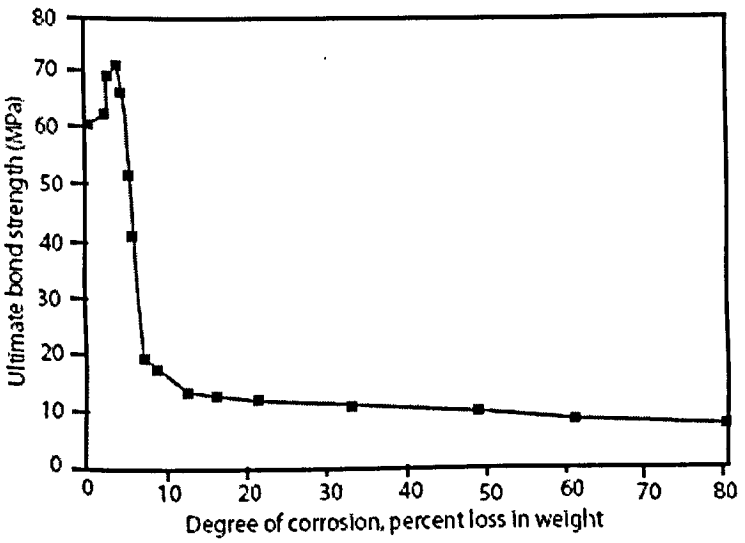

Figure 2.19: Relationship between the ultimate bond strength and different degrees of corrosion; (Almusallam, *et al.* 1995)

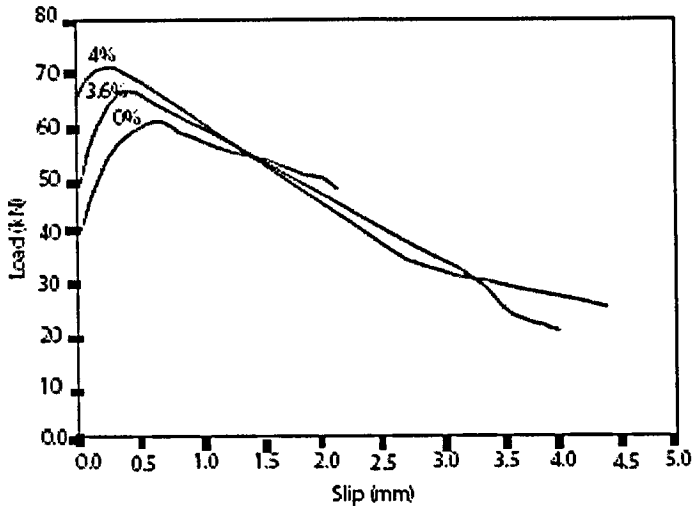

Figure 2.20: Relationship between load and slip for (0 to 6) % of weight loss; (Almusallam, *et al.* 1995)

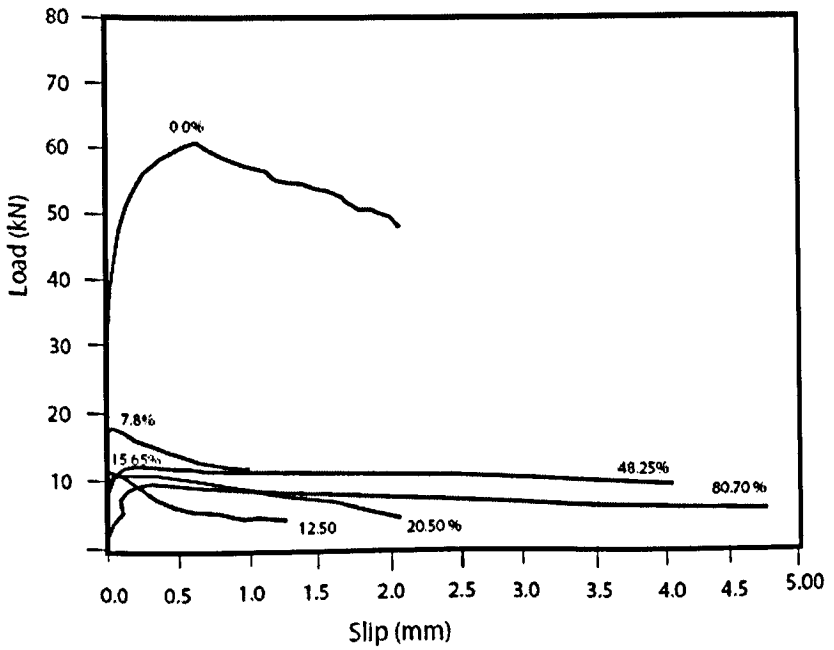

Figure 2.21: Relationship between load and slip at percentage of weight loss higher than 6%; (Almusallam, *et al.* 1995)

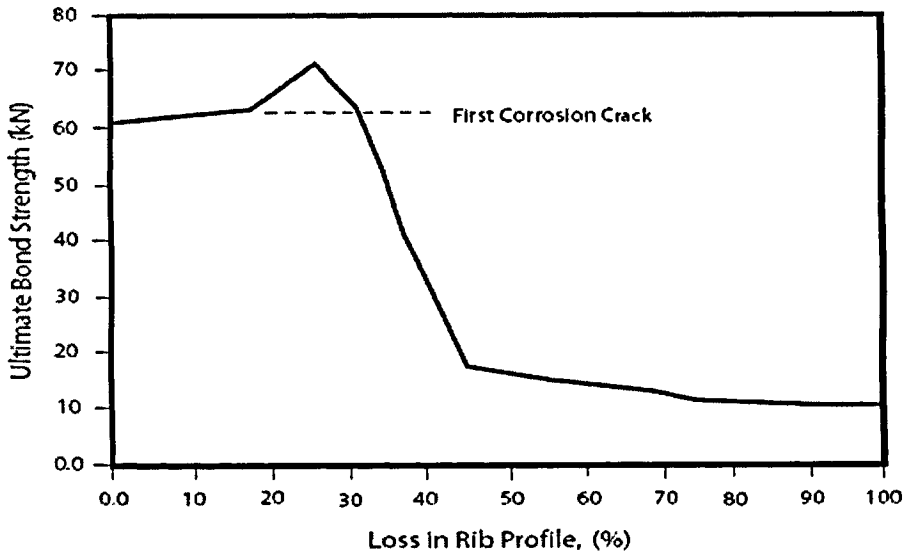

Figure 2.22: Effect of loss of rib profile on ultimate bond strength; (Almusallam, *et al.* 1995)

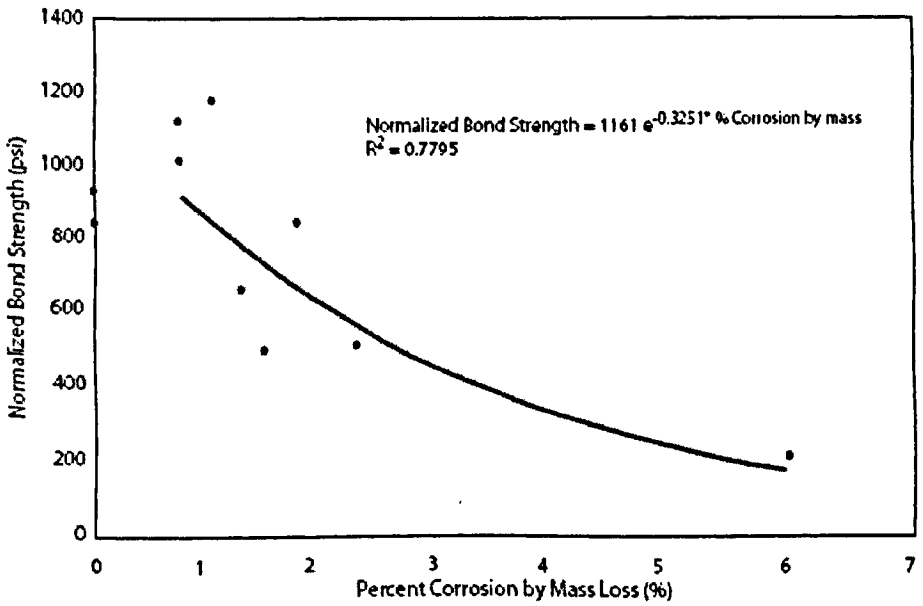

Figure 2.23: Influence of corrosion mass loss on bond strength; (Auyeung *et al*, 2000)

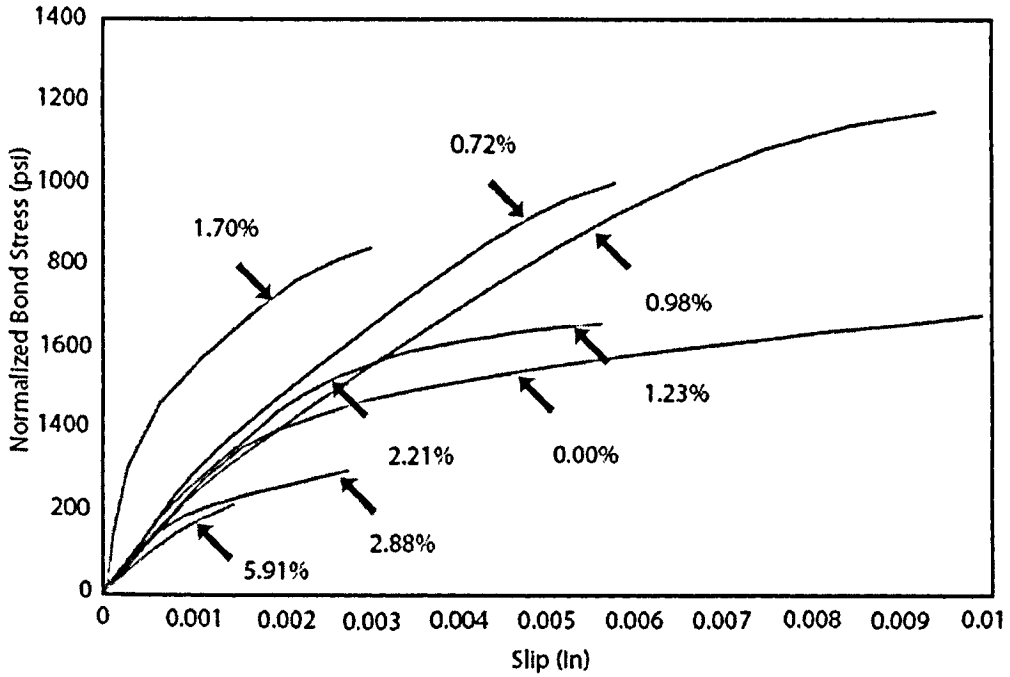

Figure 2.24: Effect of corrosion on load-slip behavior (Auyeung *et al.* 2000)

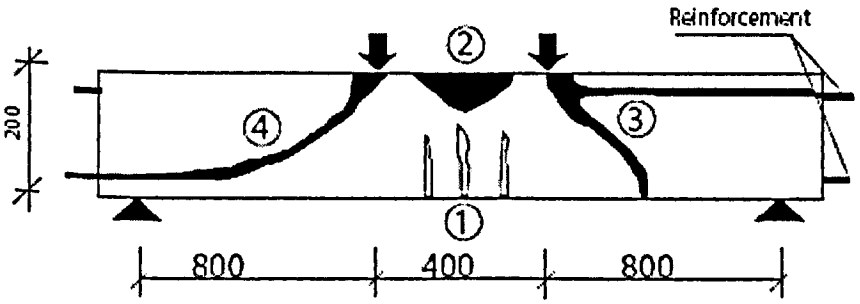

Figure 2.25 Scheme of type of failures in beams with corroded reinforcement. (1) Failure by bending (bottom tensile reinforcement), (2) Failure by crushing of concrete, (3) Failure by shear, (4) Failure by shear combined with anchorage failure of tensile bars; (Rodriguez *et al.* (1997)

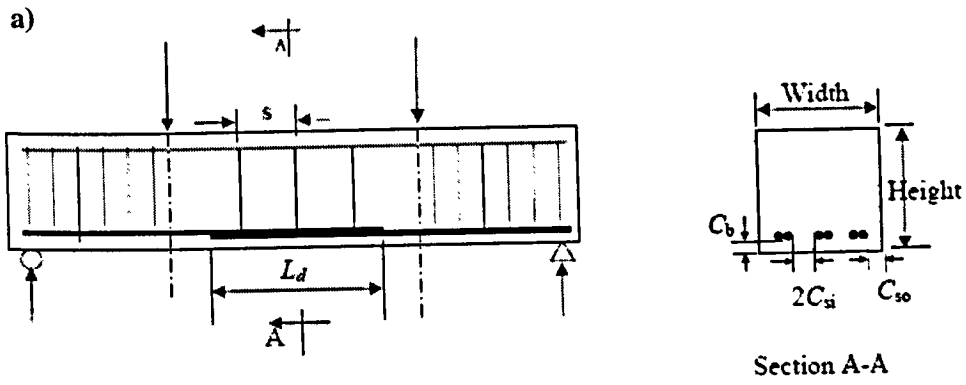

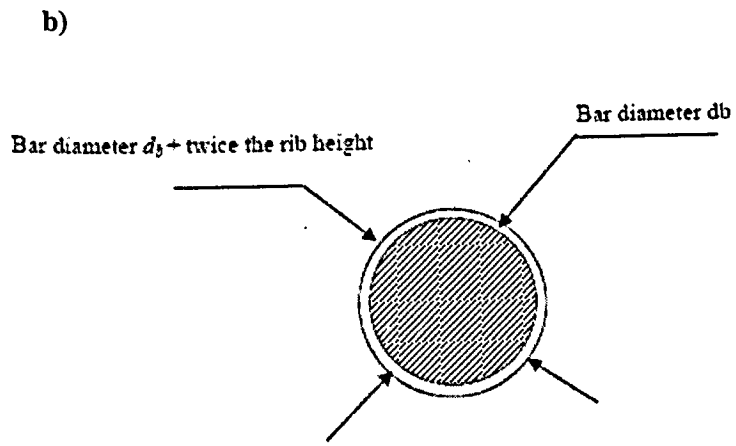

Figure (2.26) Schematic describing the physical meaning of the notations

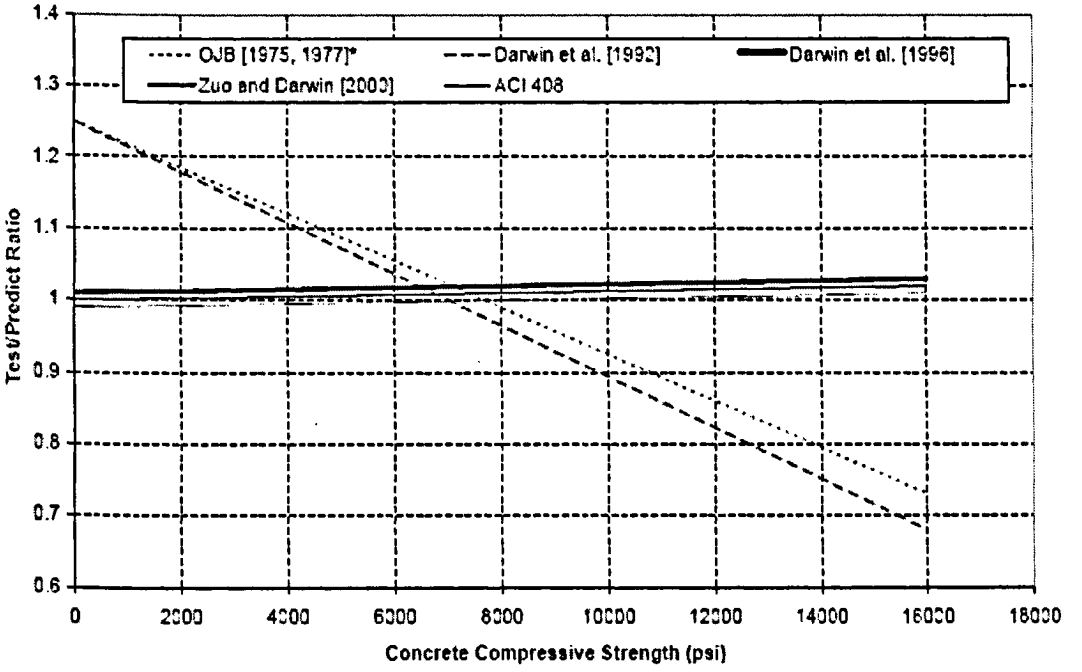

Figure (2.27) Test/Predict Ratio vs. concrete compressive strength for bars not confined with transverse reinforcement

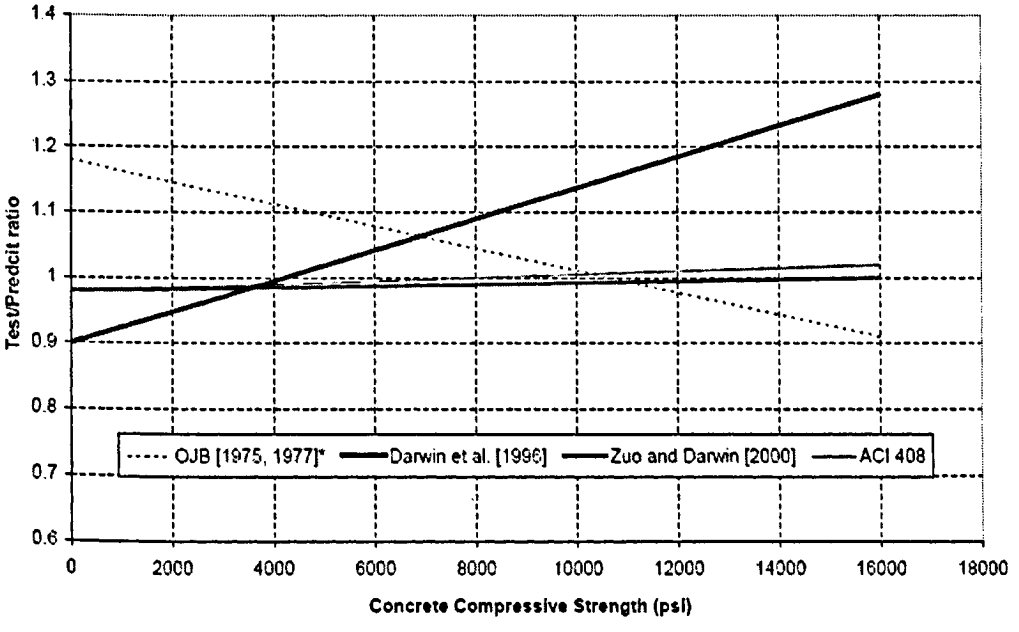

Figure (2.28) Test/Predict ratio vs. concrete compressive strength for bars confined with transverse reinforcement

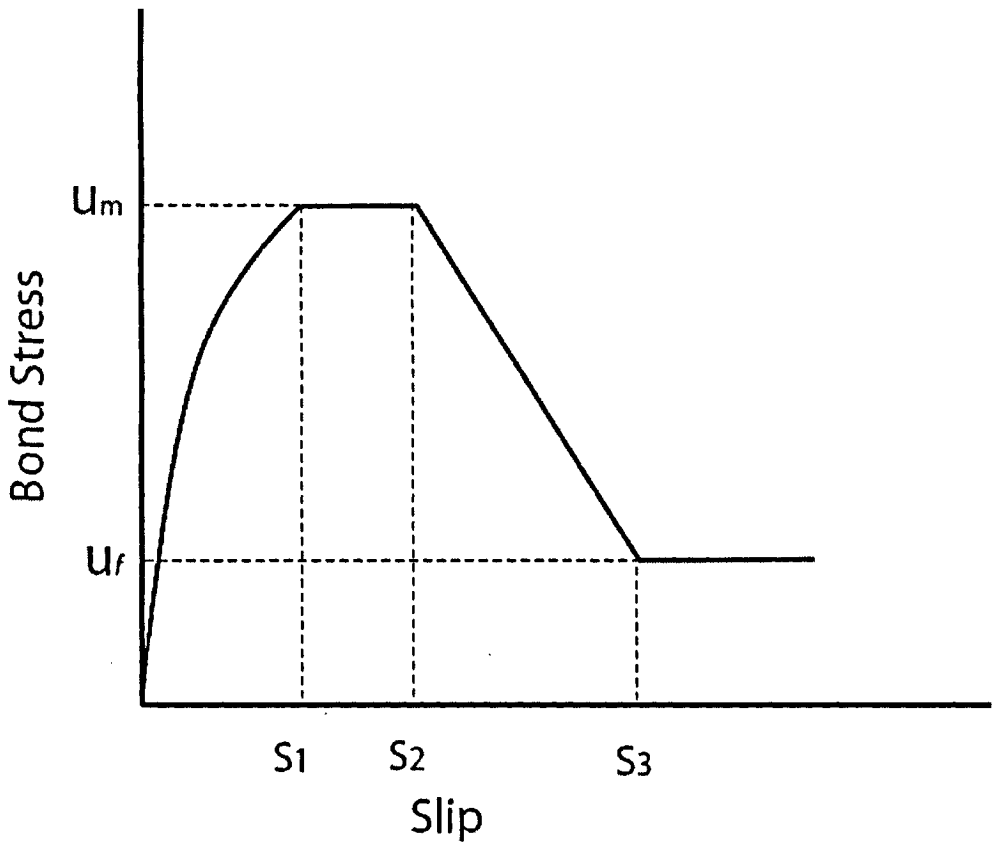

Figure 2.29 CEB bond model (Comite Euro-Internatioal du Beton, 1991)

CHAPTER 3
EXPERIMENTAL PROGRAM

This chapter describes the experimental program, which was designed to investigate the influence of corrosion on the bond behaviour at the reinforcing steel-concrete interface. It also presents the types and properties of the concrete mixtures used. A brief description of the types of the fresh and hardened concrete tests used to evaluate the concrete strength and durability is also presented. In addition, it describes the test program to simulate the prevalent conditions of severe local corrosion environments, which cause significant changes in the surface conditions of the bar and the ribs.

3.1 Experimental Program

The experimental program was designed to study the bond strength degradation for different w/c ratio concretes and concrete cover thicknesses, after subjecting them to several degrees of corrosion.

Two different w/c ratio concretes were used, one with w/c ratio of 0.37 and the second one with w/c ratio of 0.47. Regular carbon steel of a 19.5 mm diameter was used to reinforce 100 mm and 150 mm diameter cylinders.

The specimen nomenclature was derived as follows:

1. The first letter and the followed number indicate the type of concrete mixture used.
2. The number after the hyphen indicates the number of specimen.
3. The last letter indicates the size of the specimen in terms of concrete cover:

   B = 65 mm

   C = 40 mm

For example, the specimen C1-2C, the C1 is a specimen cast with concrete of w/c ratio of 0.37 and 2C refers to second specimen of a cover thickness of 40 mm.

3.2 Material Properties

The two different water cement ratios of concrete are shown in Tables 3.1, 3.2 and 3.3, with two different concrete cover thicknesses over the reinforcing steel bar (40 mm, and 65 mm), normally recommended in steel reinforced concrete structures and are exposed to severe environment. In order to limit the extent of the investigation, some variables were kept constant, such as the steel strength (400 MPa), bar diameter (19.5 mm), and concrete specimen length (200 mm and 300 mm). Four stages of corrosion were pursued in this program. At each stage of corrosion, 2 pullout specimens were tested, a number of 8 pullout specimens for each specific w/c ratio and concrete cover thickness were prepared and a total of 24 pullout specimens to test all corrosion stages of the following mix combinations;

1. w/c ratio of 0.47, and concrete cover of 40 mm.
2. w/c ratio of 0.37, and concrete cover of 40 mm.
3. w/c ratio of 0.47, and concrete cover of 65 mm

For each w/c ratio concrete mixture and each concrete cover, eight 100 x 200mm auxiliary specimens were cast for determining the compressive strength according to the CSA or the ASTM Standard C39 for 30 days and at the time of each corrosion stage, which makes a total number of 24 auxiliary cylinders. In addition, 6 other auxiliary cylinders were cast for determining the splitting tensile strength (2 cylinders for each concrete cover thickness).

3.2.1 Concrete Mix Parameters

The coarse aggregate used was dolomite with a maximum nominal size of 19mm, and the fine aggregate natural sand from Caledon – Bolton, supplied by Franchescini Bros. LTD. The results sieve analysis of the aggregate are shown in Table 3.4.

A poly-naphthalene sulfonic acid based superplasticizer was used for low workability concrete mixtures. It was used to increase the workability of the concrete with a w/c ratio of 0.37. The superplasticizer was manufactured by Euclid Admixture Canada Inc., with commercial name is "Eucon 37", conforming to the ASTM C 494 type F specifications.

The physical and chemical characteristics provided by the manufacturer are shown in Table 3.5.

Normal Portland cement CSA Type GU or ASTM Type 1 from Lafarge was used. Chemical and physical properties are shown in Tables 3.6 and 3.7 respectively.

3.2.2 Reinforcing Steel

The reinforcing steel used in this test program conforms to the CSA, G30.14-M83 (1983) which is equivalent to ASTM, A615-72 (1972). The nominal size of the steel bar is 20M with an actual size of 19.5 mm, with specified normal yield stress of 400 MPa. Each reinforcing steel bar was weighed and its length was measured as shown in Tables 3.1 through 3.3.

3.3 Specimens Preparation

The pullout specimens were prepared in the concrete laboratory of at Ryerson University; the concrete was mixed in electrical rotary mixer for about 6 minutes. Then the fresh properties of concrete i.e. the slump and the air content were measured. Then the concrete was poured in the cylinders in three layers, each layer was compacted with a rod of a diameter of (12.5 mm). Then the pre-weighed 20M reinforcing steel bar was inserted in its center, the embedded length and centricity were maintained by means of a pipe clamp tightened at the desired embedment length and a double wooden cab, as shown in Figure 3.2. The embedded length for the 100 mm diameter cylinders was 160 mm and the protruding length was 490 mm, and for those of 150 mm diameter cylinder, the embedded length was 235 mm and the protruding length was 415 mm. The total length of each bar was around 650 mm, Figure 3.3.

After casting the pullout specimens and auxiliary cylinders they were covered and left for 24 hours in the laboratory, then they were demoulded and the auxiliary cylinders were stored in the humid curing room, while the pullout specimens were soaked in water, for moist curing, to insure the steel is always kept dry. The compressive strength was obtained at an age of 30 days and at the times of pullout tests according to ASTM C39-

86, and the indirect splitting tensile strength was performed at 30 days when the first set of control specimens was tested at an age of 30 days according to ASTM C496-96. Table 3.1 shows the mix proportions and the properties of fresh concrete. The tests are shown in Figure 3.1.

3.4 Accelerated Corrosion

Typically, all conventional corrosion tests require long testing times and are expensive. There are three major types of corrosion tests: laboratory, field, and service testing. Service testing is highest reliable test followed by the field test. However, both tests are time and money consuming. The accelerated corrosion test is more realistic as the lab environment approaches that of the service environment. The accelerated corrosion test provides a qualitative data in a relatively short time on the corrosion behaviour, this data is very useful when the structure is exposed to a severe corrosive environment. It is worth mentioning that in the severe corrosive environment the current density is about 10 $\mu A/cm^2$ Rodriguez, *et al.* (1997).

Testing does not have to correlate exactly to the service environment as long as the corrosion mechanism remains the same. However, the results of accelerated testing should correlate to results from more reliable sources, e.g., service and field testing.

3.4.1 Accelerated Corrosion Experimental Setup

As mentioned earlier, corrosion of the reinforcing steel embedded in concrete occurs by an electrochemical process with the formation of an anode where electrochemical oxidation takes place, and a cathode where electrochemical reduction occurs, and an electrolyte capable of conducting the ionic current.

The pullout specimens were connected by a stainless steel clamp to a copper electrical wire and were set to serve as an anode. These wires were permitted to protrude from the specimen and to make electrical connection to the power supply. At the tank bottom, a steel mesh was connected to the power supply to serve as a cathode. The voltage was

held constant, and the current was measured on daily basis by a digital meter. Figure 3.4 shows a schematic drawing of the corrosion tank setup.

After casting and curing the 24 specimens, 18 specimens were placed 50 mm apart and subjected to accelerated corrosion by partially immersing them in 50 cm x 150 cm tank filled with salt solution (5% NaCl concentration) by weight of water. The solution was changed on weekly basis to maintain the aforementioned concentration. Two water tanks were used, one for the 100 mm diameter specimens and another for the 150 mm diameter specimens.

In this test program, the current varied between 45 - 55 mA for each pullout specimen, and the total number was 18 specimens, the other 6 specimens served as control specimens. One source of power was used and the specimens were connected in parallel. The total capacity of the source is 3 A. The first set of 6 specimens was taken off the corrosion tank after 19 days, which is after showing slight corrosion stains and hair line cracks in the concrete. The second set was taken off at 27 days after showing a considerable corrosion stains and visible cracks ranged between 0.6 mm to 1.4 mm depending on w/c ratio of the mixed concrete. Finally, the third set was removed after 36 days after it showed large size of cracks between 4 - 7 mm and in some cases a complete debonding between the reinforcing steel and the concrete.

3.5 Mass Loss Calculation

The mass loss of the steel bar is calculated as the difference between the original mass of the uncorroded and corroded bar (after removal of all loose corrosion products). For each specimen after conducting the pullout test; the corroded steel bars were cleaned and scrubbed to remove the concrete and the corrosion products from the steel bar. Then they were dipped for 2 hours in a commercial solution of "Muriatic Acid" consists of thinned hydrochloric acid with a specific gravity of 1.16 and a pH of 1.00 from Lawrasons INC., then they were dried with a piece of cloth and scrubbed again gently with a metal brush to remove the rest of loose products. Each steel bar was carefully examined for its general

conditions as a result of the corrosion process in terms of pitting and ribs degradation and then weighed for the determination of mass loss.

The mass loss of the steel bar was then obtained as the difference between the mass of the corroded bar (after the removal of the loose corrosion products) and its mass before corrosion Amleh (2000).

$$\% \text{ Mass Loss} = \frac{\text{(Uncorroded Mass)} - \text{(Corroded Mass)}}{\text{(Uncorroded Mass)}} \times 100 \qquad (3.1)$$

3.6 Chloride Ion Content Determination

The chloride ion content is very critical to the service life of reinforced concrete structures, because a small amount of chloride can attack and destroy the passive layer that protects the steel bar from corrosion. For this reason, the determination of chloride content is essential.

To determine the chloride ion content of the pullout specimens, samples of powder were collected from three different depths drilled using a hammer drill. For the concrete cover thickness of 40 mm, the drilling was at depths of 13mm, 26mm and 40mm, and for concrete cover thickness of 65mm, the drilling was at depths of 22mm, 44mm and 65mm. The drilling was uniform around all the surface area of the specimen in order to get the average chloride content at each depth; Figure 3.6 shows the drilling mode. Then an amount of 1.5 grams was mixed for 24 hours with a solution bottled in vials and prepared specially for measuring the chloride content obtained from "Germann Instruments, INC, IL, USA".

The philosophy of chloride content determination lies in measuring the voltage (x) of known chloride concentration solutions (y) and graphing lines connecting each tow sets of points (Voltage, Chloride content), each line represents the voltage that lies between an upper and lower value of chloride concentration. The concentrations supplied with

testing instrument are (0.5, 0.05, 0.02, 0.005), the test instrument and the standard concentrations are shown in Figure 3.7.

After the calibration performance, the voltage is measured for each sample collected and the corresponding chloride concentration is projected from the graph.

3.7 Mechanical Pullout Test Setup

The pullout specimens were removed from the accelerated corrosion tank after obtaining the desired level of corrosion and left to dry for 7 days. The pullout specimen was supported on an appropriate base plate in the testing machine for the standard pullout test, Figure 3.5 shows the setup of the standard pullout test. A tensile force was applied to the protruding bar end and increased monotonically in about 20 load increments until failure by either yielding of the bar, or its pullout. An LVDT is mounted on the jacking pump and its free end touches the top surface of the plate above the specimen to measure any slippage associated with applied load. The data acquisition program records the applied load and the slippage every 0.1 seconds. Each load increment was recorded by a data acquisition program through a loading cell connected to the computer.

Table 3.1 Fresh concrete mix properties and steel parameters for 0.37 w/c ratio and 40mm concrete cover thickness.

		Steel			Fresh Concrete Mix Properties						
Specimen No.	w/c Ratio	Bar Diam. (mm)	Length (mm)	Weight (gm)	Cement (kg/m^3)	Sand kg/m^3)	Gravel (kg/m^3)	W/C (kg/m^3)	SP. (kg/m^3)	Slump (mm(	Air Cont (%)
C1-1C	0.37	19.5	646	1456	400	800	800	135 *	15	131	5.3
C1-2C			656	1436							
C1-3C			643	1415							
C1-4C			650	1436							
C1-5C			642	1414							
C1-6C			639	1420							
C1-7C			648	1432							
C1-8C			639	1440							

* The w/c ratio of 0.37 includes both the water and the super plasticizer

Table 3.2 Fresh concrete mix properties and steel parameters for 0.47 w/c ratio and 40mm concrete cover thickness.

		Steel			Fresh Concrete Mix Properties						
Specimen No.	w/c Ratio	Bar Diam. (mm)	Length (mm)	Weight (gm)	Cement (kg/m^3)	Sand kg/m^3)	Gravel (kg/m^3)	W/C (kg/m^3)	SP. (kg/m^3)	Slump (mm(	Air Cont (%)
C2-1C	0.47	19.5	643	1448	400	800	800	188	/	154	5.9
C2-2C			640	1446							
C2-3C			649	1466							
C2-4C			675	1517							
C2-5C			641	1443							
C2-6C			650	1440							
C2-7C			675	1515							
C2-8C			649	1462							

Table 3.3 Fresh concrete mix properties and steel parameters for 0.47 w/c ratio and 65mm concrete cover thickness.

		Steel			Fresh Concrete Mix Properties						
Specimen No.	w/c Ratio	Bar Diam. (mm)	Length (mm)	Weight (gm)	Cement (kg/m^3)	Sand kg/m^3)	Gravel (kg/m^3)	W/C (kg/m^3)	SP. (kg/m^3)	Slump (mm(	Air Cont (%)
C2-1B	0.47	19.5	641	1461	400	800	800	188	/	150	5.8
C2-2B			638	1451							
C2-3B			640	1457							
C2-4B			642	1462							
C2-5B			640	1460							
C2-6B			640	1456							
C2-7B			652	1489							
C2-8B			644	1460							

Table 3.4 Sieve analysis for the coarse and fine aggregate.

Coarse Aggregate

Sieve No.	Opening Percentage (mm)	Cumulative Retained (%)	Passing (%)
1 in.	25	0	100.0
¾ in.	19	2.1	97.9
½ in.	12.5	47.3	52.7
3/8 in.	9.5	78	22
No. 4	4.75	99.9	.1
No. 8	2.36	100	0

Fine Aggregate

Sieve No.	Opening Percentage (mm)	Cumulative Retained %	Passing %
4	4.75	0.9	99.1
8	2.36	12.0	88.0
16	1.18	22.7	78.3
30	0.6	43.7	56.3
50	0.3	81.2	18.8
100	0.15	96.5	3.5

Table 3.5 Physical and chemical properties of superplasticizer.

Physical State	Liquid
Specific Gravity at 25oC	1.21
% of Solid by Weight	40.5%
pH	8.5 %
Colour	Dark Brown
Sulfates	1.2 %
Boiling Point	100° C (212 F)

Table 3.6 Chemical Properties of cement

Properties	Chemical Analysis
LOI	2.46
SiO_2	19.69
Al_2O_3	5.20
Fe_2O_3	2.31
CaO	62.16
MgO	2.38
SO_3	3.83
Free Lime	1.05
Insoluble (Previous month)	0.28
C_3S	54.25
C_2S	15.52
C_3A	9.87
C_4AF	7.03

Table 3.7 Physical properties of cement

Properties	Values
Residue 45μm (%)	12.9
Blaine (m^2/kg)	374
Air Content (%)	8.1
Initial Set (mins.)	121
Autoclave Exp. (%)	0.08
Sulfate Exp. (%)	0.01

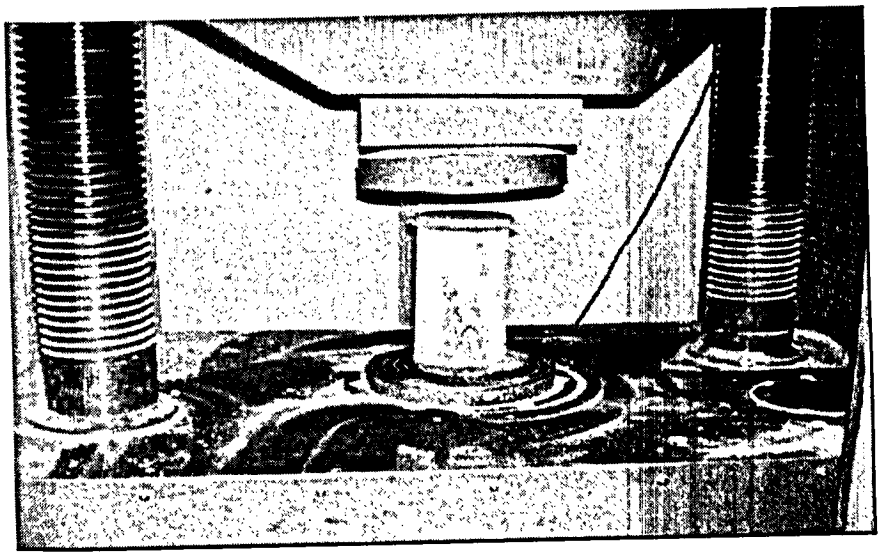

a- Compressive strength test setup

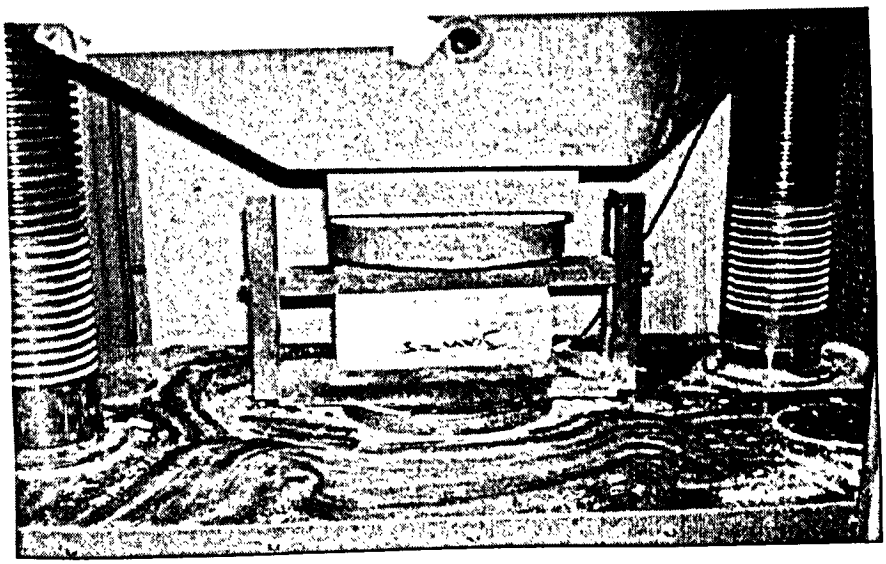

b- Indirect splitting tensile test setup

Figure 3.1 Compressive and tensile stress setup

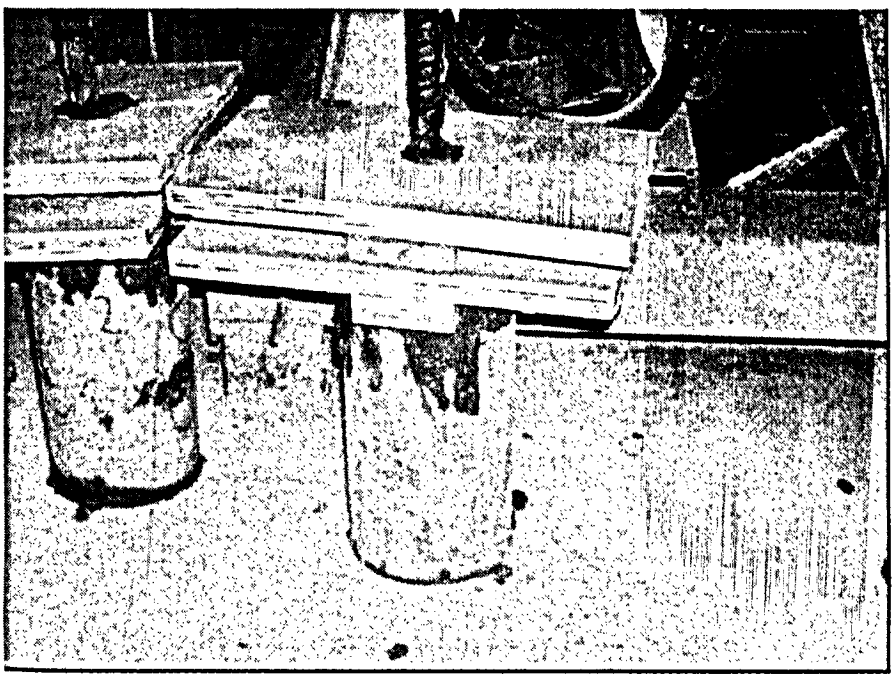

Figure 3.2 Mechanisms of centering the steel bar in pullout specimens

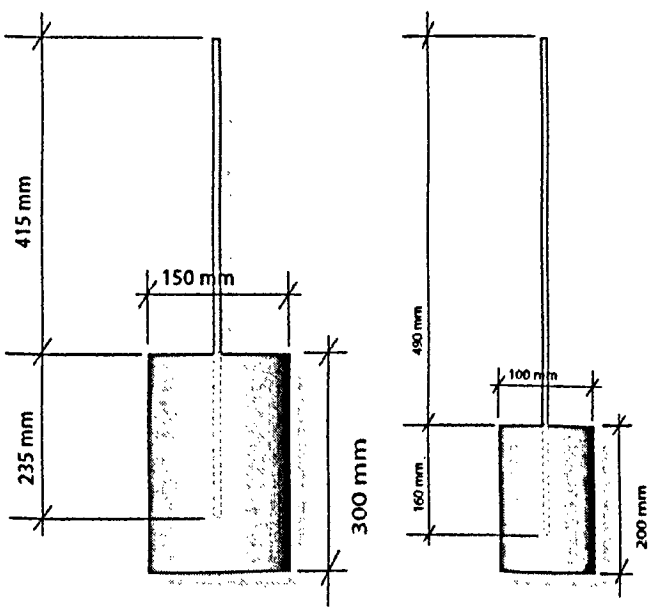

Figure 3.3 The two different sizes of pullout specimens used in this investigation

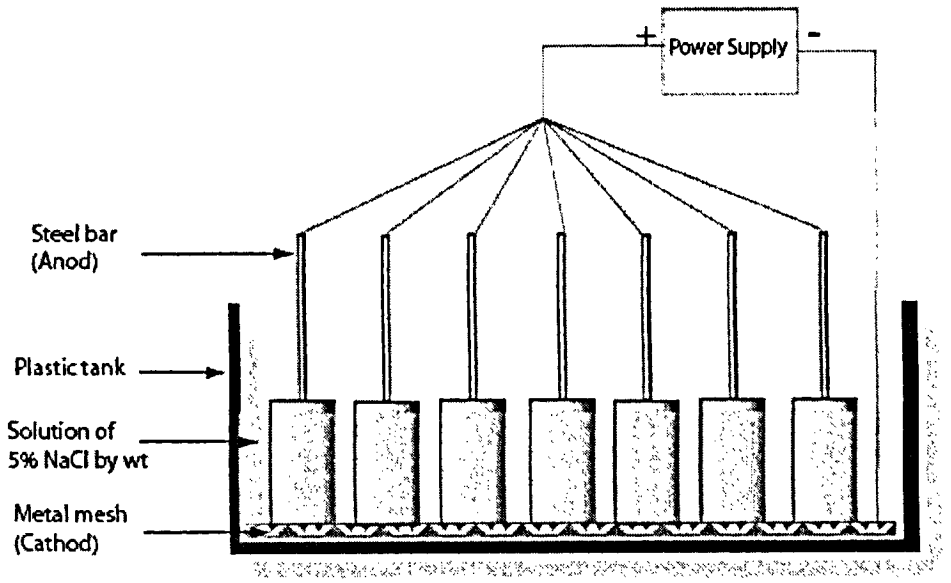

Figure 3.4 Accelerated corrosion setup for pullout specimens

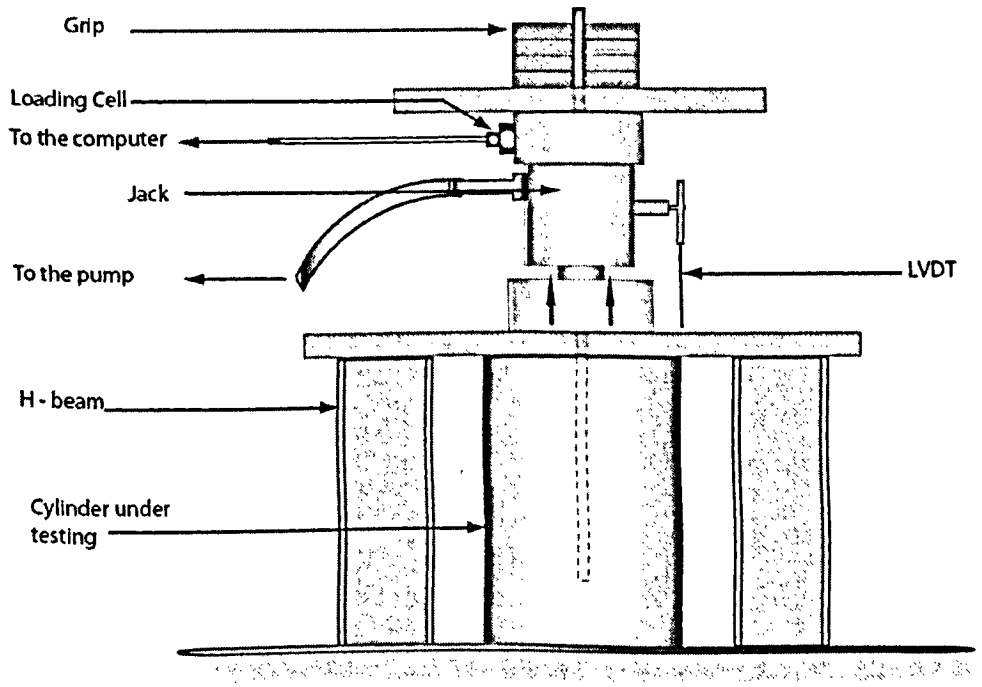

Figure 3.5 Standard pullout test setup

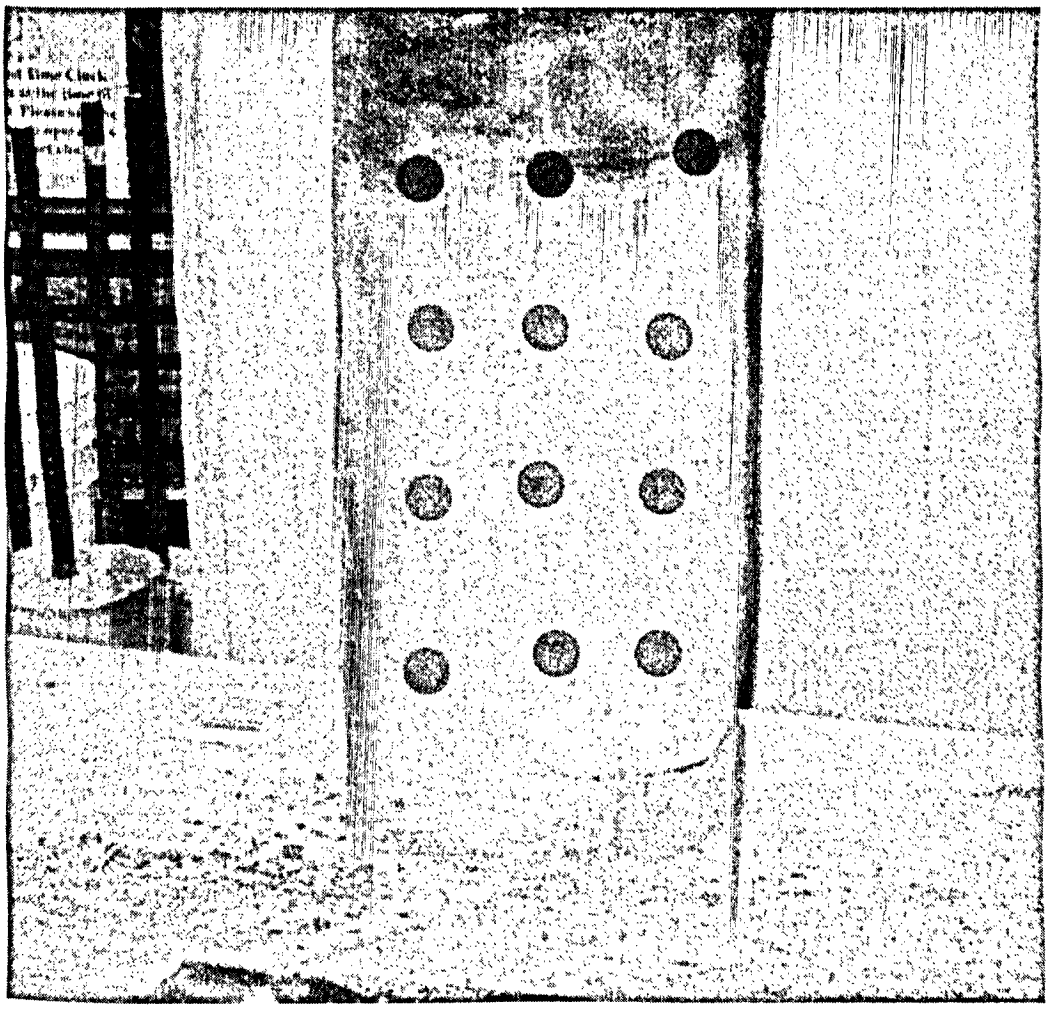

Figure 3.6 Concrete powder collection

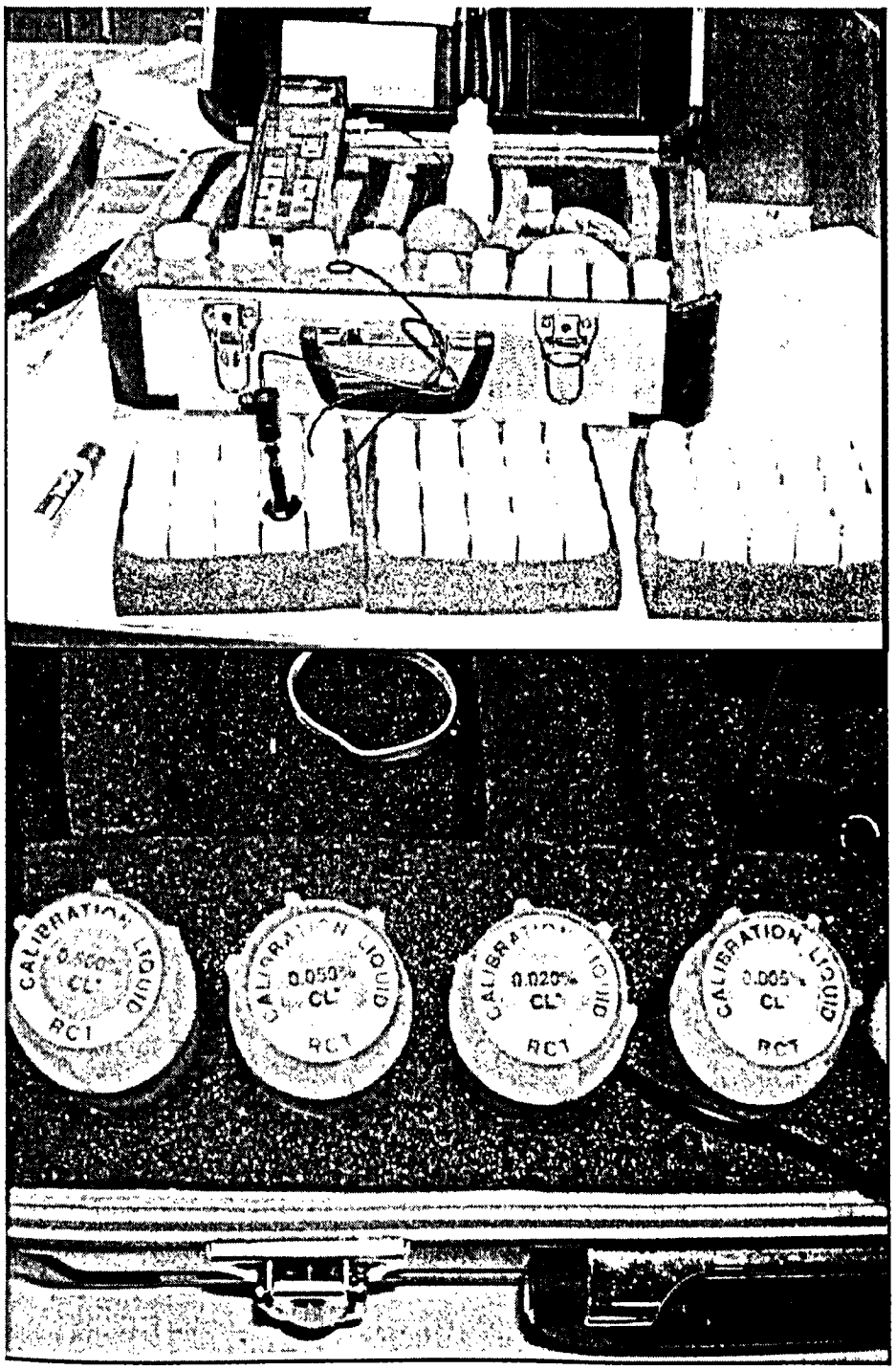

Figure 3.7 Chloride content test instrument and calibration solutions

CHAPTER 4
PULLOUT TEST RESULTS AND DISCUSSION

This Chapter reports the results of tests on pullout specimens, which investigated different aspects of the bond strength between the reinforcing steel and concrete. The main variables in the experimental test series were the effect of the level of corrosion on the degree of bond between the reinforcing steel and concrete using two different water/cement (w/c) ratio concrete mixtures and two different concrete cover thicknesses.

4.1 Effect of Different Parameters on Corrosion

As mentioned earlier, the bond strength and the failure mode are affected by several variables, such as the w/c ratios, concrete composition, tensile concrete and steel strengths, bar diameter, concrete cover thickness, embedment length, rib geometry, spacing of bars, stirrups, temperature, and corrosion. The bond characteristics of the reinforcing bars in the two different w/c ratio concrete mixtures with the control specimens (no-corrosion) are investigated first in terms of the effect of w/c ratio, concrete cover/bar diameter ratio, c/d_b, and the variation of the concrete tensile strength with the compressive strength.

4.1.1 Effect of w/c Ratio on Corrosion

The effect of w/c ratio on the transportation of harmful agents is based on the fact that the increase in w/c ratio leads to an increase in the size of the pores and permeability. Permeability of the concrete is the main factor influencing the concrete resistivity. Higher w/c ratio results in a higher permeability concrete than that of the lower w/c ratio concrete, since the excess water in the concrete matrix occupies more voids, Neville (1981).

At the same age of specimens, a low w/c ratio produces fewer pores. For example; at age of 49 days, specimen C2-4C with a cover thickness of 40 mm and w/c ratio of 0.47 suffered a mass loss of 13.25 %, while specimen C1-7C with the same cover thickness and w/c ratio of 0.37 suffered a mass loss of 10.75 %. Also by comparing specimen C2-4B with a cover thickness of 65 mm and w/c ratio of 0.47 with the aforementioned specimens, it is noticed

that it suffered a mass loss of 10.25 % which is less then specimen C1-7C despite the higher w/c ratio, and far less than C2-4C. Table 4-1 shows the percentage mass loss of each specimen in the program

4.1. 2 Effect of w/c Ratio on Compressive Strength

There is a general agreement that the concrete strength has a significant influence on the bond behaviour. Perry and Thompson (1966) studied the influence of the concrete strength on the bond stress distribution over the anchorage length. They found that in eccentric pullout specimens, the location of the maximum bond stress for the same force in the bars moved closer to the loaded end as the concrete strength was increased. This indicates a lower slip with the higher strength concretes. Compressive strength is considered to be a key parameter in bond behaviour, because the force is transferred by bearing and bond, and failure can occur by tensile splitting and shearing of the concrete Orangun, Jirsa and Breen, (1977). Tepfers (1973) showed that with a higher concrete strength, the slope of the bond stress distribution varies considerably over the splice length when compared to that with lower concrete strengths.

The results of this investigation were in agreement with the earlier researchers; which are that the higher the w/c ratio, the lower the compressive strength. Feret in 1892 found that the compressive strength is proportional to the w/c:

$$f'_c = \frac{1}{(1+(w/c))^2} \qquad (4.1)$$

It should be noted that the splitting tensile stress depends directly on the compressive strength of a given concrete mixture. Pillai and Kirk (1988) found that for normal density concrete the splitting tensile strength varies between 0.52 to 0.58 times the square root of compressive strength of the same concrete.

$$f_t = 0.56\,(f'_c)^{1/2} \qquad (4.2)$$

Table 4.2 summarizes the measured values of compressive and tensile strengths after 30 days of curing (for an age of 30 days). Appendix A Figure 1 through 4 show the test results of auxiliary specimens for compressive and the splitting tensile strengths at each individual stage.

It should be noted that the crack width was found to develop faster and longer in specimens with lower compressive strength, this is attributed to the higher corrosion rate in a relatively weaker and more porous concrete. Figure 4.1 shows two different crack widths for two specimens with same variables except in w/c ratio.

4.1.3 Effect of Concrete Cover Thickness on Corrosion

An adequate concrete cover will delay the corrosion onset. The chloride travels from the outer to the inner surface of concrete, and the larger the concrete cover the longer the time the chloride ions to reach the steel bar. However, excessively large thickness of concrete cover thicknesses would result in the presence of a considerable volume of unreinforced concrete. And yet, the steel is required to control shrinkage and thermal stresses, and to prevent cracking due to the above mentioned stresses. The large thickness of cover is proved to be detrimental. In practical terms, the cover thickness should not exceed 80-100 mm, Neville (1995), but the decision on cover forms part of structural design. ACI 318 recommends a minimum cover thickness of 37.5 mm in most structures, and a cover of 50 mm where deicing salt is used, and ACI 357 recommends a minimum of 62.5 mm in marine structures.

The testing program results as exhibited in Table 4.1 showed that the specimens with a concrete cover of 65 mm suffered less corrosion than those with concrete cover of 40 mm for the same w/c and the same immersing time. For example; specimens C2-7B (with a concrete cover thickness of 65 mm) and C2-1C (with concrete cover thickness of 40 mm) suffered a mass loss of 21.17 % and 23.62 % respectively. Moreover, specimen C2-7B showed less mass loss than that of specimen C1-2C, with a mass loss of 21.84 % despite the latter was a lower w/c ratio of 0.37. It shows that to a certain cover thickness, the w/c ratio and the cover thickness could compromise each other. The lower w/c ratio concrete

means lower penetrability than that of higher w/c ratio, and thus, smaller cover thickness would result in a situation where the chloride ion can not be transported rapidly through the concrete despite the smaller cover thickness, Neville (1995).

4.2 Chloride Ion Content

As mentioned earlier, the concrete provides a protective alkaline environment within a normal, uncontaminated reinforced concrete structure, which chemically protects the steel reinforcement from corrosion. However, when chlorides reach the steel surface, the chemical protection normally imparted is eliminated and the steel may then corrode, provided a sufficient supply of moisture and oxygen is available, Amleh (2000).

Chlorides penetrate concrete by the transport of water containing the chlorides, by diffusion of the ions in the water, and by absorption. Prolonged or repeated ingress can, with time, result in a high concentration of chloride ions at the surface of the steel bar. The chloride content of the concrete is critical to the life of the reinforcement, because small amounts of chloride can disrupt the passive layer that protects the steel from corrosion. Therefore, to assess the condition of the deteriorating concrete, it is essential to determine the chloride content in the concrete.

The chloride ion concentration was measured using a Rapid Chloride testing instrument to determine the chloride ion profile for each specimen according to the ASTM Standard C 1152-90 method with known chloride concentrations and then the calibration graph was established as shown in Figure 4.3. The equation of each line was determined as shown in Appendix A Figure 5

The concentration of chloride content was determined for each sample at three depths from the surface to the steel bar level by using the appropriate equation. The results are shown in Appendix A Figure 6 through 8. The results were as expected, in the uncracked specimens, the chloride ion concentration decreased from the exterior concrete surface to the steel bar surface. This phenomenon is basically the migration of chloride ions into the concrete through diffusion. However, in the cracked specimens, the chloride concentration was

higher at the surface and at the reinforcing steel bar, this because the chloride penetrated directly through the crack to the reinforcing steel bar and then into the micro – cracks around the reinforcing bar. Figures 4.4 through 4.6 show the chloride ion profiles for different stages of corrosion.

4.3 Effect of Immersing Time on Corrosion

The current measurements for each specimen were recorded periodically (every 24 hours) by means of a SMART Digital Multimeter that read both the current and the voltage. The relationship between the current and immersing time is shown in Figure 4.7. The results of current measurements seen in Figure 4.7 show that all specimens displayed small values at the beginning of the corrosion process and even slightly lower after few days, and this was basically because of the formation of the protective layer around the steel bar. The corrosion initiation in specimens C2-3C, C1-8C and C2-7B were 16, 22, 26 days respectively. The difference in the initiation time between specimens C2-3C and C1-8C is attributed to the difference in w/c ratio, that is the lower w/c ratio resulted in lower transportability of the chloride ion to the surface of the reinforcing steel bar and thus longer time to destroy the protective layer. Once the depassivation of the protective layer occurred and the rate of current increased steadily indicating the start of corrosion propagation stage. This propagation stage generally coincides with the specimen cracking. Lounis & Mirza (2001) in their study of the service life prediction of deteriorating concrete structures, found similar behaviour to the one found in this investigation as shown in Figure 4-8

As seen in Figure 4-7, the specimen C2-3B took longer corrosion initiation time than that of C1-8C, because of the larger concrete cover thickness and the longer distance for the chloride ion to travel through the concrete to the surface of the reinforcing steel bar.

4.4 Effect of Corrosion on Bond Strength

4.4.1 Bond Stress – Slip Relationship

As the steel bar corrodes, the increased volume of the corrosion products results in a "bursting" pressure, which causes longitudinal splitting cracks in the specimens, with the crack width increasing with the corrosion level. This results in the breakdown of adhesion and friction at the steel-concrete interface, excepting at low corrosion levels, when there is no longitudinal cracking, and the corrosion products have a beneficial effect of improving the bond characteristics at the steel-concrete interface. At higher corrosion levels, the steel bars display localized pitting and loss of some of the ribs over the bar length, thereby weakening the rib-concrete mechanical interlocking force transfer mechanism. An examination of the number and spacing of the transverse cracks shows that as the level of corrosion increases, the transverse crack spacing also increases, reflecting the deterioration of bond characteristics at the steel-concrete interface, Amleh and Mirza, (1999).

The bond strength for different stages of corrosion was calculated for each type of concrete cover thickness and w/c ratio. The average bond stress, u, for each load level was calculated as the average stress between the reinforcing steel bar and the surrounding concrete along the embedded portion of the bar, using the relationship.

$$u = P/L\,(\pi\, d_b) \tag{4.3}$$

where P is the maximum measured load, L is the embedded length of the reinforcing steel bar, and d_b is the reinforcing bar diameter (No. 20 bars were used in all of the pullout specimens).

In addition, for each pullout test the slip at the loaded end was measured for the various load increments up to failure. Failure was defined as the point of maximum bond strength, and the corresponding maximum slip value was then defined as the value at the point of failure. Bond stress was calculated at each load level and plotted against the loaded end slip for each specimen as shown in Figures 4.9 through 4.11.

4.4.1.1 Uncorroded Control Specimens

As shown in Figures 4.9 through 4.11, uncorroded specimens, at the early stage of loading there was very small values of slip associated with ascending values of bond stress, followed by another stage with no gain in bond stress (bond stress reached the maximum) but a relative slip, and after that some longitudinal cracks appeared and a sudden drop in bond stress followed by an explosive failure. This behaviour is similar to the Comite Euro-International du Beton (CEB) (1990) Model Code Figure 2.27- presented in Chapter 2 in the literature review. The bond stress-slip relationship, which consisted of three distinct regions that adequately describes the complete bond stress-slip behaviour. The demarcation of the three regions would be based on the behavioural trends which would be similar to that of the CEB Model Code (where $s_1 = s_2$ in Equation 3.18). In this model, the shear stress initially increased with slip up to a maximum shear stress of u_m. The second region was then illustrated by an increase in the slip with a small drop in the applied load, or constant shear stress for a short distance (between s_1 and s_2) followed by a sharp drop in the applied load with longitudinal splitting cracks. The bond behaviour between s_1 and s_2 is associated with the concrete shearing off between the ribs and splitting open, hence, s_1 was associated with the breakdown of the bond.

4.4.1.2 Corroded Specimens

The variation of the calculated bond stress with the associated slip is shown in Figures 4.9 to 4.11. The increase in corrosion level is manifested by the increase in slip due to the formation of longitudinal cracks caused by corrosion. The increase in corrosion level produces corrosion products which have flaky shapes act as a lubricant and reduce the friction component of the bond, Almussalam (1995), Amleh and Mirza (1999).

At advanced levels of corrosion (10% mass loss or more), the corrosion products at the bar surface are relatively loose. A significant degradation of the lugs occurs causing the deformed steel bar to act like a plain bar. Therefore, the horizontal component of the bearing force produced as a result of mechanical interlocking of the ribs is significantly reduced and the pullout is facilitated at lower load.

At very advanced levels of corrosion, the corrosion products increased to such an extent that the steel bar is unable to grip the concrete and continues to slip at very low pullout load values. At this stage, it is believed that the only bond mechanism that is still performing is the friction bond stress.

For example, Figure 4.9 shows clearly the different corrosion stages. The control specimens C2-6C and C2-2C have the highest value of bond strength and the lowest value of slip and thus the highest slope. Then followed by specimens C2-8C and C2-4C at the first stage of corrosion; when some debonding at the interface of the reinforcing steel bar and the surrounding concrete took place, the value of bond strength dropped and the associated slip increased. Some staining was observed through the hair cracks developed in this stage. The slope between the slip and bond stress observed in Figure 4.9 shows to be less than that of the control specimens indicating a loss of bond within the specimen. Specimens C2-7C and C2-5C, which have higher corrosion level (2^{nd} corrosion level) showed even flatter slope and further debonding between the reinforcing steel bar and the surrounding concrete. The size of the cracks at this stage was determined to be between 0.6 – 1.4 mm. At the final stage of corrosion, the corrosion products almost completely debonded the interface between the reinforcing steel bar and the surrounding concrete, the slope between the bond stress and the slip was almost horizontal. The cracks' sizes were between 4 – 7 mm.

4.4.2 Bond Strength - Mass Loss

The percentage mass loss of each steel bar was obtained as the difference between the mass of corroded steel (after cleaning the loose products) and the mass before corrosion. Figure 4.12 shows the relationship between the normalized bond strength calculated using the highest value of bond stress of specimen C2-3B = 8.63 MPa, obtained from the pullout test taken as 100 %, and the other values of bond stress as a percent of this value. As seen from the figure, the specimens of C2-B series with a w/c ratio of 0.47 and a concrete cover thickness of 65 mm, showed the least bond loss and kept values even higher than those of C1-C series of w/c of 0.37 and concrete cover thickness of 40 mm, this is obviously due to the longer embedded length and larger concrete cover thickness.

However, specimens of C2-C (w/c of 0.47) showed more degradation in bond stress and relatively lower values of mass loss compared with specimens of C1-C (w/c ratio of 0.37), that is due to the higher w/c ratio in specimens C2-C.

Table 4.1 shows the values of the bond strengths corresponding to the associated mass loss. The higher values of bond stresses at the early stages of corrosion of the specimens were not studied, since they were not captured because they were not in the objective of this investigation.

4.4.3 Effect of Chloride Content on Bond Strength

The detrimental action of chloride on bond strength for a given time depends mainly on two factors; the permeability of the concrete, and the distance the chloride ion travels from the surface of the embedded steel bar. The relationship between the chloride ion content at the steel bar level and the bond strength for different w/c ratios is shown in Figure 4.13. The general trend indicates that the higher the chloride concentration at the interface between the reinforcing steel bar and the surrounding concrete, the more bond deterioration. Specimens of C2-C series with higher w/c ratio of 0.47 experienced more bond deterioration with less concentration of chloride ion content than that of specimens C1-C series due to higher w/c ratio and more permeable concrete.

Since specimens C2-B series have larger concrete cover thickness, the chloride ions needed longer time to reach the steel bar, and the bond was less degraded than both other specimens.

Table 4.1 Bond strength vs mass loss and corresponding chloride ion content

65mm/0.47				40mm/0.47				40mm/0.37			
Specimen #	ML %	Measured bond strength (MPa)	Cl^- %	Specimen #	ML %	Measured bond strength (MPa)	Cl^- %	Specimen #	ML %	Measured bond strength (MPa)	Cl^- %
C2-3B	0.00%	8.63	0.00%	C2-6C	0.00%	6.32	0.00%	C1-3C	0.00%	8.05	0.00%
C2-2B	10.95%	5.70	0.19%	C2-8C	9.44%	3.59	0.16%	C1-5C	9.22%	4.13	0.15%
C2-4B	11.89%	5.19	0.21%	C2-4C	13.25%	2.72	0.22%	C1-7C	10.75%	2.82	0.23%
C2-8B	12.53%	4.89	0.23%	C2-7C	13.66%	2.55	0.31%	C1-1C	11.40%	1.98	0.35%
C2-5B	13.96%	4.18	0.29%	C2-5C	14.48%	2.02	0.58%	C1-6C	12.07%	1.60	0.59%
C2-7B	21.17%	2.67	0.55%	C2-1C	23.62%	0.20	0.70%	C1-2C	21.84%	0.76	0.81%
C2-6B	28.81%	0.54	1.14%	C2-3C	29.06%	0.10	0.89%	C1-8C	21.61%	0.62	0.79%

Table 4.2 Values of compressive and tensile strengths at age of 30 days

Auxiliary Specimen	w/c Ratio	Age of curing (day)	Measured compressive Strength. (MPa)	Measured Tensile Strength. (MPa)	Calculated Tensile Strength $[0.56 (f'c)^{1/2}]$ (MPa)
C2 - C	0.47	30	42.00	3.94	3.63
C1 - C	0.37	30	59.60	5.31	4.32
C2 - B	0.47	30	42.00	3.99	3.63

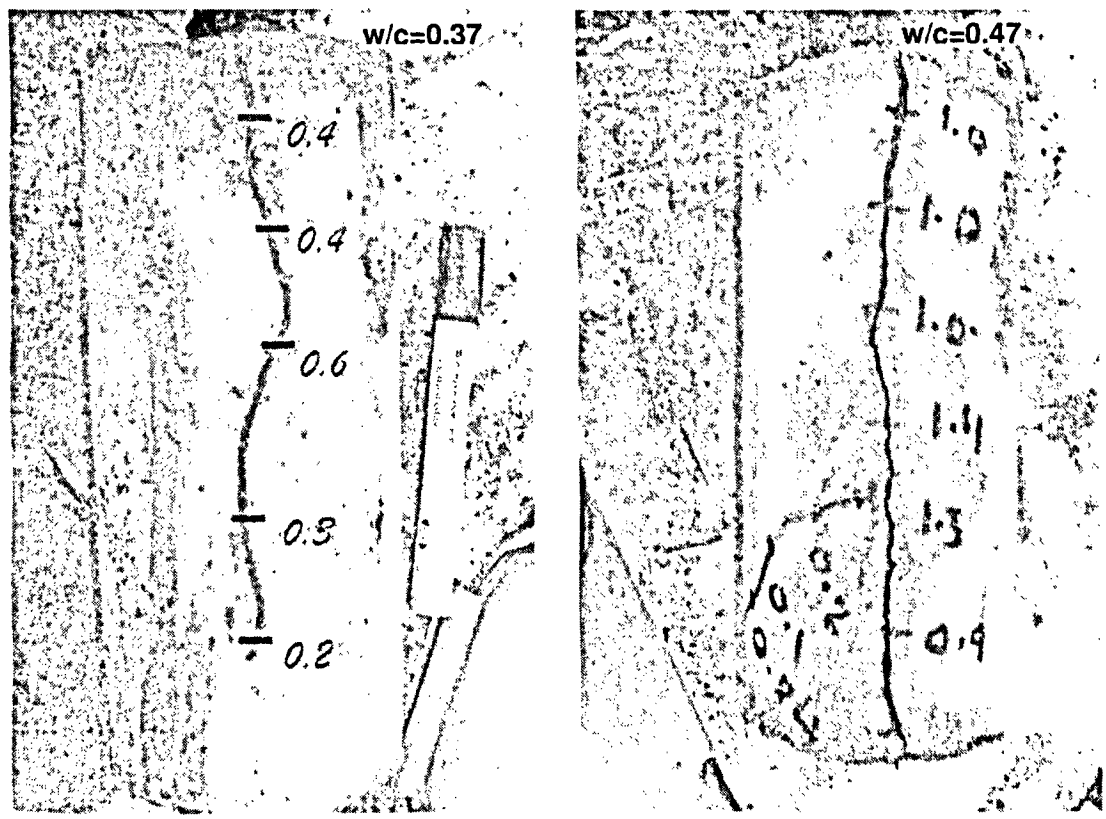

Figure 4.1 Crack widths for specimens with different w/c ratio, with the same immersing time in corrosion tank

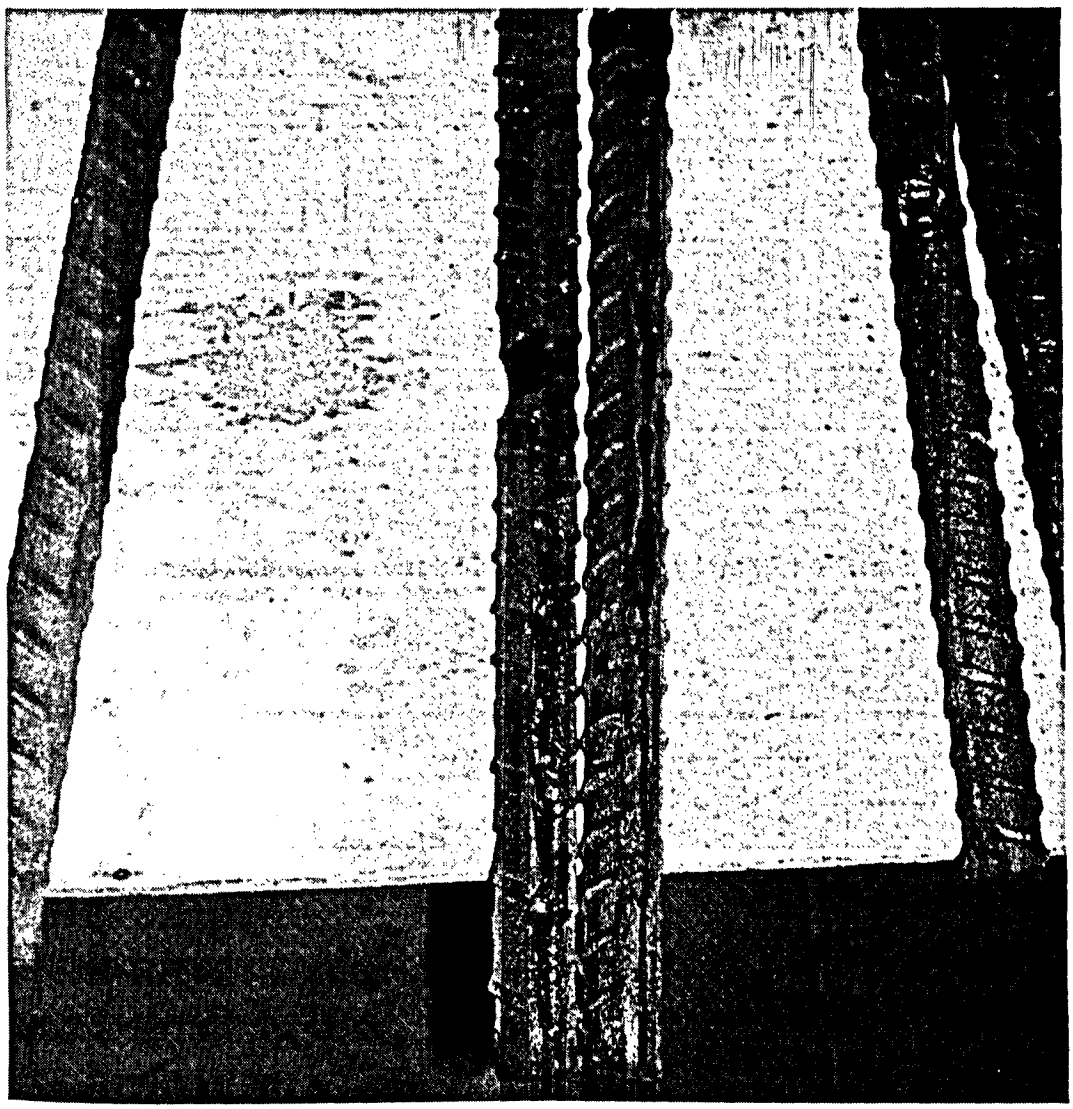

Figure 4.2 Corrosion in different embedment lengths.

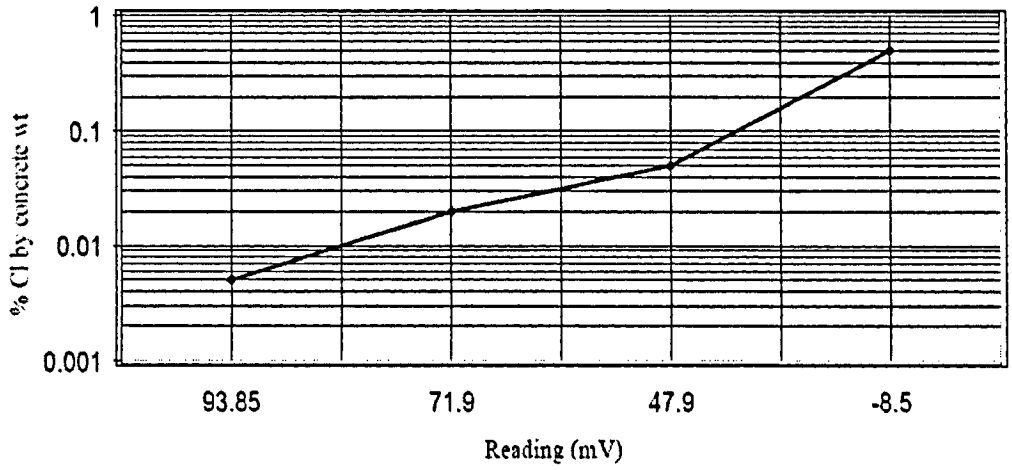

Figure 4.3 Calibration graph for chloride ion content (%) determination

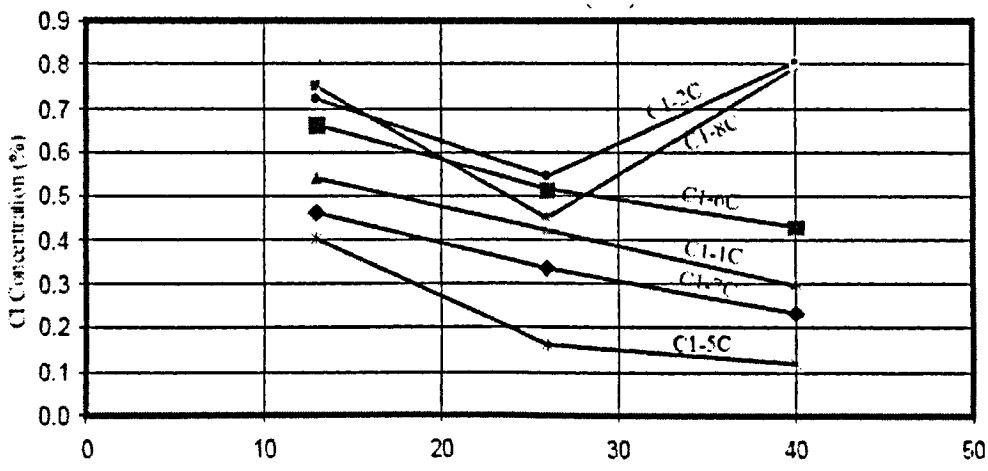

Figure 4-4 Chloride ion profile for different corrosion stages for concrete specimens with w/c ratio of 0.37 and 40 mm concrete cover thickness

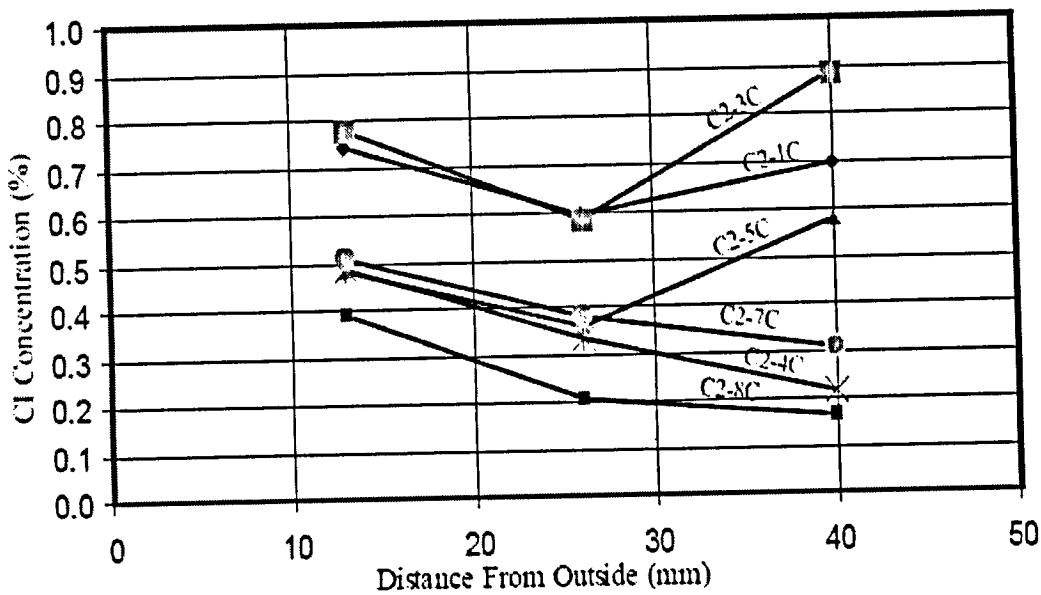

Figure 4-5 Chloride ion profile for different corrosion stages for concrete specimens with w/c ratio of 0.47 and 40 mm concrete cover thickness.

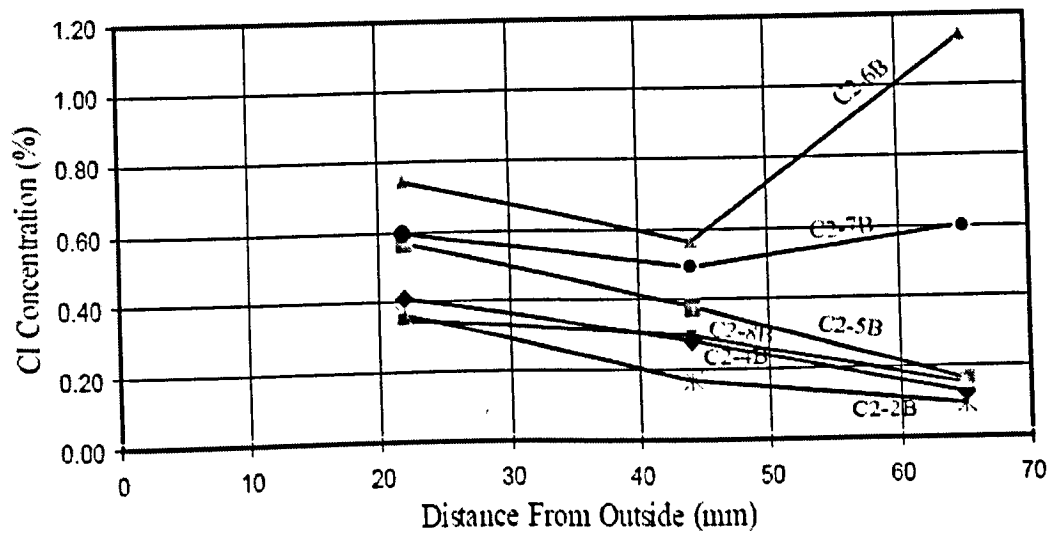

Figure 4-6 Chloride ion profile for different corrosion stages for concrete specimens with w/c ratio of 0.47 and 65 mm concrete cover thickness.

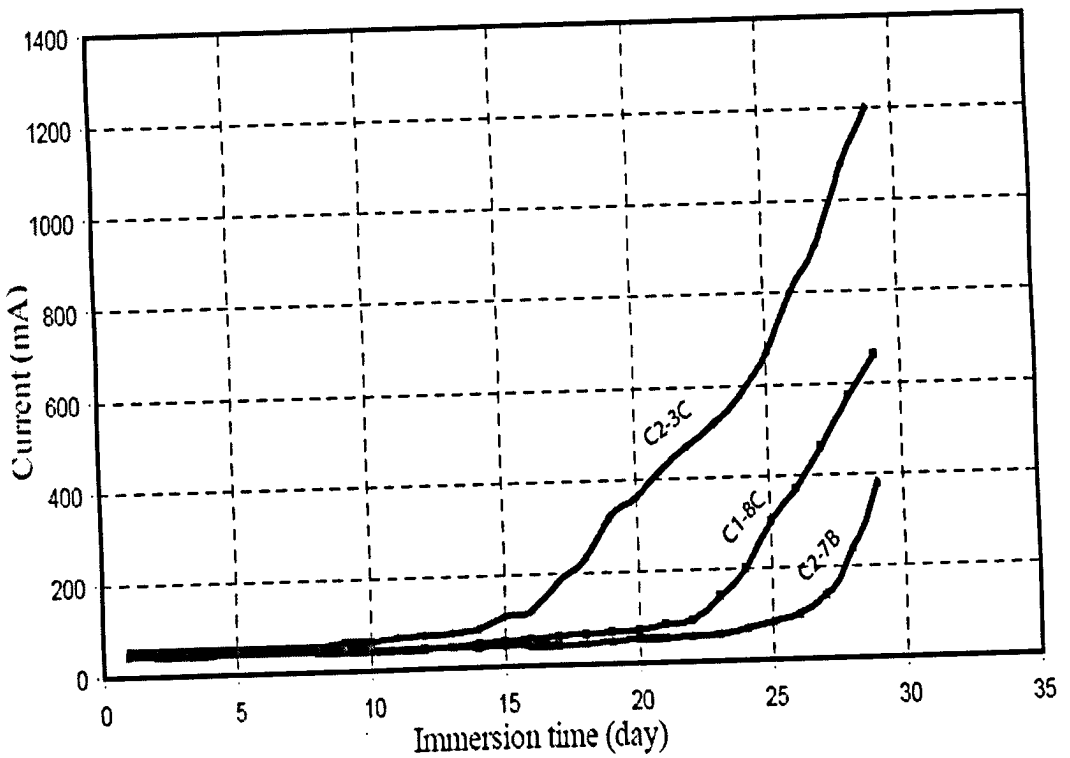

Figure 4.7 Current readings for different w/c ratios and different concrete cover thicknesses

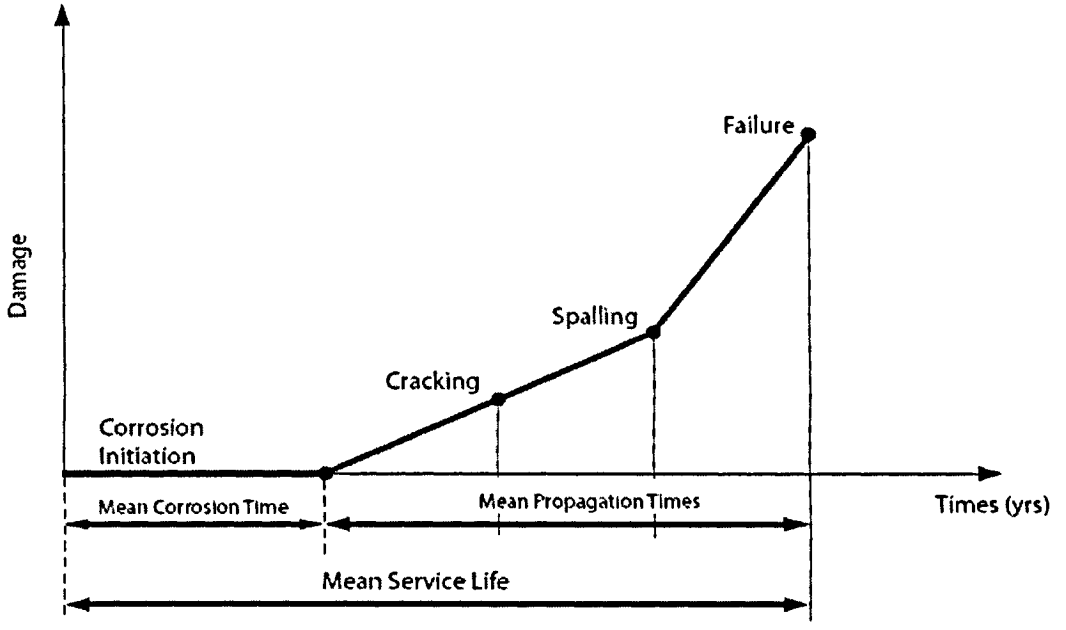

Figure 4.8 Idealized deterioration stages of reinforced concrete structures, Lounis& Mirza (2001)

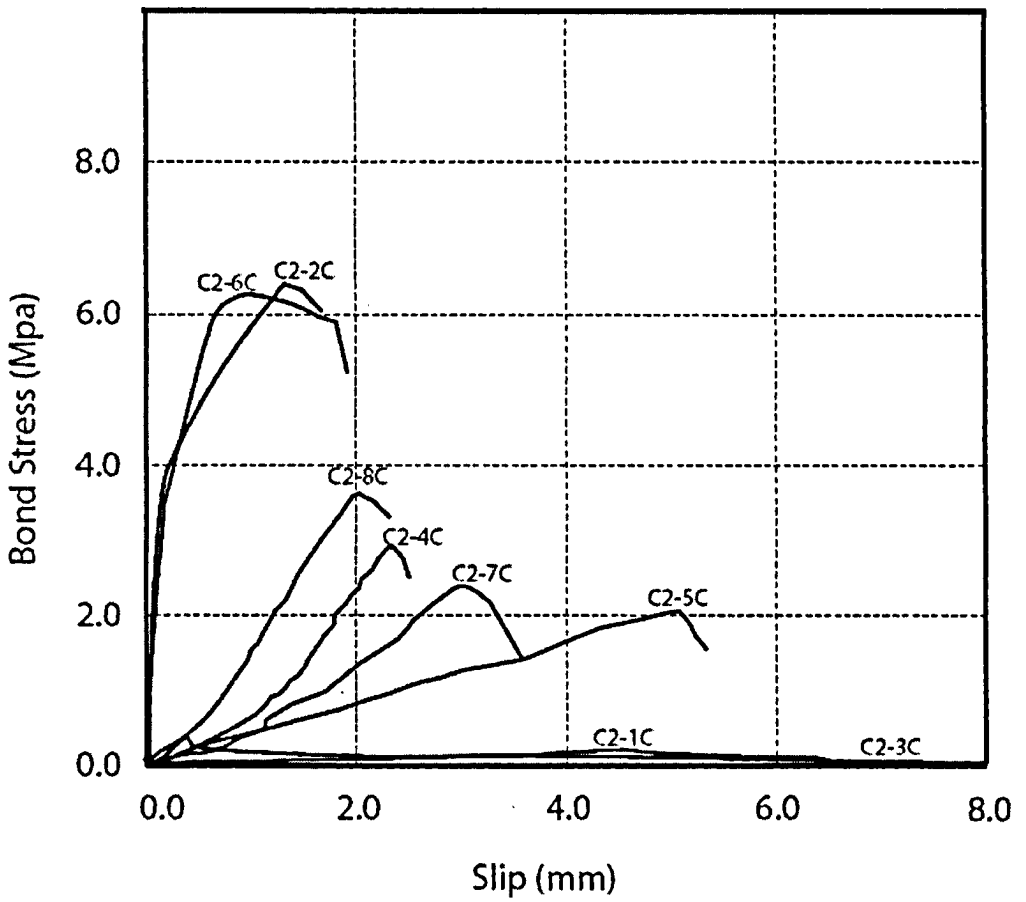

Figure 4.9 Bond stress vs slip for series of C2-C specimens with a concrete cover thickness of 40 mm and w/c ratio of 0.47.

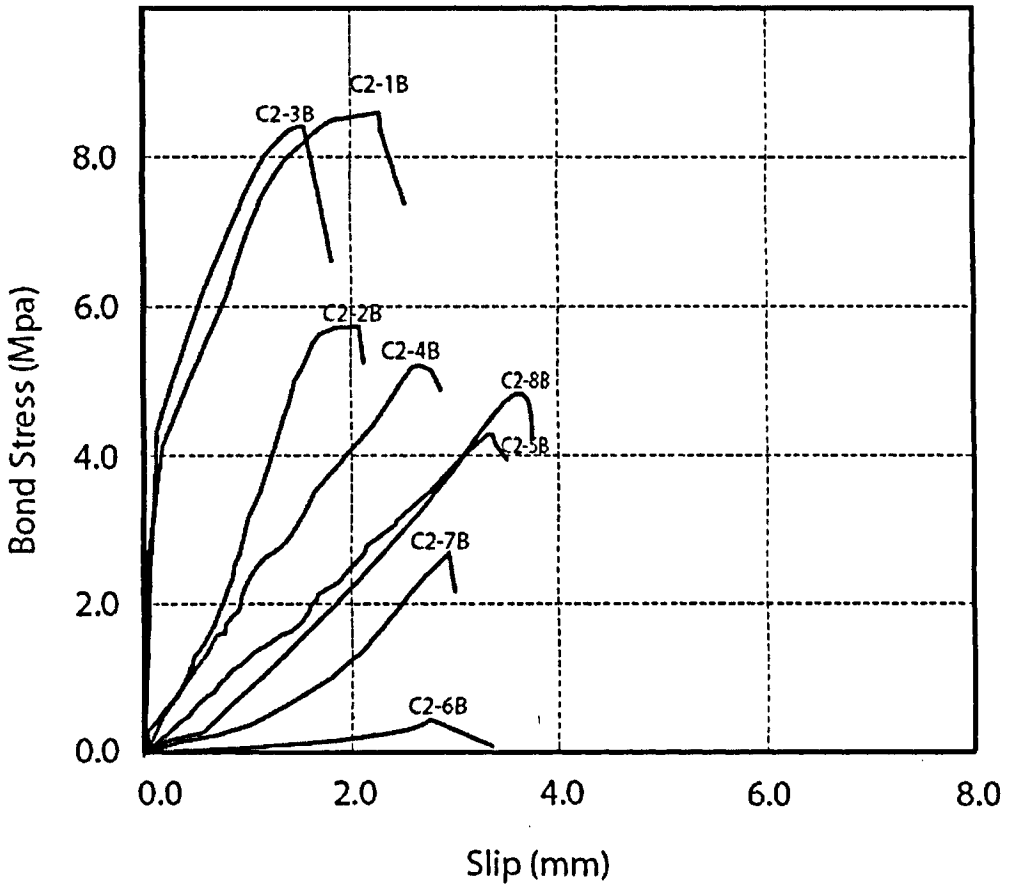

Figure 4.10 Bond stress vs slip for series of C2-B specimens with a concrete cover thickness of 65 mm and w/c ratio of 0.47.

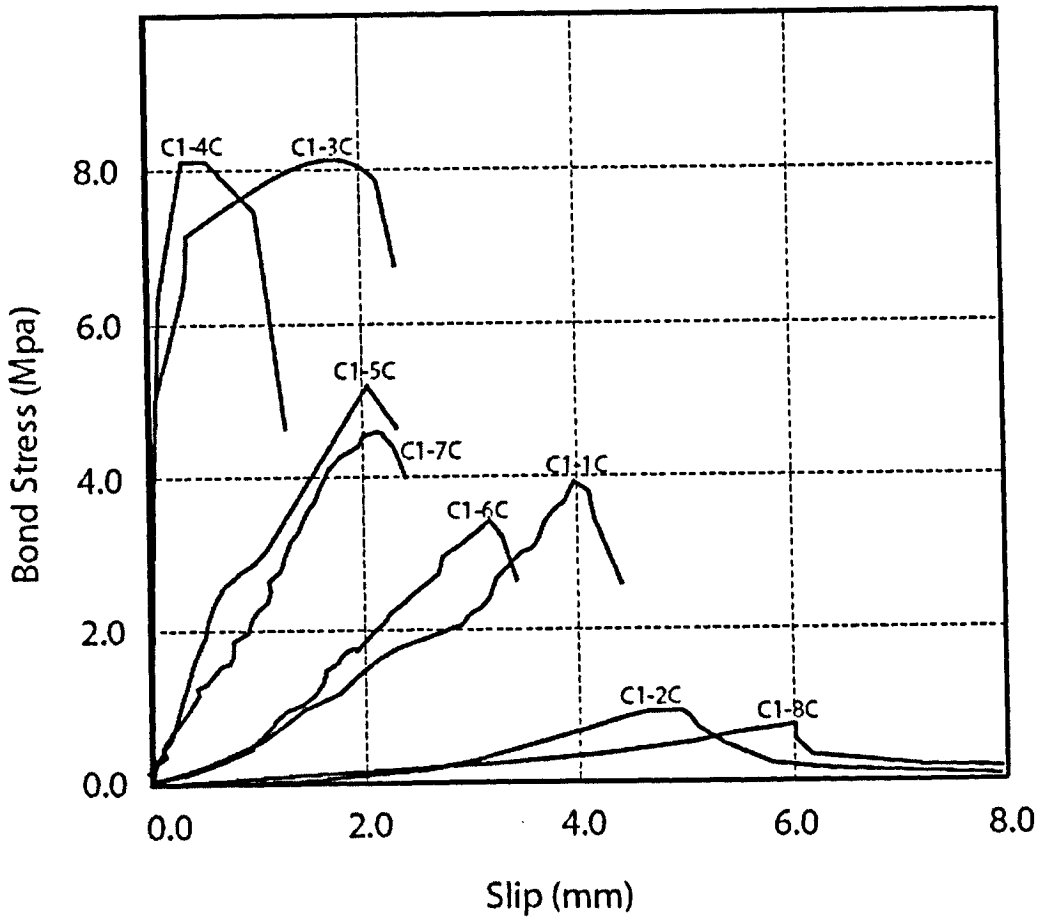

Figure 4.11 Bond stress vs slip for series of C1-C specimens with a concrete cover thickness of 40 mm and w/c ratio of 0.37.

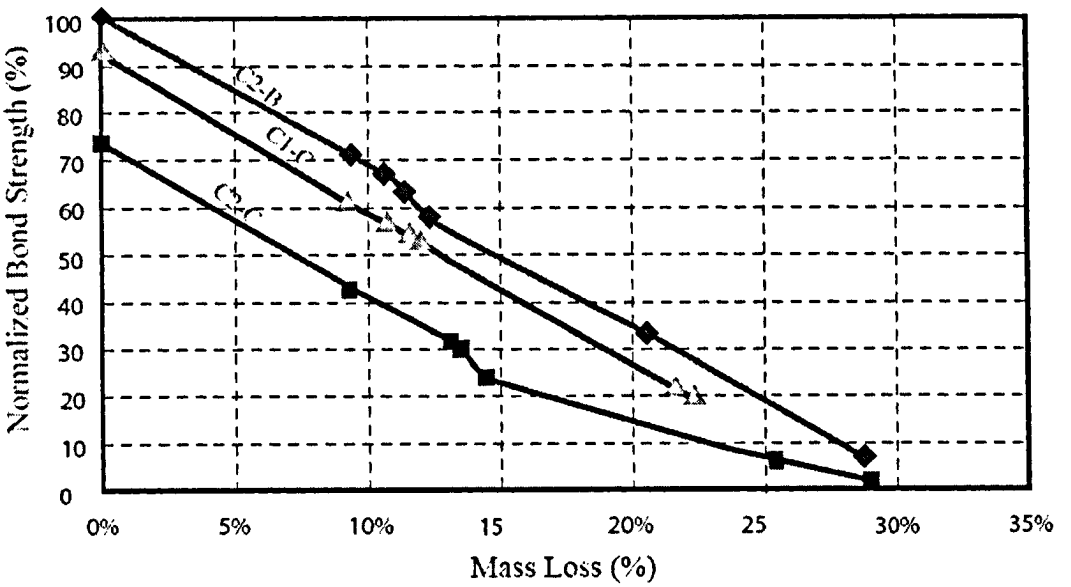

Figure 4.12 Normalized bond strength vs mass loss for the different series of specimens

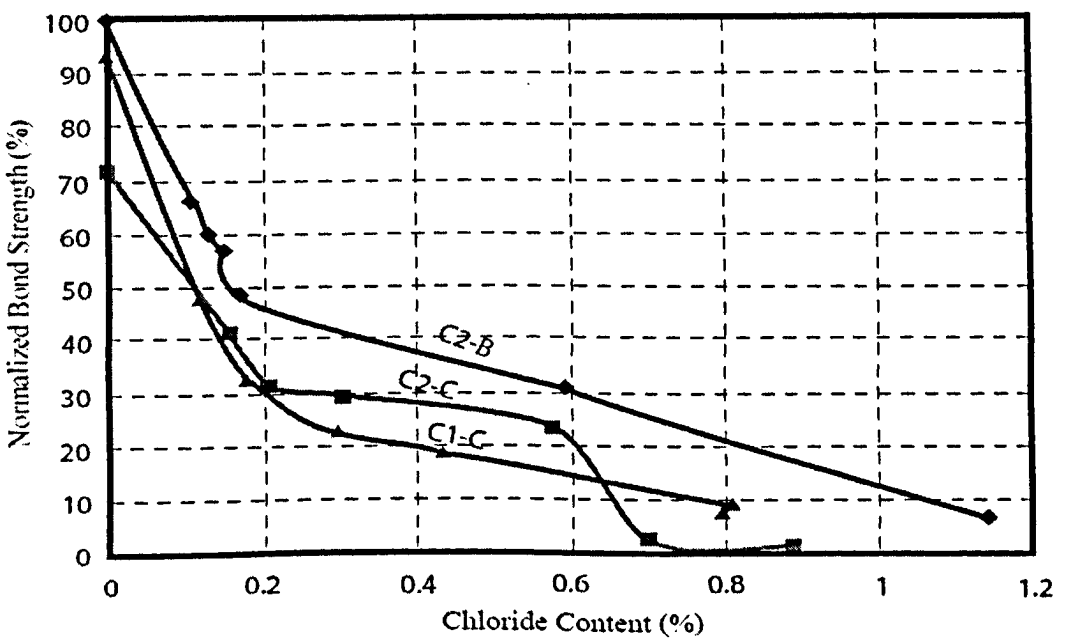

Figure 4.13 Normalized bond strength vs chloride ion concentration for all different series of specimens

CHAPTER 5
OPTIMIZATION PROGRAM

This chapter reports the analytical discussion of the complete responses until failure of all of pullout specimens, tested after the development of the different required levels of corrosion. Also, this chapter deals with the practical aspects of the effect of corrosion on bond behaviour at the reinforcing steel-concrete interface. Where possible, appropriate design equations are formulated (using optimization); for bond strength in structural concrete at a given stage of corrosion deterioration after being subjected to an aggressive environment for a given time. This chapter presents the development of mathematical equations using the data obtained by Amleh (2000), and this investigation.

5.1 Definition of Optimization (Curve Fitting)

Optimization is a mathematical procedure for determining optimal allocation of scarce resources to make a system or design as effective or functional as possible.

In general, the optimization or known as curve fitting will produce an equation that can be used to find points anywhere along the curve. In some cases, finding an equation is not the main goal that is pursued, instead, using a curve fitting to smooth the data and improve the appearance of a plot is the essential goal.

The curve fitting can be divided into three main categories: least squares curve fitting, nonlinear curve fitting, and smoothing curve fitting, Kaleida Graph Guide to Curve Fitting (1988).

1. Least Squares Curve Fitting

Least Squares is a method of curve fitting that has been popular for a long time. Least Squares minimizes the square of the error between the original data and the values predicted by the equation. While this technique may not be the most statistically robust method of fitting a function to a data set, it has the advantage of being relatively simple

and of being well understood. The major weakness of the Least Squares method is its sensitivity to outliers in the data. If a data point is widely different from the majority of the data, it can skew the results of the regression. For this reason, the data should always be examined for reasonableness before fitting.

There are five known Least Squares fits; Linear, Polynomial, Exponential, Logarithmic, and Power.

2. Nonlinear Curve Fitting

The General curve fit in this technique is based on the Levenberg-Marquardt algorithm and is calculated using an iterative procedure. It starts with initial guesses for the unknown parameters that were supplied with the equation. It then calculates a Chi Square value that represents the sum of the squared error between the original data and the calculated fit. It takes a user-defined equation and uses it to fit a set of plotted data. This technique of fitting is the most powerful.

3. Smooth Curve Fitting

The smoothing fits is different from the other two types of fits as these curve fits do not generate an equation for the resulting curve. This is because there is no single equation that can be used to represent the curve. These curve fits are useful when the goal is to improve the appearance of the plot by drawing a smooth curve through the data.

5.2 Data Used in This Optimization Program

Two sets of data were used to develop a baseline model for predicting residual bond strength using pullout specimens. The data obtained by Amleh (2000) were modeled due to the use of correlations derived from it as a recommended method. Tables 5.1 and 5.2 show the experimental results obtained by Amleh (2000). The tables exhibit the bond strength, crack width and the chloride ion contents for 2 mixtures of concrete. The w/c ratio for the pullout specimens starting with C4 was 0.32, and the w/c ratio for those of C5 was 0.42. The corrosion level as well as the percentage of the mass loss due to corrosion were also exhibited for each specimen of the two concrete types. Table 5.3

shows the compressive strength obtained at an age of 365 days for both mixtures and the calculated splitting tensile strength of both mixes.

The bond stress at the beginning of corrosion process (around 5% mass loss) was observed to have higher values than the values without corrosion, this is attributed to the increase of confinement of the bar in concrete, as the amount of corrosion products increase and develop an expansive mechanical pressure on the surrounding concrete, Almusallam (1995), Amleh and Mirza (1999). Thus such values were discarded and the optimization was carried out with the other values.

Relationships between the mass loss and bond strength and between the chloride ion content and bond strength were obtained. Then a linear curve fitting for each curve was performed resulting in a line where its equation and correlation to the real data are shown in Figures 5.1 through 5.8. A polynomial curve fitting was performed on the same data yielded a second degree curve with a correlation almost the same with linear curve fitting, yet there was not any tangible trend that can relate all the equations of the fit curve

5.3 Bond Stress as a Function of Concrete Cover Thickness, Bar Diameter, Compressive Strength, w/c Ratio and Chloride Ion Content.

5.3.1 Bond Stress For Control Specimens (No Corrosion)

Tepfers (1973) studied theoretically the circumferential stress distribution over the thickness of the concrete cylinder confining the bars. These circumferential tensile stresses are caused by the outward redial stresses from the action of the deformed bars on the concrete cylinder as shown in Figure 5.6. He assumed three stages in the bond response of the concrete cylinder: the uncracked stage, partially cracked stage, and the plastic stage. The analyses of the cracked and partially cracked stages were based on the elastic theory. In the plastic stages, a uniform tensile stress distribution was assumed over the thickness of the concrete cylinder.

Assuming short anchorage lengths, Tepfers (1973) derived equations for the three stages, and found good agreement between the measured values of the short anchorage tests with partly cracked theory. If partially cracked elastic behaviour is assumed, then the bond strength u, at the cracking of the concrete cover, is given by:

$$u = 0.6(0.5 + c/d_b) f_t \quad \text{MPa} \qquad (5.1)$$

where:

u = bond stress

c = concrete cover thickness

d_b = bar diameter

f_t = concrete tensile strength

Applying Pillai and Kirk formula, as the splitting tensile strength f_t for normal density concrete varies between 0.52 to 0.58 times $(f_c)^{1/2}$, an average was taken as:

$$f_t = 0.56 (f_c)^{1/2} \quad \text{MPa} \qquad (5.2)$$

By substituting equation 5.2 into 5.1, Equation 5.1 becomes;

$$u = (0.17 + 0.336\, c/d_b) (f_c)^{1/2} \qquad (5.3)$$

Equation 5.3 represents the bond stress in terms of the compressive strength, concrete cover thickness and bar diameter for normal density concrete

Following these equations, Amleh (2000) performed a detailed analysis of the chloride ion content for all of the pullout specimens in the two different concretes and the results of a detailed regression analysis led to two equations in Table 5.4 relating the bond strength to chloride content. The correlation coefficients are listed for each case showing confidence in the equations developed.

To verify the validity of the first part of these equations, u is calculated from the equation and compared to the value obtained in Table 5.1:

For a concrete cover of 50 mm and w/c ratio of 0.32:

$u = [0.35 + (0.3 * 50/19.5)] (60)^{1/2} = 8.67$ MPa

u from Table 5.1 = 9.28 MPa

Table 5.5 shows the results obtained from Equation 5.3 and Table 5.1. This comparison shows that using Equation 5.1 along with Equation 5.2 gave reasonable results, and thus using these equations would simplify the calculations of the anticipated bond strength.

5.3.2 Bond Stress with Corrosion

The second part of each equation in Table 5.4 represents the loss of bond due to corrosion and was exhibited as the amount of chloride at the reinforcing steel bar level. The mass loss of the reinforcing steel bar is generally related to the chloride content of the concrete. These chlorides would normally permeate or diffuse through the concrete cover, however, as cracks form and widen much of the chlorides flow directly through the cracks to the surface of the reinforcing steel bar and destroy the passive layer to initiate corrosion. Nevertheless, if the cracks are fine, 0.1 mm or less in width, this flow of chlorides to the bar surface is not significant, Amleh (2000).

By examining the two equations in Table 5.4, it is noticed that the amount of chloride required in the equation at water cement ratio of 0.32 is almost twice the amount for one of 0.42 for the same concrete cover thickness and bar diameter; this is obviously attributed to the change of water cement ratio.

According to Fick's second law of diffusion for non steady-state diffusion, the ingress of chloride is a function of the concrete diffusivity. The water-cement ratio is a major factor influencing diffusivity in the mix proportion of ordinary Portland cement concrete, Tanaka *et al.* (2001). Thus the second part of the equation in Table 5.4 can be written as follows:

$$u = [0.35 + 0.3\, c/db](f'c)^{1/2} - f(w/c) * Cl^-,$$

where; f(w/c): is a function of w/c ratio and Cl^- is the percent chloride ion content at reinforcement.

Furthermore, Tanaka *et al.* (2001) in their study on the required cover depth of concrete highway bridges in coastal environment, found that the diffusion factor is proportional to the w/c ratio, for ratios between 0.25 – 0.55. Figure 5.5 shows the result of the fitting performed on the multiplier of Cl^- for the two different w/c ratios. Thus, applying the Power Least Square Fitting to the chloride multiplier of the equations from the results of Amleh (2000) and incorporating the w/c ratio, the equation can be written as follows:

$$u = [0.35 + 0.3\ c/db](f'c)^{1/2} - [1.667\ (w/c)^{-2.3588}]Cl^- \qquad (5.4)$$

5.3.3 Validation of Derived Equation with Mass Loss Equations

The equations of the relationship between the bond stress and the mass loss are shown in Figures 5.1, 5.2, 5.3 and 5.4, and summarized in Table 5.6.

The mass loss of the reinforcing steel bar is generally related to the chloride ion content, Amleh (2000). If the mass loss is plotted against the chloride ion content from the data in Tables 5.1, 5.2, and the bond stress is calculated from Equation 5.5 and, the mass loss was verified by using the calculated bond strength in the equations of Table 5.6.

Example

The residual bond strength is calculated at a chloride ion content of (0.2%) from Equation 5.5:

For a concrete cover thickness of 75mm and w/c ratio of 0.32

$u = [0.35 + (0.3* 75/19.5)] * (60)^{1/2} - [1.667\ (0.32)^{-2.3588}] * 0.2$

$u = 6.75$ MPa

Apply $u = 6.75$ MPa in the corresponding equation in Table 5.6

$6.75 = (0.35+0.3 * 75/19.5) * (60)^{1/2} - 0.42\ (ML)$

$ML = 11.66\ \%$

ML from Figure 5.7 is 11.0 %

Table 5.7 shows the results of the obtained and calculated mass loss

5.3.4 Validation of the Derived Bond Equation with the Pullout Test Results

In Tables 5.8, through 5.10, the bond stress with its corresponding percentage mass loss and chloride ion content are summarized. Equation 5.5 will be applied for the chloride content to check the validity of this equation for different cover thicknesses and w/c ratios from this program study.

For a concrete cover of 65 mm, w/c ratio of 0.47 and chloride ion content of 0.21%:

$u = [0.35 + (0.3 * 65/19.5)] * (42)^{1/2} - [1.667 (0.47)^{-2.3588}] * 0.21$

u = 6.78 MPa

u obtained from the pullout test 5.19 MPa

Tables 5.8, 5.9, 5.10 show the results of the obtained and calculated bond stress.

5.4 Generalized Formula

The studies have indicated that the different variables, such as w/c ratio and the accelerated corrosion behaviour including immersing time and induced current play a major role in determining a general loss of structural capacity, also the effect of interaction between the process of corrosion behaviour variables cannot be neglected. Therefore, the effect of such variables is also studied using by using analytical techniques.

5.4.1 Effect of Immersing Time on Chloride Ion Content

Figure 4.7 shows the relationship between the current in mA and the immersing time in days. The initial low current passing through the concrete specimens is an indication of the higher resistivity of the concrete. Permeability of the concrete is the main factor influencing the concrete resistivity, higher w/c ratio results in a higher permeability concrete than lower w/c ratio concrete, since the excess water in the concrete matrix occupies more voids, Neville (1981).

As mentioned previously, Equation 5.4 was derived based on the work done by Amleh (2000). The immersing time of specimens in the salt solution was 220 days for w/c ratio of 0.32, and 150 days for w/c ratio of 0.37, and the induced average current was less than 2.5 mA. In this study the immersing time was 35 days and the induced average current was around 50 mA. Therefore, the corrosion process is incomparable for the two studies. At 2.5 mA and a time of 150 days, the corrosion process is closer to the natural and better representing the real world. While in the second case, the steel bar was forced to corrode by applying higher current, and not by the concentration of chloride accumulated at the reinforcing steel bar surface.

In order to establish a scientific comparison, a factor should be introduced to account for the difference in time and induced current. Tables 5.8 through 5.10 show the calculated using Equation 5.4 and obtained values of bond strength. By examining the difference between the calculated and the obtained values, and by using the trial and error method, a constant could be derived to magnify the second term and adjust for the under-calculated bond loss caused by not accounting for the induced current and the immersing time. Equation 5.4 can be written as follows:

$$u = [0.35 + 0.3\ c/db](f'c)^{1/2} - [1.667\ (w/c)^{-2.3588}]\ (I/2.5)^{0.16}Cl^{-} \qquad (5.5)$$

where I is the current in m Amp.

Example

For specimen C2-4B with a w/c ratio of 0.47, concrete cover thickness of 65 mm and steel bar diameter of 19.5 mm. The chloride ion content is 0.21 % and the average current is 50 mA,

$u = [0.35+(0.3*0.065/0.0195)]*(42)^{0.5}-[1.667*(0.47)^{-2.3588}]*(50/2.5)^{0.16} * 0.21$

u = 5.39 MPa

u calculated from the pullout test is 5.19 MPa

The new calculated bond stress for each specimen using Equation 5.5 is summarized in Tables 5.11 to 5.13.

It is noticed that Equation 5.5 gives reasonable results for a bond loss of around 50%, beyond this loss the equation does not work efficiently. This was expected since the behaviour of the structure after this much of bond loss is unpredictable and considered in the collapse stage from structural view point.

Table 5.1: Test data for NPC with 0.32 w/c ratio concrete pullout specimen (Amleh 2000).

Specimen No.	Cover thickness	Corrosion Level	Mass Loss due to Corrosion (%)	Width of Longitudinal Crack due to corrosion (mm)	Chloride Ion Content at Bar Level (%)	Bond Strength (MPa)
C4-1B		0	0.00	0.00	0.00	10.96
C4-2B		0	0.00	0.00	0.00	11.64
C4-4B		1	2.65	0.00	0.01	12.60
C4-7B	75mm	2	8.46	0.50	0.13	8.08
C4-5B		3	9.23	0.65	0.15	7.78
C4-6B		4	10.43	0.80	0.17	7.68
C4-8B		5	18.70	3.20	0.45	3.84
C4-3B		6	24.30	5.00	0.82	1.14
C4-1C		0	0.00	0.00	0.00	9.28
C4-2C		0	0.00	0.00	0.00	9.79
C4-6C		1	1.61	0.00	0.00	9.95
C4-8C		2	2.85	0.20	0.06	9.45
C4-5C	50mm	3	7.26	0.40	0.13	6.37
C4-4C		4	12.50	0.90	0.23	3.84
C4-3C		5	18.25	3.00	0.48	1.47
C4-7C		6	19.94	4.00	0.59	1.28

Table 5.2: Test data for NPC with 0.42 w/c ratio concrete pullout specimen (Amleh 2000).

Specimen No.	Cover thickness	Corrosion Level	Mass Loss due to Corrosion (%)	Width of Longitudinal Crack due to corrosion (mm)	Chloride Ion Content at Bar Level (%)	Bond Strength (MPa)
C5-1B	75mm	0.00	0.00	0.00	0.00	9.53
C5-2B		0.00	0.00	0.00	0.00	9.80
C5-5B		1.00	2.25	0.00	0.04	11.52
C5-7B		2.00	4.95	0.08	0.13	9.79
C5-8B		3.00	9.86	0.60	0.17	7.74
C5-3B		4.00	18.34	1.20	1.00	3.20
C5-6B		5.00	20.85	2.00	1.23	2.58
C5-4B		6.00	21.85	3.00	1.45	2.18
C5-1C	50mm	0.00	0.00	0.00	0.00	9.12
C5-2C		0.00	0.00	0.00	0.00	8.60
C5-5C		1.00	1.3	0.00	0.01	9.60
C5-7C		2.00	2.5	0.00	0.10	9.60
C5-8C		3.00	5.1	0.20	0.15	8.14
C5-6C		4.00	13.23	1.00	0.82	4.16
C5-3C		5.00	17.56	1.40	0.97	3.13

Table 5.3 Values of compressive and splitting tensile strengths (Amleh 2000).

Concrete Mix.	Compressive Strength, f'_c	Tensile Strength, $0.56\ (f'_c)^{1/2}$
NPC, w/c= 0.32	60 MPa	4.34 MPa
NPC, w/c= 0.42	51 MPa	4.00 MPa

Table 5.4 Relationship between bond stress and chloride ion content (Amleh 2000).

Concrete cover, mm	**w/c ratio**	**Optimized equations of Amleh (2000)**	**R^2**
50	0.32	$u=(0.35 + 0.3\ c/d_b)\ (f'_c)^{1/2}-24.5\ (Cl^-*)$	0.94
75			
50	0.42	$u=(0.35 + 0.3\ c/d_b)(f'_c)^{1/2}-12.9(Cl^-*)$	0.80
75			

*Cl^- is the chloride ion content as % of concrete

Table 5.5 Results obtained from Equation 5.3 and from Table 5.1.

Concrete Cover (mm)	w/c Ratio	u obtained from Eq. 5.3 (Mpa)	u obtained from Table 5.1 (Mpa)
50	0.32	8.67	9.28
75	0.32	11.65	10.96
50	0.42	8.00	9.12
75	0.42	10.74	9.53

Table 5.6 Equations of the bond stress vs the mass loss.

Concrete Cover (mm)	w/c ratio	Optimized equations of Amleh (2000)	R^2
50mm 75mm	0.32	$u = (0.35 + 0.3c/d_b)(f'_c)^{1/2} - 0.42\ ML$	0.97
50mm 75mm	0.42	$u = (0.35 + 0.3c/d_b)(f'_c)^{1/2} - 0.34\ ML$	0.90

Table 5.7 Results of the obtained and calculated mass loss.

Concrete Cover (mm)	w/c Ratio	u obtained from Eq. 5.4 (Mpa)	ML obtained from Table 5.6 (%)	ML obtained from Figure 5.7 (%)
50	0.32	3.77	11.66	10.50
75	0.32	6.75	11.66	11.00
50	0.42	5.42	7.56	4.50
75	0.42	8.16	7.58	6.50

Table 5.8 Comparative results of bond strength obtained from Equation 5.4 for 65mm cover thickness and w/c ratio of 0.47.

65mm/0.47						
Specimen #	% Cl^-	Obtained Bond MPa	% Bond Loss	Calculated Bond MPa	Difference	% Difference
C2-3B	0.00%	8.63	0.00%	8.75	0.12	1.38%
C2-2B	0.19%	5.70	33.99%	6.97	1.27	22.30%
C2-4B	0.21%	5.19	39.81%	6.78	1.56	30.09%
C2-8B	0.23%	4.89	43.38%	6.57	1.68	34.46%
C2-5B	0.29%	4.18	51.59%	6.03	1.86	44.41%
C2-7B	0.55%	2.67	69.03%	3.57	0.90	33.52%
C2-6B	1.14%	0.54	93.70%	-1.91	-2.46	-451.80%

Table 5.9 Comparative results of bond stresses obtained from Equation 5.4 for 40mm cover thickness and w/c ratio of 0.47.

40mm/0.47						
Specimen #	% Cl^-	Obtained Bond MPa	% Bond Loss	Calculated Bond MPa	Difference	% Difference
C2-6C	0.00%	6.32	0.00%	6.26	-0.06	-1.01%
C2-8C	0.16%	3.59	43.23%	4.74	1.15	31.99%
C2-4C	0.22%	2.72	57.01%	4.24	1.53	56.16%
C2-7C	0.31%	2.55	59.69%	3.35	0.81	31.64%
C2-5C	0.58%	2.02	68.03%	0.84	-1.18	-58.57%
C2-1C	0.70%	0.20	96.82%	-0.29	-0.49	-244.60%
C2-3C	0.89%	0.10	98.42%	-2.05	-2.15	-2153.73%

Table 5.10 Comparative results of bond stresses obtained from Equation 5.4 for 40mm cover thickness and w/c ratio of 0.37.

40mm/0.37						
Specimen #	% Cl^-	Obtained Bond MPa	% Bond Loss	Calculated Bond MPa	Difference	% Difference
C1-3C	0.00%	8.05	0.00%	7.45	-0.60	-7.42%
C1-5C	0.15%	4.13	48.74%	4.73	0.61	14.73%
C1-7C	0.23%	2.82	64.94%	3.32	0.49	17.48%
C1-1C	0.35%	1.98	75.40%	1.19	-0.79	-40.00%
C1-6C	0.59%	1.60	80.14%	-3.12	-4.72	-295.36%
C1-2C	0.81%	0.76	90.60%	-6.88	-7.64	-1010.00%
C1-8C	0.79%	0.62	92.28%	-6.67	-7.29	-1172.89%

Table 5.11 Comparative results of bond stresses obtained from Equation 5.5 for 65mm cover thickness and w/c ratio of 0.47.

65mm/0.47				
Specimen #	% Cl^-	Obtained Bond (MPa)	% Bond Loss	Calculated Bond (MPa)
C2-3B	0.00%	8.63	0.00%	8.75
C2-2B	0.11%	5.8	32.79%	5.71
C2-4B	0.13%	5.19	39.86%	5.39
C2-8B	0.15%	4.89	43.34%	5.07
C2-5B	0.17%	4.18	51.56%	4.12
C2-7B	0.59%	2.67	69.06%	-0.04
C2-6B	1.14%	0.54	93.74%	-9.47

Table 5.12 Comparative results of bond stresses obtained from Equation 5.5 for 40mm cover thickness and w/c ratio of 0.47.

40mm/0.47				
Specimen #	% Cl^-	Obtained Bond (MPa)	% Bond Loss	Calculated Bond (MPa)
C2-6C	0.00%	6.32	0.00%	6.26
C2-8C	0.16%	3.64	43.23%	3.70
C2-4C	0.22%	2.82	57.01%	2.74
C2-7C	0.31%	2.55	59.69%	1.30
C2-5C	0.58%	2.02	68.03%	-3.01
C2-1C	0.70%	0.2	96.82%	-4.93
C2-3C	0.89%	0.1	98.42%	-7.97

Table 5.13 Comparative results of bond stresses obtained from Equation 5.5 for 40mm cover thickness and w/c ratio of 0.37.

40mm/0.37				
Specimen #	**% Cl^-**	**Obtained Bond (MPa)**	**% Bond Loss**	**Calculated Bond (MPa)**
C1-3C	0.00%	8.05	0.00%	7.45
C1-5C	0.12%	5.10	36.65%	4.42
C1-7C	0.18%	4.60	42.86%	3.78
C1-1C	0.30%	3.91	51.43%	1.86
C1-6C	0.44%	3.54	56.02%	-1.97
C1-2C	0.81%	1.13	85.96%	-5.49
C1-8C	0.79%	0.82	89.81%	-5.17

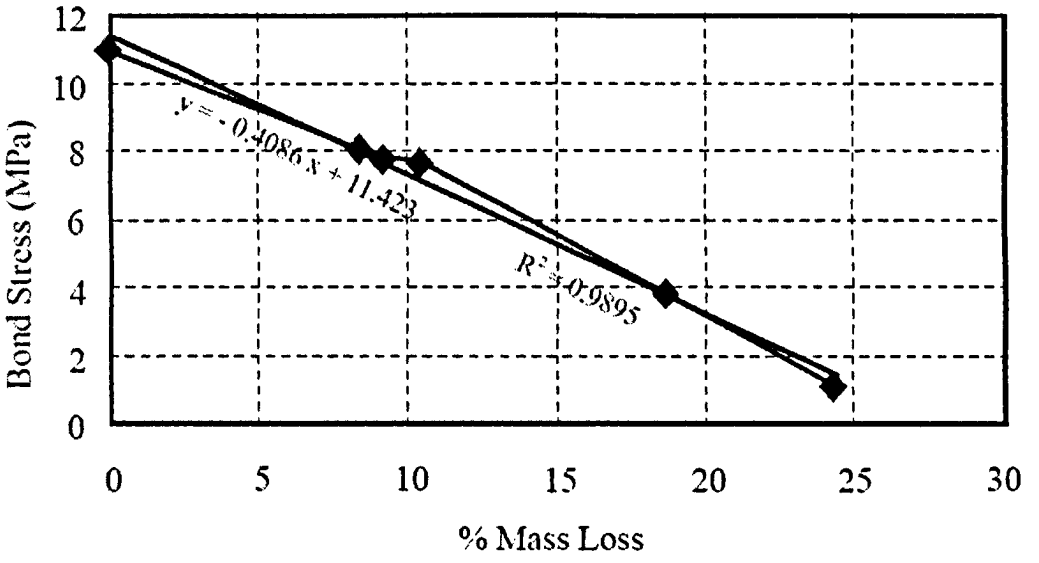

Figure 5.1 Mass loss vs bond stress for a cover of 75 mm and w/c 0.32, Amleh (2000).

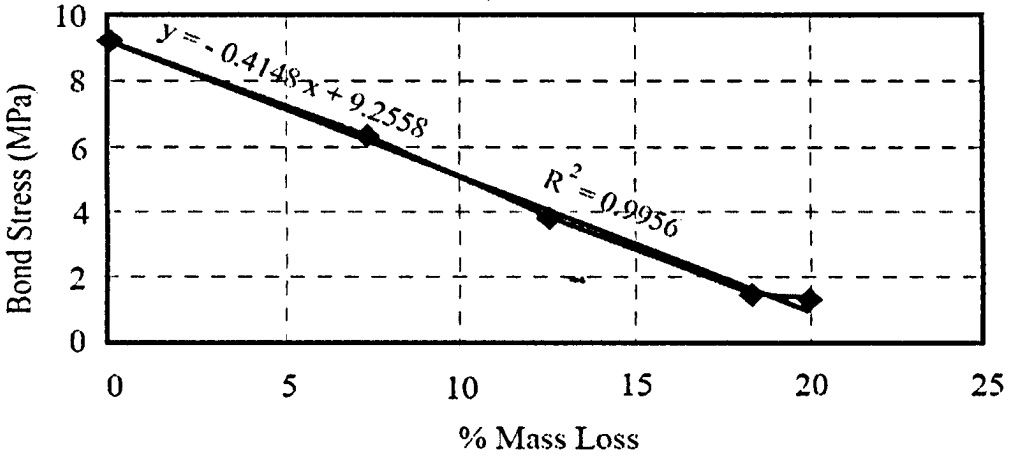

Figure 5.2 Mass loss vs bond stress for a cover of 50 mm and w/c 0.32, Amleh (2000).

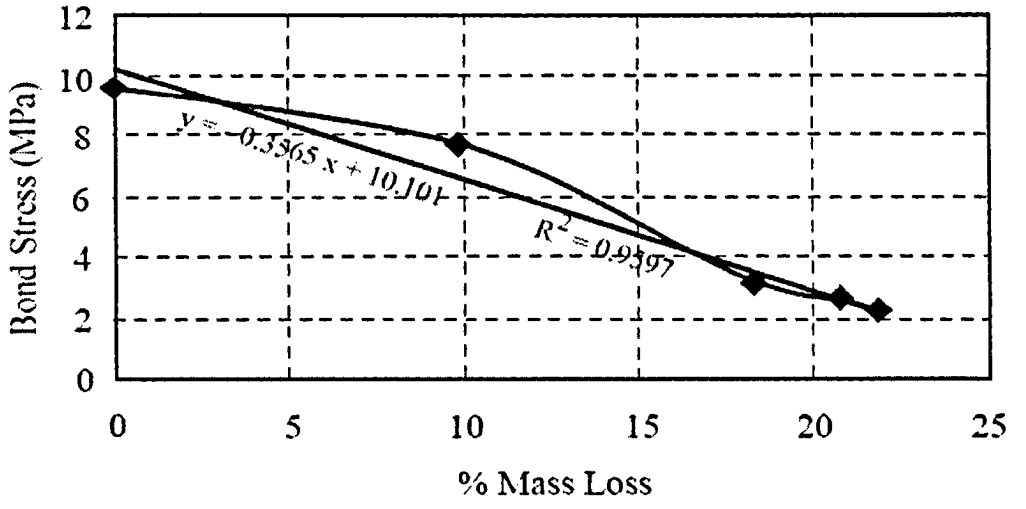

Figure 5.3 Mass loss vs bond stress for a cover of 75 mm and w/c 0.42, Amleh (2000).

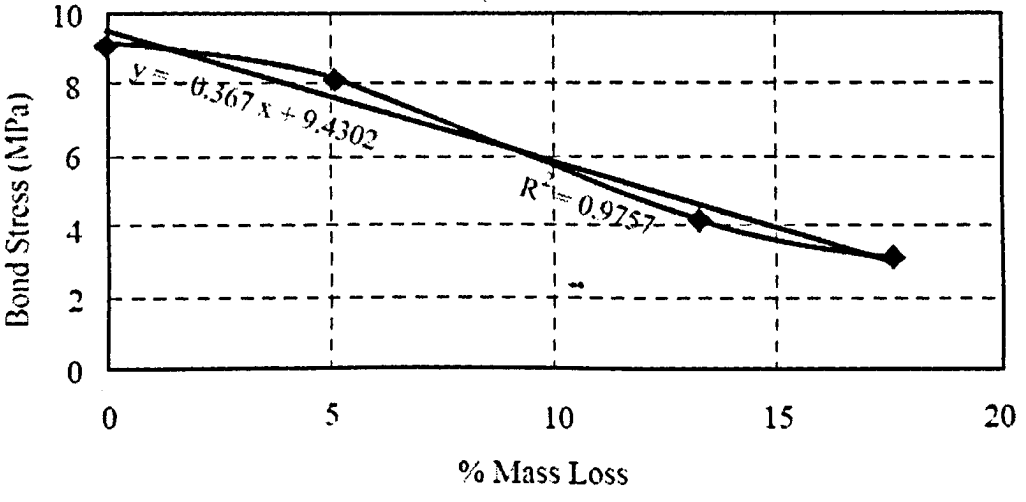

Figure 5.4 Mass loss vs bond stress for a cover of 50 mm and w/c 0.42, Amleh (2000).

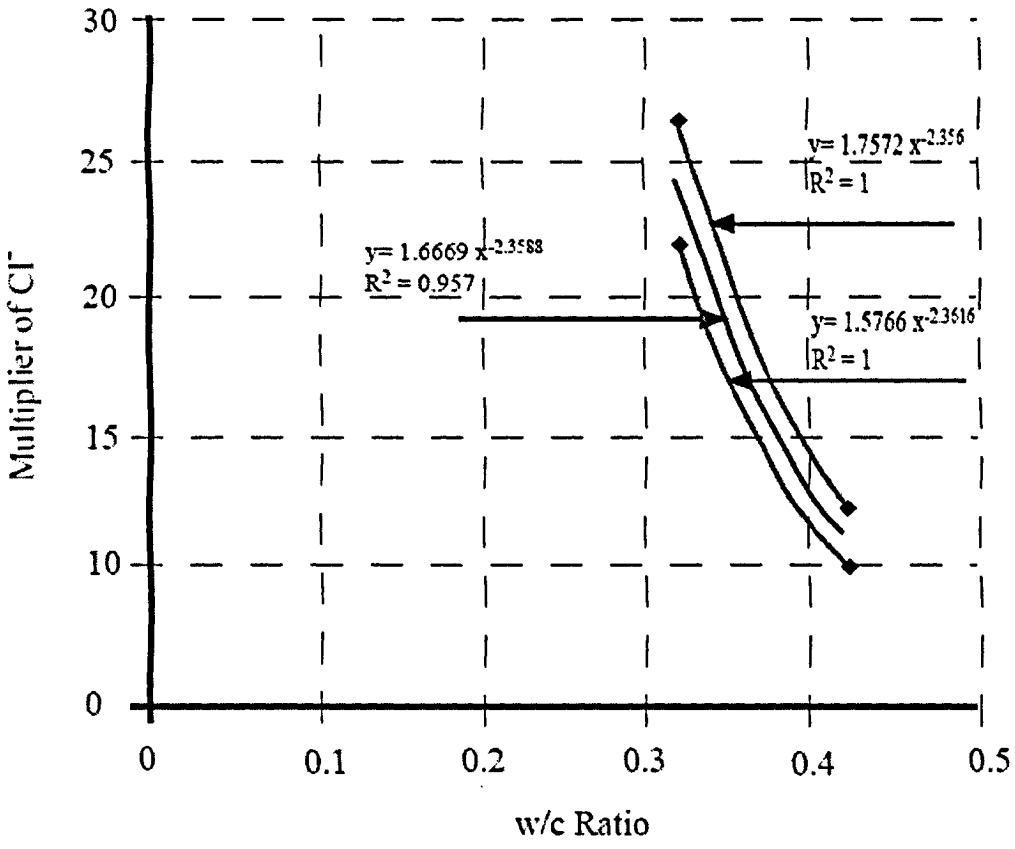

Figure 5.5 Relationship between the different w/c ratios and the multipliers of Cl^- from date of Amleh (2000).

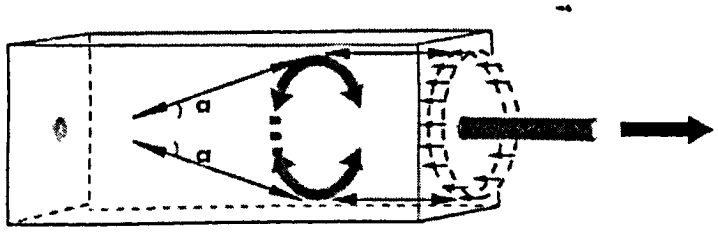

Figure 5.6 Tensile Stress Ring Tepfers, (1973).

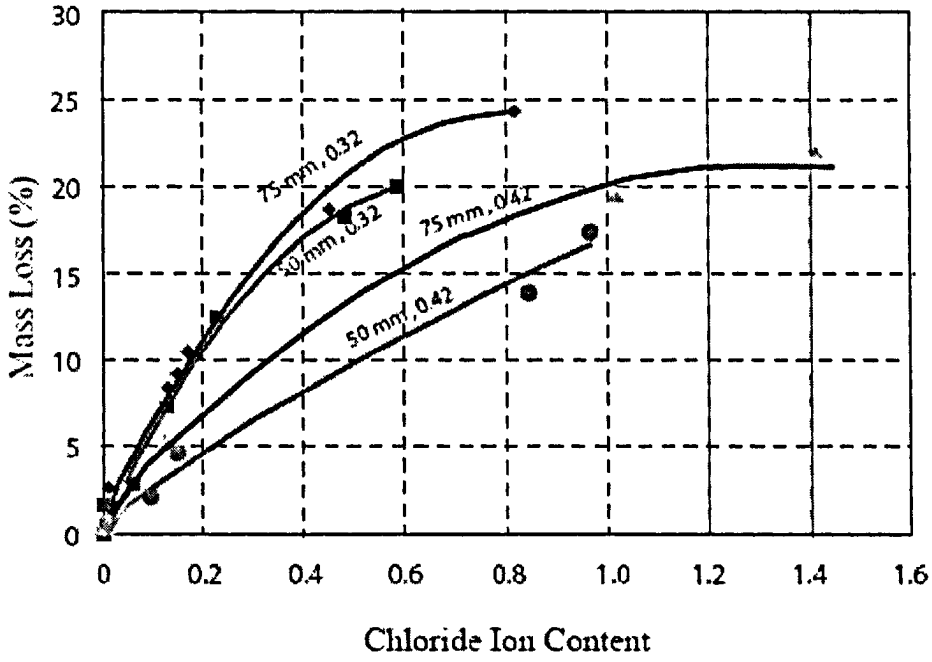

Figure 5.7 The mass loss corresponding to the chloride content.

CHAPTER 6

CONCLUSIONS AND FUTURE DIRECTIONS

6.1 Summary

Bond characteristics between concrete and reinforcing bars are one of the major structural properties that influence the strength and the performance of flexural concrete members. The objective of the research work presented in this thesis is to determine experimentally the effect of corrosion on bond behavior of deformed reinforcing steel bars embedded in concrete. The research included evaluation of the data obtained by Amleh (2000) to predict the bond strength at different stages of corrosion. In this regard, two phases of investigations were conducted. The first phase was experimental work to determine the bond loss due to chloride ion ingress at the interface between the reinforcing steel bar and the surrounding concrete using different w/c ratios. The second phase was to generalize and further develop the equations of bond loss derived by Amleh (2000) to be used for different water to cement ratio concretes and different accelerated corrosion processes.

In the experimental work; two different w/c ratio concretes were used, one with w/c ratio of 0.37 and the second one with w/c ratio of 0.47. Regular carbon steel bar of a 19.5 mm diameter was used to reinforce 100 mm and 150 mm diameter cylinders. Four stages of corrosion were pursued in this program. At each stage of corrosion, 2 pullout specimens were tested, 8 pullout specimens for each specific w/c ratio and concrete cover thickness were prepared and a total of 24 pullout specimens to test all corrosion stages.

Accelerated corrosion of steel reinforcing bars embedded in concrete was used by immersing the specimens in a 5% sodium chloride (NaCl solution) and applying a fixed voltage of 30 volts while the current was recorded at 24-hour intervals. This procedure enabled achieving high levels of corrosion (20 – 25 %) within a few weeks.

During the corrosion process; the specimens were monitored, and visually examined for any cracks. The level of corrosion was verified by removing the corroded bar from the

specimen and determining its mass loss as compared with the originally measured mass of the uncorroded specimen.

6.2 Conclusions

Based on the results of this research program, the following points can be concluded:

1. The overall behaviour of the tested pullout specimens conforms to that reported in the literature, in terms of crack widths and chloride ion content, the concrete cover thickness and immersing time, and bond strength with the slip for different corrosion stages.

2. It was found that for the same conditions of the pullout specimens, the effect of the rate of corrosion is proportional to w/c ratio, i.e. the higher the w/c ratio, the higher the rate of corrosion and therefore the lower the bond strength. Also, it is noticed that the larger size of the concrete cover thickness could help reduce the rate of corrosion. The greater the cover thickness, the longer the time it takes the chloride ions to reach the surface of the reinforcing steel.

3. The compressive strength is also found to be -as expected- inversely proportional to the w/c ratio, which coincide with the findings of Feret (1892). The bond stress is indirectly dependent of the tensile strength and is therefore, affected by the w/c ratio which agrees with Perry and Thompson (1966), Orangun, Jirsa and Breen, (1977) and Tepfers (1973).

4. The visual test revealed an increase in the crack width development with rising of corrosion level.

5. The research study clearly indicated that the bond stress-slip response of the embedded bar in the pullout specimen, was adversely affected by the width of the crack, and the level of corrosion. The crack width was found to develop faster and longer in specimens with lower compressive strength and as a result; the maximum bond strength in the

pullout test is affected significantly by the number and size of cracks and thus, the level of corrosion.

6. For a given crack width due to corrosion, it is observed that within the range of cover depths covered in this study, the available bond strength is higher for larger concrete cover thicknesses than for smaller cover thicknesses, this shows the significance of larger concrete cover thickness for protection of reinforcing steel in structural concrete elements. Certainly, the quality of concrete in terms of its permeability is equally important for the corrosion protection.

7. The bond strength in the pullout specimens is observed to decrease with an increase in the chloride ion content at the steel bar surface, which is directly related to the mass loss. This finding agrees with the findings of Amleh (2000) and Hassan (2003). The chloride ion would normally permeate or diffuse through the concrete cover, however, as cracks form and widen; much of the chlorides flow directly through the cracks to the surface of the reinforcing steel bar and destroy the passive layer to initiate corrosion.

8. With corrosion taking place at the interface between the reinforcing steel bar and the surrounding concrete, the bond strength deteriorates. Hence, the bond stress is expressed as a function of the concrete cover thickness, the reinforcing steel bar diameter, the tensile or compressive strength, and the percentage of chloride ion concentration at the surface of the steel bar as in the equations in Table 5.4, Amleh (2000). A relationship between w/c ratio on chloride ingress was developed to count for the deterioration in bond stress as in Equation 5.4 expressed as a function of the percentage of chloride ion content and the w/c ratio.

9. The validation of Equation 5.4 with the pullout specimens test results did not show a good correlation, that is due to the difference in the immersing time and the intensity of the current used to corrode the specimens in the laboratory. For this reason, a constant represents the used current intensity to corrode the reinforcing steel bars is introduced to

the second term of Equation 5.4 to consider for the lack of chloride ion concentration at the reinforcing steel bar as in Equation 5.5.

10. Equation 5.5 could be used to compare results from real life with those obtained from laboratory tests in terms of the rate of current intensity to be used in the laboratory to obtain the same level of bond loss.

In conclusion, a generalized relationship involving the prediction of bond stress at different levels of corrosion was developed. Furthermore, the results of this research study have led to a better understanding, both qualitatively and quantitatively, of the impact of corrosion on bond strength of corroded reinforced structures.

6.3 Recommendation for future research

- It is recommended to measure the steel reinforcing tensile strength after the corrosion takes place, because the corrosion products could severely affect the steel reinforcing tensile strength due to the corrosion concentration in some spots at the reinforcing steel bar, and also measuring the modulus of elasticity due to possible embrittlement during the corrosion process.

- It is highly recommended for future investigation to do more testing to verify Equation 5.5, and possibly to make some enhancement for a better performance with all types of concrete and with different concrete mixtures.

- Since there is a great deal of variables to consider when dealing with bond between the reinforcing steel and the surrounding concrete, more testing is required to include these variables in Equation 5.5. These variables are concrete permeability, steel strength, type of steel deformation in terms of lug size and shape.

- More investigation is required to study the effect of pozzolanic supplementary cementing materials on bond behaviour similar to that done by Hassan (2003) and Amleh

(2000), and incorporate the effect of these materials as a percentage in permeability reduction.

Finally, the development of practice- oriented equations for the evaluation of bond stress would contribute to the structural engineering community. However the determination of the input parameters could pose a major limitation to equations, which must be overcome before they can be used to facilitate the assessment of structures in the field. For instance, there are currently no methods available to conveniently determine the cross-section reduction, the location and distribution of pits and respectively the bond stress at these locations. The development of these methods would make the practice-oriented equations feasible, which in turn would prove to be a great asset to the engineers in the field.

APPENDIX A

Compressive and tensile strengths at an age of 30 days

Sample #	Age (Day)	W/C Ratio	Comp Str (Mpa)	Ave. Comp Str. (Mpa)	Splitting Tension Test (Mpa)
C2-2C	30	0.47	42.28	42.00	4.04
C2-6C	30		41.71		3.84
C1-3C	30	0.37	60.98	59.60	5.12
C1-4C	30		58.22		5.5
C2-3B	30	0.47	43.59	42.00	4.2
C2-1B	30		40.40		3.77

Figure 1 Obtained compressive and tensile strengths at an age of 30 days

Compressive strength at an age of 49 days

Sample #	Age (Day)	W/C Ratio	Comp Str (Mpa)	Ave. Comp Str. (Mpa)
C2-4C	49	0.47	42.77	42.84
C2-8C	49		42.90	
C1-5C	49	0.37	61.30	61.68
C1-7C	49		62.06	
C2-2B	49	0.47	43.40	43.04
C2-4B	49		42.68	

Figure 2 Obtained compressive strength at an age of 49 days

Compressive Strength at an age of 57 days

Sample #	Age (Day)	W/C Ratio	Comp Str (Mpa)	Ave. Comp Str. (Mpa)
C2-5C	57	0.47	42.90	42.83
C2-7C	57		42.76	
C1-1C	57	0.37	61.78	61.89
C1-6C	57		61.99	
C2-5B	57	0.47	43.21	43.23
C2-8B	57		43.24	

Figure 3 Obtained compressive strength at an age of 57 days

Compressive Strength at an age of 66 days

Sample #	Age (Day)	W/C Ratio	Comp Str (Mpa)	Ave. Comp Str. (Mpa)
C2-1C	66	0.47	43.36	43.78
C2-3C	66		44.20	
C1-2C	66	0.37	62.84	63.83
C1-8C	66		64.81	
C2-6B	66	0.47	44.30	43.98
C2-7B	66		43.65	

Figure 4 Obtained compressive strength at an age of 66 days

Equation of CL^- between (0.005 - 0.02)

		1st point	2nd point
y	% CL^- Ave.	0.005	0.02
x	mV	93.85	71.9

Slope

m =(y1 -y2)/(x1 - x2)

m -0.0007

y = mx + b

0.0050 = -0.0641 + b ➡ b= 0.0691

y= -0.0007 x + 0.0691

Equation of CL^- between (0.02 - 0.05)

		1st point	2nd point
y	% CL- Ave.	0.02	0.05
x	mV	71.9	47.9

Slope

m =(y1 -y2)/(x1 - x2)

m -0.0013

y = mx + b

0.0200 = -0.0899 + b ➡ b= 0.1099

y= -0.0013 x + 0.1099

Equation of CL- between (0.05 - 0.5)

		1st point	2nd point
y	% CL- Ave.	0.05	0.5
x	mV	47.9	-8.5

Slope m =(y1 -y2)/(x1 - x2)

m -0.0080

y = mx + b

0.0500 = -0.3822 + b ➡ b= 0.4322

y= -0.0080 x + 0.4322

Figure 5 Establishing the equations of the calibration curve

		Depth from outside (mm)		
		13	26	40
C2-1C	mV	-39.30	-20.70	-33.50
	%CL-	0.75	0.60	0.70
C2-8C	mV	5.60	28.20	33.80
	%CL-	0.39	0.21	0.16
C2-5C	mV	-6.30	9.00	-18.40
	%CL-	0.48	0.36	0.58
C2-3C	mV	-43.30	-18.90	-57.00
	%CL-	0.78	0.58	0.89
C2-4C	mV	-7.00	12.30	27.20
	%CL-	0.49	0.33	0.22
C2-7C	mV	-9.60	6.70	15.30
	%CL-	0.51	0.38	0.31

Figure 6 Measured concentration of chloride ion content for series C2-C

		Depth from outside (mm)		
		13	26	40
C1-7C	mV	-3.70	12.00	31.00
	%CL-	0.46	0.34	0.18
C1-8C	mV	-39.60	-2.00	-45.40
	%CL-	0.75	0.45	0.79
C1-1C	mV	-13.70	1.00	17.00
	%CL-	0.54	0.42	0.30
C1-6C	mV	-28.80	-10.40	-0.40
	%CL-	0.66	0.52	0.44
C1-5C	mV	3.50	33.70	39.00
	%CL-	0.40	0.16	0.12
C1-2C	mV	-36.60	-13.90	-46.90
	%CL-	0.72	0.54	0.81

Figure 7 Measured concentration of chloride ion content for series C1-C

		Depth from outside (mm)		
		22	44	65
C2-4B	mV	2.70	18.70	37.50
	%CL-	0.41	0.28	0.13
C2-8B	mV	10.60	17.20	35.00
	%CL-	0.35	0.29	0.15
C2-6B	mV	-38.90	-16.50	-88.60
	%CL-	0.74	0.56	1.14
C2-5B	mV	-16.80	6.70	32.80
	%CL-	0.57	0.38	0.17
C2-2B	mV	8.80	33.10	40.30
	%CL-	0.36	0.17	0.11
C2-7B	mV	-20.30	-7.30	-20.20
	%Cl-	0.59	0.49	0.59

Figure 8 Measured concentration of chloride ion content for series C2-B

REFRENCES

ACI Committee 222R, 2002, "Protection of Metals in concrete Against Corrosion"

ACI Committee 318, 2002, Building Code requirements for structural Concrete(318-02) and Commentary (318R-02), American Concrete Institute, Farmington Hills, MI.

ACI Committee 408, 1966, "Bond Stress – The State of the Art," ACI Journal, Proceedings V. 63, No. 11, Nov., pp. 1161-1188.

ACI Committee 408, 2002, "Bond and Development of Straight Reinforcing Bars in Tension," Draft Report, ACI 408R-XX, Jul., pp. 130.

Al-agroudi, H. (2003) "Bond Characteristics of Micro-Composite Multistructural Formable Steel Used in Reinforced Concrete Structures", a Master of Science thesis submitted to the Graduate Faculty of North Carolina State University

Almusalam Abdullah, A, Al-Gahtani Ahmad S., Aziz Abdur Rauf and Rasheeduzzafar., (1995), "effect of reinforcement corrosion on bond strength. Construction and Building Material", Vol. 10, No.2, pp. 123-129.

Amleh, L., (2000), "Bond Deterioration of Reinforcing Steel in Concrete Due to Corrosion," Ph.D thesis Dept of Civil Engineering and Applied Mechanics, Mc Gill University.

Amleh, L. & Gosh, A. (2006) "Modeling The Effect of Corrosion on Bond Strength at The Steel–Concrete Interface With Finite-Element Analysis.

Amleh, L. and Mirza, M.S., (1999), "Corrosion Influence on Bond Between Steel and Concrete,"ACI Structural Journal, May June, pp. 415-423.

Auyeung, Yubun, Balaguru, P., and Chung, Lan. , (2000), "Bond Behavior of Corroded Reinforcement Bars," ACI journal. No. 97-M28, pp. 214-220.

Bavarian, Behazad, PhD., Lisa, Reiner (March, 2002) "Corrosion Protection of Steel Rebar in concrete using Migrating Corrosion Inhibitors, MCI 2021 & 2022". Dept. of Manufacturing Systems Engineering & Management, College of Engineering and Computer Science, California State University, Northridge pp. 2-4.

Beeby, A.W. (1979), "The Prediction of Crack Widths in Hardened Concrete" The strudctural Engineer, Vol. 5 No. (2), pp. 35-40.

Bentz, D. P., Ehlen, M. A., Ferraris, C. F., and Garboczi, E. J. (2001), "Sorptivity-Based Service Life Predictions For Concrete Pavements" 7th International Conference on

Concrete Pavements. Proceedings (1991), Volume 1. International Society for Concrete Pavements. September 9-13, 2001, Orlando, Florida, pp. 181-193, 2001.

Berkeley, K.G.C., and Pathmanaban, S. (1990), "Cathodic Protection of reinforcement Steel in Concrete", Butterworth & Co., London, UK, PP. 1-52.

Bertolini, L., Elsener, B., Pedeferri, P., and Polder, R. (2004). "Corrosion of Steel in Concrete." Wiley-VCH Verlag GmbH & Co. KGaA, Weinheim, 28, 49, 91.

Borgard, B. Warren, C., Somayaji, S., and Heidersbach, R. (1990), "Mechanisms of Corrosion of Steel in Concrete," Corrosion Rates of Steel in Concrete, ASTM STP 1065, N. S. Berkr, V. Chaker, and D. Whiting, Eds., American Society for Tesing and Materials, Philadelphia, pp 174-188.

Cabrera J. G., and Ghodussi, P., (1992), "Effect of reinforcement corrosion on the strength of steel concrete bond." Proc mt. Conf. On Bond in Concrete- from research to practice. Riga, Latvia. pp. 10.11-10.24.

Cairns J. and Ramli Abdullah., (1994), "Fundamental Tests on the Effect of an Epoxy Coating on Bond Strength," ACI Journal /July- August No. 91- M32, pp. 331-338.

CEB-MC90 (1990), "CEB-FIP Model Code 1990", Thomas Telford Services Ltd., London, England

Choi, Oan. Chul, Lee, Woong Se., (2002), "Interfacial Bond Analysis of Deformed Bars to Concrete," ACI journal, No. 99-S75, pp. 750-755.

Clark, A. P., 1949, " Bond of Concrete Reinforcing Bars, "ACI Journal, Proceedings V. 46, No. 3, Nov., pp. 161-184.

Coronelli D., Gambarova P.G. (2000) "A MECHANICAL MODEL FOR BOND STRENGTH OF CORRODED REINFORCEMENT IN CONCRETE.", Proc. 14th Engineering Mechanics Conference of the Amerişan Society of Civil Engineers (EM2000), Austin, TX (USA), May 21-24, 2000.

Darwin, D.; McCabe, S. L.; Idun, E. K.; and Schoenekase, S. P., 1992, "Development Length Criteria: Bars Not Confined by Transverse Reinforcement," ACI Structural Journal, V. 89, No. 6, Nov.-Dec., pp. 709-720.

Darwin, David, and Ebeneze, K. Graham., (1993), "Effect of Deformation Height and Spacing on Bond Strength of Reinforcing Bars," AC! Structural Journal, V. 90, No. 6, Nov-Dec, pp. 646-657.

Darwin, D.; Tholen, M. L.; Idun, E. K.; and Zuo, J., 1996a, "Splice Length of High Relative Rib Area Reinforcing Bars," ACI Structural Journal, V. 93, No. 1, Jan.-Feb., pp. 95-107.

Darwin, D.; Tholen, M. L.; Idun, E. K., 1996b, "Development Length Criteria for Conventional and High Relative Rib Area Reinforcing Bars," ACI Structural Journal, V. 93, No. 3, May-June, pp. 347-359.

David W., (1941), "Bond Stress in Concrete Pullout Specimens," American Concrete Institute, Vol 13, No.1, September, pp. 37-50.

Davis, J.R. (2000), "Corrosion: Understanding the Basics" ASTM International, The Materials Information Society.

Elsener, B., (2001), "Corrosion for Steel in Concrete: State of the Art Report" European Federation of Corrosion Publications, Great Britain.

Ferguson, P. M. and Thompson, J. N., 1965, "Development Length of High Strength Reinforcing Bars," *ACI Journal*, V. 62, No. 1, Jan., pp. 71-94.

Goto, Y., 1971, "Cracks Formed in Concrete Around Deformed Tension Bars," *ACI Journal*, V. 68, No. 4, Apr., pp. 244-251.

Hassan, A. (2003), "Bond of Reinforcement in Concrete With Different Types of Corroded Bars", a Master of Science thesis presented to Ryerson University.

Ingraffea, A.R., Gerstle, W. H., Gergely, P. & Sauoma V. (1984), "Fracture Mechanics of Bond in Reinforced Concrete", Journal of Structural Engineering, 110:871-890.

Isecke, B., (1982), "Collapse of the Berlin Congress Hall Prestressed Concrete Roof," *Materials Performance*, NACE, December.

Jirsa, J.O. et al., (1979), "Rationale for Suggested development, Splice, and Standard Hook Provisions for deformed bars in Tension" Concrete International, No. 7, pp. 47-61.

Kaleida Graph Guide to Curve Fitting, Synergy Software (1988), Maxwell resources INC. PP. 5-18.

Kimura, H., and Jirsa, J., (1992), "Effects of Bar Deformation and Concrete Strength on Bond of Reinforcing Steel to Concrete," PMFSEL Report No. 92-4, Phil M. Ferguson Structural Engineering Laboratory, University of Texas at Austin.

Lounis, Z., & Mirza, M.S., (2001), "Reliebility-Based Service Life Prediction of deteriorating Concrete Structures", 3 Int. Conf. on Concrete under Severe Conditions pp.965-972.

Lutz, Leroy A.; Gérgely, Peter; and Winter, George.,(1966), "Mechanics of Bond and Slip of Deformed Reinforcing Bars in Concrete," Research Report No. 324, Department of Civil Engineenng, Cornell University, Ith aca, New York.

Lutz, L. A. and Gergely, P., 1967, "Mechanism of Bond and Slip of Deformed Bars in Concrete," *ACI Journal*, V. 64, No. 11, Nov., pp. 711-721.

Maslehuddin M., Ibrahim M. Allam, Ghazi J. Al. Sulaimani, Abdulaziz L. Al-Mana, and Sahel N. Abdulijauwad., (1990), "Effect of Rusting of Reinforcing Steel on its Mechanical Properties and Bond With Concrete," ACI Journal ,No. 87-M53, pp. 496-500.

Mathey, R.; and Watstein, D., 1961, "Investigation on Bond in Beam and Pull-out Specimens with High-Yield –Strength deformed Bars," ACI Structural Journal, V. 90, No. 6, Nov. –Dec., pp. 646-657.

Mehta, P.K., and Monteiro, P.J.M. (1992), "Concrete Structure – Properties and Materials" , Prentice –Hall Inc. Englewood Cliffs, N.J.

Neville, A. (1995), "Chloride Attack of Reinforced Concrete: An Overview", Materials and Structures, 1995.

Neville, A.M., (1981),"Properties of Concrete," 3rd Edition, Pitman Publishing Ltd., London, Chapter I. of Corroded Reinforcement in Concrete", Politecnico di Milano.

Orangun, C. O.; Jirsa, J. O.; and Breen, J. E., 1975, "The strength of anchored Bars: A Reevaluation of Test Data on Development Length and Splices," Research Report No. 154-3F, center for High way Research, The University of Texas at Austin, Jan., 78 pp

Orangun, C. O., Jirsa, J.O., & Breen, J.E., (1977), "A Re-evaluation of Test Data on Development Length and Splices" ACI Journal, PP 114-122.

Park, R., and Paulay, T., (1975), "Reinforced Concrete Structure," Ultimate strength design of reinforced concrete structures, vol. 1, printed by the University of Canterbury for extension study seminars conducted for practicing structural engineers in New Zealand.

Perry, S. E. and Thompson, J. N. (1966), "Bond Stress Distribution on Reinforcing Steel in Beams and Pullout Specimens", ACI Journal, Proceedings, Vol. 63, No. 8, pp 865 – 874.

Pillai, S.U. & Kirk, D.W. (1988) "Reinforced Concrete Design", McGraw Hill Ryerson.

Rehm, G., (1961), "Uber die Grunlagen des Verbundes Zwischen Stahl und Beton," Deutscher Ausschuss für Stahlbeton, Heft 138, Wilhelm Ernest und Sohn, Berlin.

Reynolds, G. C. (1982), "Bond Strength of Deformed Bars in Tension" Cement and Concrete Association, C & CA Technical Report 548.

P. Desay, and K.B. Rao, "Probabilistic analysis of the cracking or RC beams" Materials & Structures, Rilem 20 (1987), (120), pp. 408 -417.

Rodriguez J., Ortega, L. M., Casal, J. (1997), "Load Carrying Capacity of Concrete Structures With Corroded Reinforcement", Construcrion and Building Materials, Vol. II, No. 4. pp. 239-248.

Soretz, S., and Holzenbein, H., (1979), "Rib Dimension Influence on Bond and Bendability," ACI journal. Proceedings V. 76, pp. 87-91.

Stanish, K.D., Hooton, R.D., and Thomas, M.D.A (1997). "Testing the Chloride Penetration Resistance of Concrete: A Literature Review." Department of Civil Engineering, University of Toronto.

Tanaka Y., Kawano H., Watanabe H. & Nakajo T. (2001), "Study on Required Cover Depth of Concrete Highway Bridges in Coastal Environment" 17th U.S. – Japan Bridge Engineering Workshop, 2001, Tsukuba

Tepfers, R. (1973), "A Theory of Bond Applied to Overlapped Tensile Reinforcement Splices for deformed bars" Dividion of Concrete Structures, Chalmers University of Technology, Goteborg, Sweden, Publication. 73:2, 328p.

Tepfers, R., (1979), "Cracking of Concrete Cover Along Anchored Deformed Reinforcing Bars" Magazine of Concrete Research, Vol. 31, No. 106 PP.3-12.

Treece, R.A., & Jirsa, J.O. (1989), "Bond Strength of Epoxy-Coated Reinforcing Bars" ACI Materials Journal, Vol. 86, No. 2, PP. 167-174.

Watstein, D. W. & Mathey, R. G. (1959), "Width of Cracks in Concrete at the Surface of Reinforcing Steel Evaluated by Means of Tensile Specimens" ACI Journal, Proceedings, Vol. 31, No. RP 1545, pp 1-24.

Welch G.B.and Patten B.J.F., (1967), "Reduction in concrete-Steel Bond with Horizontally Embedded Reinforcement,"UNCIV Report No R-8, university of New South Wales, pp 26.

Zuo, J.; and Darwin D., 2000, "Splice Length of Conventional and High Relative Rib Area Reinforcing Bars in Normal and High Strength Concrete," ACI Structural Journal, V. 97, No. 4, Jul.-Aug., pp. 630-641.